AD NUMBER

AD829538

NEW LIMITATION CHANGE

TO

Approved for public release, distribution unlimited

FROM

Distribution authorized to DoD only; Administrative/Operational Use; 30 SEP 1967. Other requests shall be referred to Office of Naval Research, Attn: Air Programs [code 461], Washington, DC 20360.

AUTHORITY

onr ltr, 24 sep 1973

AD-829 538

RADAR REFLECTIVITY OF SEA TARGETS, Volume I

Prepared for
DEPARTMENT OF THE NAVY
OFFICE OF NAVAL RESEARCH
AIR PROGRAMS
Washington, D. C. 20360
Under
Contract Nonr-991(12)

H. A. Corriher, Jr., Berry O. Pyron,
R. D. Wetherington, and A. B. Abeling
Project A-914

30 September 1967

Engineering Experiment Station
GEORGIA INSTITUTE OF TECHNOLOGY
Atlanta, Georgia

GEORGIA INSTITUTE OF TECHNOLOGY
Engineering Experiment Station
Atlanta, Georgia 30332

FINAL REPORT, Vol. I

Project A-914

RADAR REFLECTIVITY OF SEA TARGETS, Volume I

by

H. A. CORRIHER, JR., BERRY O. PYRON,
R. D. WETHERINGTON, and A. B. ABELING

30 September 1967

Prepared for
DEPARTMENT OF THE NAVY
OFFICE OF NAVAL RESEARCH
AIR PROGRAMS
WASHINGTON, D. C. 20360
Under
Contract Nonr-991(12)

ABSTRACT

Volume I of this two-volume survey presents a broad overview of the state of knowledge of radar reflectivity of sea targets. All forms of targets are considered, including ships and boats, submarines, periscopes and snorkels, wakes, buoys, icebergs, and splashes. Also discussed are the statistical properties of returns, glint, and camouflage. Several approximate theories which have been advanced to explain the radar return of sea targets are reviewed and compared, and additional theoretical work is reported which indicates that there are serious limitations inherent in the commonly used coherent model. The effective cross-section of a target on a reflective surface is emphasized as being the product of the inherent ("free-space") cross-section times F^4, the fourth power of the pattern propagation factor. Suggestions are made for interpreting World War II cross-section values for present-day systems studies. It is recommended that extensive experimental measurement data be obtained on a few targets rather than fragmentary data on many targets. This should lead to better understanding of the general problem and, eventually, to possible techniques for predicting the radar cross-sections of sea targets.

FOREWORD

Work on this program has resulted in two technical reports, each issued in two volumes. Technical Report No. 1 is entitled "Abstracts on Radar Reflectivity of Sea Targets" and covers literature which was issued from World War II until late 1966. The present two-volume report summarizes the findings of a number of these and other investigations, and reports on studies conducted during the present contract program. Volume I gives a general overview of the state of knowledge of radar reflectivity of sea targets and describes results of some specific studies. Volume II is primarily devoted to classified experimental results.

During the course of this program, we have endeavored to contact all groups known to be currently engaged in studies directly or closely related to reflectivity of sea targets and many of the agencies have been visited. Although the list is too extensive to give here, we wish to thank the numerous persons who have assisted in providing information, both written and oral.

In addition to the authors, several other persons at Georgia Tech made appreciable contributions to this work. We wish especially to acknowledge the many helpful discussions with Mr. W. K. Rivers, Jr. and Dr. M. W. Long, and the assistance of Mr. J. M. Corbitt and Dr. H. A. Ecker in theoretical studies associated with appendix material of this volume. We also wish to thank Mrs. Linda N. Black and Mrs. Jean A. Nichols for the final typing of this volume.

TABLE OF CONTENTS

TABLE OF CONTENTS (continued)

I. INTRODUCTION

Meaningful description and measurement of the radar cross-section of a target on the sea are extremely difficult. Targets of interest range from small and relatively simple shapes such as a periscope to large and very complex shapes such as a ship. Under some circumstances, the presence of the sea as a rough, reflecting surface causes the target to be illuminated by a field having appreciable phase and amplitude variations with height. When these complications are combined with relative motion between target and radar, and with variations in propagation near the surface, the problem of understanding and characterizing radar target return becomes a formidable one.

It is the purpose of the present study to collect and analyze information on reflectivity of sea targets from all known sources. Abstracts of over 300 reports and papers have been given in the two volumes of Technical Report No. 1 on this program [1, 2]. Here we present information from some of these sources in a more organized and detailed form, together with results from analysis performed during the current program. The body of this report is primarily concerned with experimental studies and interpretation of the results; theoretical aspects of the problem are summarized in an appendix.

Much of the basic information on scattering by targets over a reflecting surface is readily available elsewhere, and is therefore not covered here. We have found the treatments by Kerr [3], Durlach [4], and Katzin [5] to be particularly valuable, although many other useful sources also exist. Our references to material in Volume 13 of the MIT Radiation Laboratory series are so frequent that we will often simply use the designation "Kerr."

The great interest in radar reflectivity of aircraft during World War II continued thereafter and developed into consideration of missile problems. In comparison with this, both theoretical and experimental aspects of reflectivity of targets on the sea have been largely neglected. While there have been several individual measurements programs and theoretical studies, the vigorous concentrated effort on aircraft reflectivity, with attendant cross-fertilization through interchange of ideas and results, seems not to have been duplicated for sea targets. In summarizing the main findings from literature accessible to us through about mid-1967, we point out what is known with reasonable certainty and what is known sketchily or not at all. In one sense, this must be considered an interim study since, as will be made apparent, the present

knowledge of reflectivity of sea targets falls short of being adequate for design of sophisticated radar systems.

We have approached the question of radar cross-section of sea targets as involving an inherent ("free-space") cross-section which is modified by a factor F^4, the fourth power of the pattern propagation function, to obtain an effective cross-section. When numerical values of cross-section are given in this report they must be viewed with caution, since the problem of accounting for F^4 is difficult. We recommend that the user obtain copies of the actual documents containing the measured data and interpret them for his own needs in light of the discussions which follow.

One of the most unfortunate aspects of the situation is that there is great demand for statistical descriptions of the targets, whereas such characteristics as run-to-run variability in data have not been established for most measurements. It is particularly difficult to interpret fragments of information from many sources and arrive at numerical values appropriate to specific targets. What we are able to say with confidence is that returned power (and, hence, effective cross-section) for a sea target undergoes wide variations within relatively short times, these fades being typically 20 dB or more. When multiple runs have been made on targets, there is also spread in the smoothed values, sometimes a little and sometimes a great deal. The number of replicated runs on a target has usually not been sufficient to establish the true variability of the data, or to determine whether its causes are inherent in the target or created by the environment.

In design of future radar systems which incorporate new techniques in equipment and signal processing, it is unlikely that previously obtained cross-section data can do much more than provide gross estimates of target properties and indicate the direction for additional studies. A single cross-section value cannot possibly represent a complex target for all wavelengths, all polarizations, all pulse lengths, all aspects, all schemes of signal processing, etc. In many cases design of a new system may require data obtainable only by measurements using the technique under development. Therefore, while preliminary studies may rely on fundamental aspects of the reflection process in the target environment to make extrapolations of known information, it is likely that such work will need to be followed by target measurement programs specifically designed to answer particular system-oriented questions. This need for experimental data will be reduced if reliable methods of predicting cross-section can be developed for sea targets.

II. SURFACE-BORNE CROSS-SECTION MEASUREMENTS ON SHIPS AND SUBMARINES

During 1944-1946, the Naval Research Laboratory (NRL) conducted an extensive series of cross-section measurements on ships, boats, and submarines using shore-based radars at their Chesapeake Bay Annex (CBA). The large quantity of data makes the reports [6-13] valuable as a source of low-angle information. We will describe the measurement program in general, comment on the interpretation of quantitative cross-section data from these and other similar early tests, and present examples of data on aspect variation of cross-section.

2-2. Description of Measurements

Operational radars were used by NRL for measurements on about thirty ships of various types. Dihedrals, trihedrals, and flat-screen reflectors placed on barges in Chesapeake Bay were used for system calibration and their free-space cross-sections were modified to account for interference-lobe effects. A-scope pip heights were measured using pulsed signal generators or calibrated gain-control dials. The radars operated at frequencies from about 100 MHz to 9200 MHz, and all had pulse lengths of the order of microseconds and beamwidths of the order of several degrees; most were horizontally polarized. As examples, Table I gives a few characteristics of the radars used to make the measurements described in Section 2-3 below; all those listed used horizontal polarization.

Table I

Characteristics of Radars at CBA*

Radar	Freq. (MHz)	PRF (pps)	Pulse Length (μsec)	Antenna Ht. (ft)
SCR-270	107	300	5-40	133.8
SC-2	200	60	5	110.1
Mk-4	700	1600	1.5	115.5
Mk-12	970	500	1.2	125.2
SG-1	3060	800	2	137.0
SU	9200	600	0.5	137.0

*Frequency and antenna height from NRL reports; other values are approximate, based on Reference 14.

In the earliest tests, data were taken as the maximum return in some fairly long time interval (typically 30 seconds) as the target opened or closed in range or made a tight circle in a short time. Later tests were standardized on four basic types of ship maneuvers during the measurements, as described below.

The first type was a slow circle, with a rate of turn of about 12° per minute (i.e., a complete circle in half an hour). The diameter of the circle was as small as possible, consistant with the turning rate of the ship, and was usually about 1000 yds but was sometimes larger. The ship announced the relative bearing of the Chesapeake Bay Annex, when visible, every 5° during the circle; when the station was obscured, the ship's true heading was reported. Announcements of the heading were heard by all radar operators and the maximum signal during the preceeding 5° interval was then recorded. In general, two complete circles (720°) were executed by the ship.

The second type consisted of fast circles at various ranges during which the radar operator recorded only the maximum signal obtained. Each circle took about 8-10 minutes and was about 1200 yds in diameter. Ship's true heading was announced every 30° so that the radar operators could anticipate the large broadside echoes which usually were the maximum returns.

In a third type, the ship followed a base course which kept the radar stations abeam, and then periodically varied the heading $\pm$ 5° about this course. The purpose of this zig-zag course was to assure that the broadside aspect was presented to the shore-based radars a number of times at each range.

A fourth type was for the purpose of obtaining cross-section for bow or stern aspect. It consisted of having the ship follow a base course which kept the radar station at a relative bearing of 0° for bow aspect (or 180° for the stern aspect), and then varying the heading of the ships $\pm$ 5° about this base course. The largest echo observed was recorded during each zig-zag period. These measurements actually gave the peak amplitude of the principal lobe in a narrow sector about the bow or stern of the ship.

With the above procedures, the operators were able to obtain consistent results using manual recording of the visual observations of A-scopes. However, as discussed below, the numerical data which resulted are believed to be strongly biased toward high cross-section values (in comparison with currently accepted practices) and must not be accepted as "the cross-section" without interpretation.

Low-level meteorological soundings were taken during most of the radar measurements, except for the early ones. Meteorological conditions were found to be of paramount importance in propagation over Chesapeake Bay, with most of the significant variation occurring below a height of 800 ft. It was observed that surface ducts could increase the radar return power by a factor as large as 40 dB over standard conditions, thereby grossly affecting the cross-section measurements.

2-2. Interpretation of World War II Data

Emphasis in the NRL tests appears to have been on determining the maximum expected cross-section for conditions associated with long-range detection. Therefore, most of the numerical data presented in the reports are for broadside aspects, though some apply to bow or stern aspects. Because the variation of received power with range may be approximated by two forms, R^{-4} and R^{-8}, which are at least partially justified on both theoretical and experimental grounds, NRL found it convenient to define different radar cross-sections for the two regions. In their terminology, these are called the "near-zone cross-section," σ_n, and the "far-zone cross-section," σ_f, and must be used with two different forms of the radar equation (see Section 6-5 of Kerr).

Based on the approximate theory for the coherent flat plate employed in their analysis, the two forms of cross-section are related to the "free-space cross-section," σ_o, as follows:

$$\sigma_n = 4\sigma_o, \text{ and}$$

$$\sigma_f = (4\pi h/\lambda)^4 \, \sigma_o/9,$$

where h is the effective height of the target. It then follows that σ_n and σ_f are related as

$$\sigma_f = (4\pi h/\lambda)^4 \, (\sigma_n/36) = (R_t/h_1)^4 \, \sigma_n \, ,$$

where h_1 is the antenna height and R_t is the transition range at which the R^{-4} and R^{-8} regions meet and for which the NRL approximation gives

$$R_t = 4\pi h_1 h/\sqrt{6}\,\lambda = 5.13\, h_1 h/\lambda \, .$$

The approximate theory used by NRL in deriving these definitions of cross-section is really equivalent to using $\sigma_o F^4$ in the standard radar equation (see Eq. (A-8)) and making separate approximations to F^4 for the two range-law regions: $F^4 = 4$ for the R^{-4} region, and $F^4 = (4\pi h_1 h/\lambda R)^4/9$ for the R^{-3} region. The very large numerical values which are found for σ_f are balanced in its associated radar equation for the R^{-8} region by a factor $(h_1/R)^4$ which is split off from the F^4 approximation (i.e., $(h_1/R)^4\ \sigma_f = \sigma_o F^4$). Conversion of σ_n or σ_f to the conventional free-space cross-section is not entirely straightforward because neither the effective target height h nor the transition range R_t is available as an entirely accurate value for treating σ_f, and the factor of 4 is somewhat suspect for use with σ_n (see Section A-4).

It is unfortunate that most of the NRL data are for σ_f, since it would probably be more satisfactory to have σ_n and modify it for use in the R^{-8} region. Certainly, to take σ_f as being the conventional free-space cross-section used in the standard radar equation would be a serious error, and the numerical values of σ_f would be unreasonably high. Except for possible biases discussed below, the values of σ_f determined under standard propagation conditions should be appropriate for use in the R^{-8} region when the standard radar equation has been multiplied by $(h_1/R)^4$. (Note that this is R and not R_t; along with the R^{-4} already in the radar equation this gives the R^{-8} dependence.)

Turning now to the question of bias in the numerical data, it should be noted that these NRL data (and most other values from the World War II era) are not the median values of many points taken over some interval of time or aspect as would probably be used now (see, for example, Chapter III). Instead, they are peak readings and are statistically likely to be several dB above the median value for any reasonable probability distribution.

The long period of observation makes it likely that many independent samples were obtained, say 100 or so. Assuming that the cross-sections are Rayleigh distributed, there is a 50% chance that at least one out of the 100 independent samples will be 7 dB above the mean value which specifies the distribution, or 8.6 dB above the median value. This implies that the peak observations made by NRL in these early tests are biased strongly upward from the median values which might be reported today for the same targets.

A second possible bias may appear in some of the values because of the way straight lines were fitted to the data points (plotted as log P_r vs. log R) from which cross-sections were calculated. Almost all of these curves are

fitted to the upper points in a set which usually has fairly large spread. Examination of many of these plots leads to an estimated bias of 1 to 5 dB above curves which would put about the same number of data points over and under the fitted lines. Also, when the data points were in the R^{-4} region, the lines were placed at the top of the "hump" which is theoretically predicted just inside the transition range and which appears rather clearly on at least some experimental plots (see also Sections A-2 and 5-1).

Finally, the experimental procedures used in collecting these data greatly increased the probability of observing specular returns from large flat or nearly flat surfaces at bow, stern, and broadside aspects. Therefore, we would expect the data to be biased in the high direction over that expected for most aspects of a complex target. Although the exact form of probability distribution which would fit these data cannot be determined, it is safe to say that the returns occurring during the observation period would probably show an excess of high cross-section values over that predicted by a Rayleigh distribution with the same mean value. Recording only values from this high cross-section tail, as was done, would result in an estimate of median return which would be high, but the specific amount cannot be established.

Taking into account the above three bias-producing factors--peak rather than median values of many independent samples, curve fitting to extreme data points, and samples from an expected probability distribution having a high cross-section tail--the NRL figures should be useful if adjusted downward to more nearly approximate median data. While an exact correction cannot be determined, we suggest that a downward adjustment of about 15 to 20 dB seems reasonable and should give results which are within the expected spread of experimental data. The correction might be different at different aspects if the statistical distributions are aspect dependent. It is again cautioned that σ_f values are appropriate only when the standard radar equation has been multiplied by $(h_1/R)^4$ and that these data were sometimes influenced strongly by meteorological conditions.

Although the NRL data comprise most of the calibrated cross-section values available for ships viewed at low elevation angles, some data were obtained by the MIT Radiation Laboratory and are given in Reference 15 (from which Table 6-2 of Kerr was extracted). Many details of the measurement procedures are lacking in this report, but the data points were the maximum returns in 15-second intervals and probably have a substantial upward bias. It is suggested

that these values be reduced at least 15 dB to make them more comparable to median figures.

2-3. Aspect Variation of Cross-Section

In this section, we present examples of the results of slow-circle measurements made by NRL. These plots were taken from Reports V, VII, and VIII in their series [10, 12, 13], and show the aspect variation of return power as the ships turned through one or more complete circles. Because the range variation is small during a circle, the variation can be taken to be due to variation in cross-section. All plots have been normalized to the largest value observed during any of the replicated runs. Most of the plots are for data in the R^{-8} region and show the aspect variation for four or five frequencies ranging from 107 MHz to 3060 MHz. In some cases the plots show different information, as discussed below. The value of σ_f or σ_n corresponding to the normalized peak is given for each plot. Propagation was approximately standard during these measurements; however, the cautions discussed above apply to these numerical values. Data are for the peak power in a 5° interval.

Fig. 1 shows slow-circle data taken at a range of 20,000 yds on the aircraft carrier USS Antietam (CV-36), and the plots show data taken on four circles of the ship. The data points were not identified with each particular circle, and hence represent the overall spread of cross-section measurements, rather than run-to-run variations. The broadside returns are largest in these plots and show an asymmetry between port and starboard for some runs. Although this might be expected because of the presence of the island on one side of the ship, results are not consistent for all five frequencies.

The top four plots of Fig. 2 show the aspect variation for the battleship USS Missouri (BB-63) at four frequencies and a slow circle range of 10,000 yds. The maximum peaks occur at broadside, with port and starboard not necessarily the same. A secondary peak is usually observed for bow aspect but a corresponding peak is not observed for stern aspect.

The bottom two plots in Fig. 2 contrast the aspect variation obtained in the R^{-4} and R^{-8} regions. The bottom plot was for a slow circle at 25,000 yds, when the target was in the R^{-8} region at 3060 MHz. The plot just above shows the variation for the ship at 10,000 yds, when it was in the R^{-4} region at 3060 MHz. The broadside return is relatively larger, with respect to other aspects, when the target is in the R^{-4} region than is the case for the R^{-8} region. In other tests not illustrated here, the 17-ft paraboloid of the SK-2

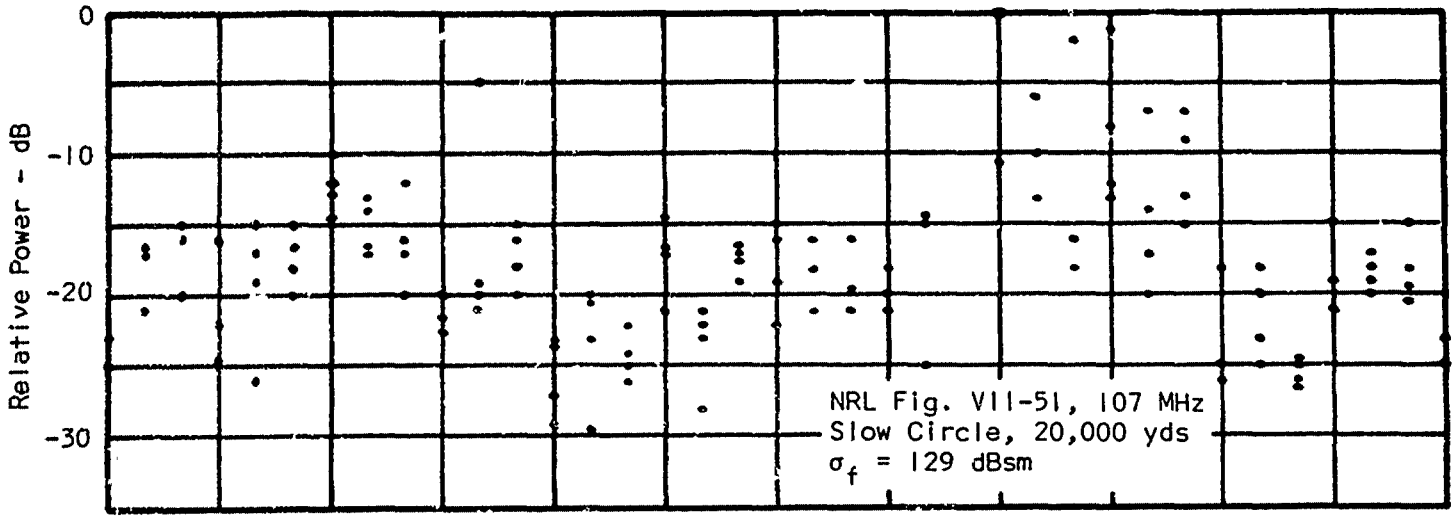
0
-10
-20
-30
Relative Power - dB
NRL Fig. VII-51, 107 MHz
Slow Circle, 20,000 yds
σ_f = 129 dBsm

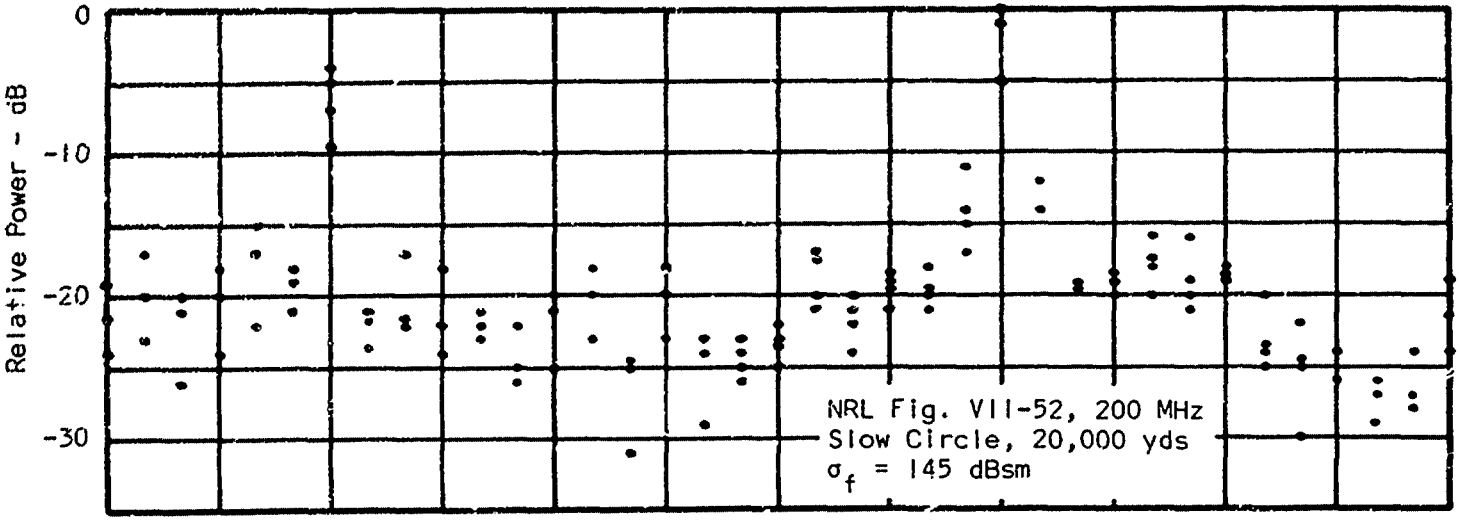
0
-10
-20
-30
Relative Power - dB
NRL Fig. VII-52, 200 MHz
Slow Circle, 20,000 yds
σ_f = 145 dBsm

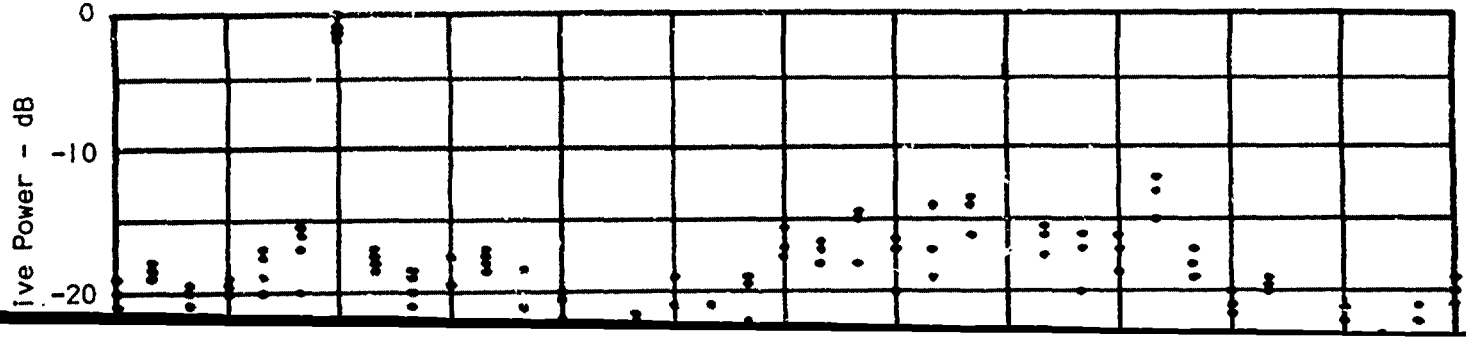
0
-10
-20
ive Power - dB

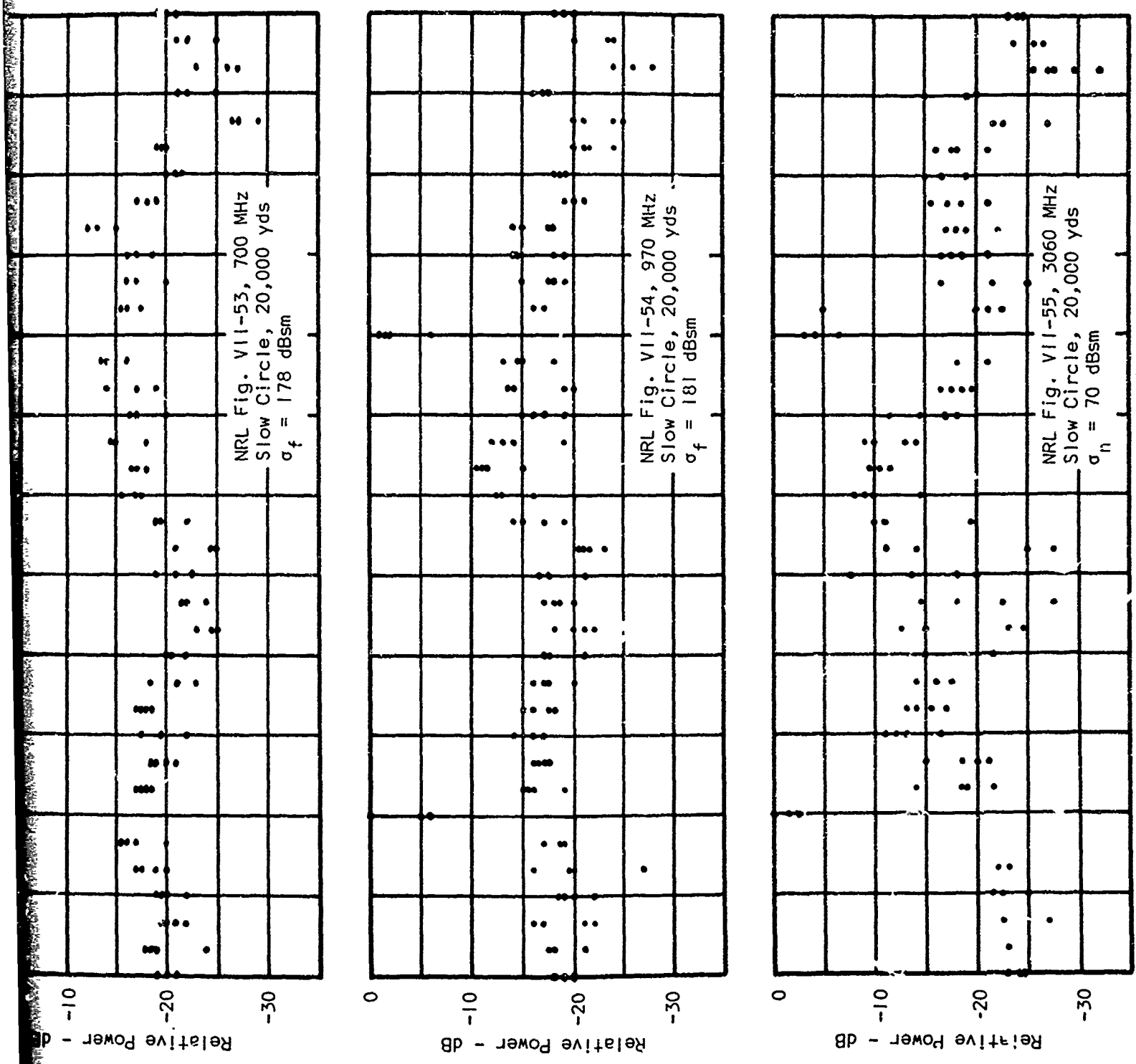
NRL Fig. VII-53, 700 MHz
Slow Circle, 20,000 yds
σ_f = 178 dBsm
NRL Fig. VII-54, 970 MHz
Slow Circle, 20,000 yds
σ_f = 181 dBsm
NRL Fig. VII-55, 3060 MHz
Slow Circle, 20,000 yds
σ_n = 70 dBsm
Relative Power - dB
0
-10
-20
-30
Port
Stern
Starboard
Bow

2

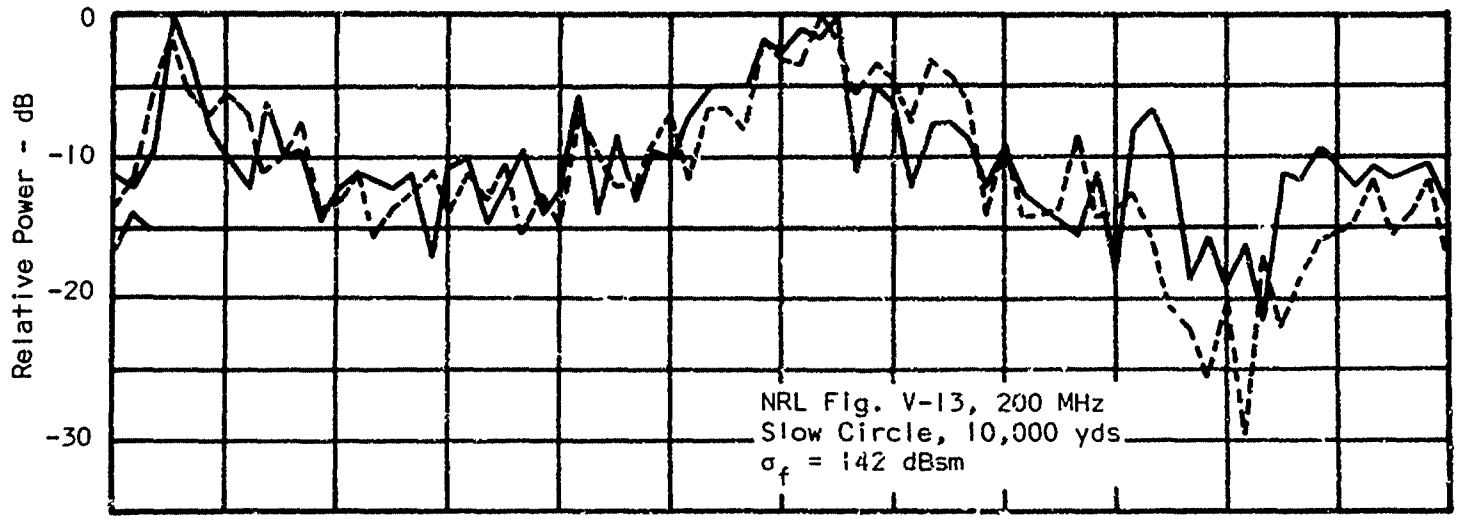
0
-10
-20
-30
Relative Power - dB
NRL Fig. V-13, 200 MHz
Slow Circle, 10,000 yds
σ_f = 142 dBsm

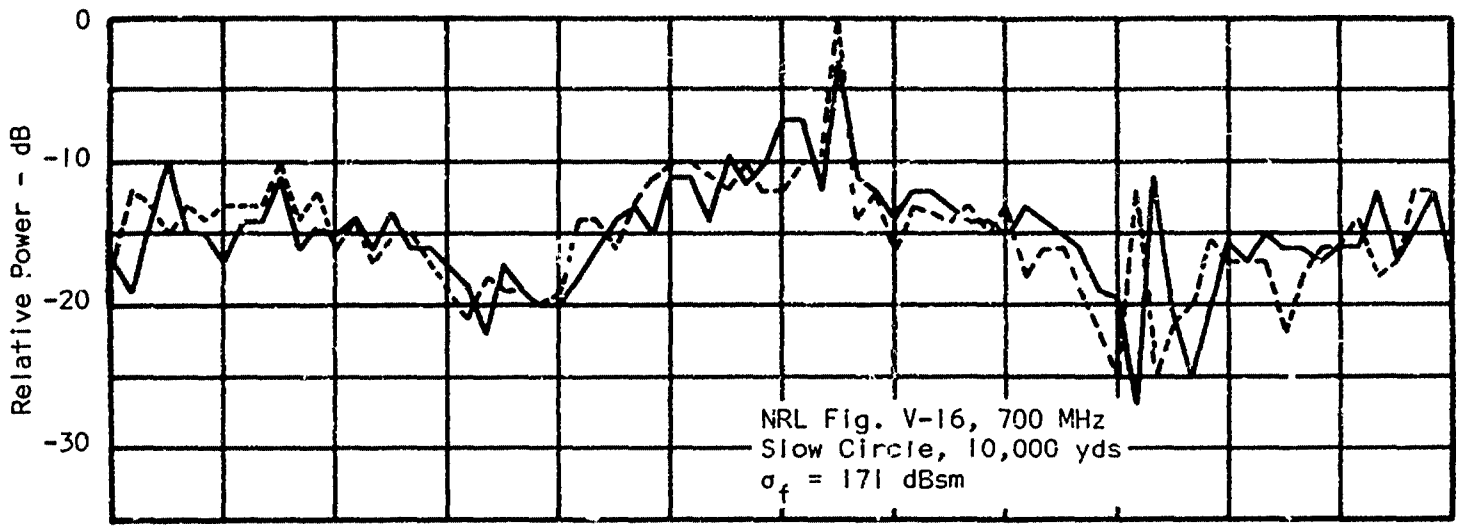
0
-10
-20
-30
Relative Power - dB
NRL Fig. V-16, 700 MHz
Slow Circle, 10,000 yds
σ_f = 171 dBsm

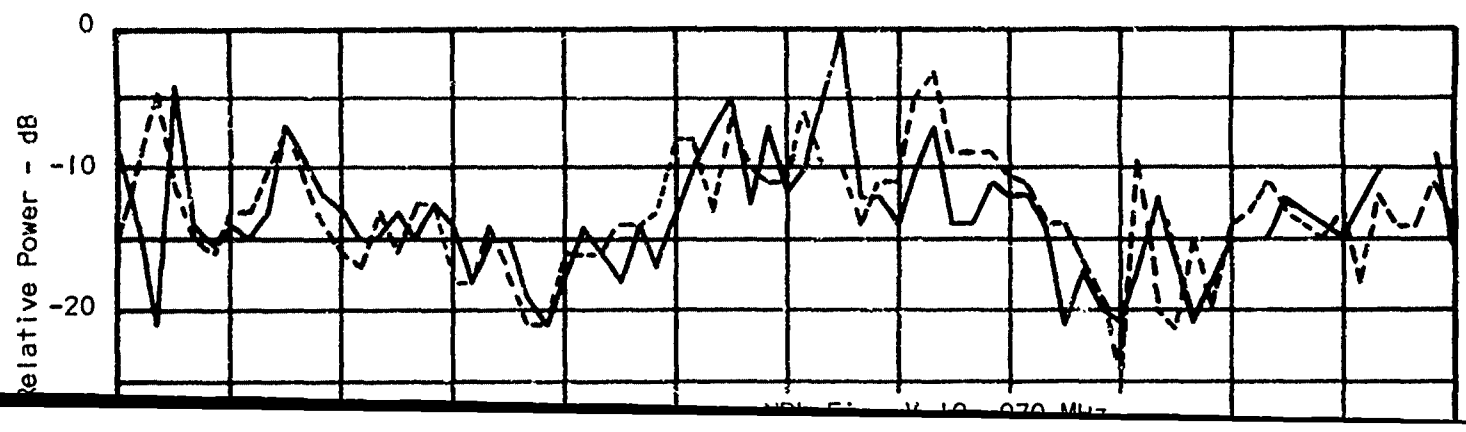
0
-10
-20
Relative Power - dB

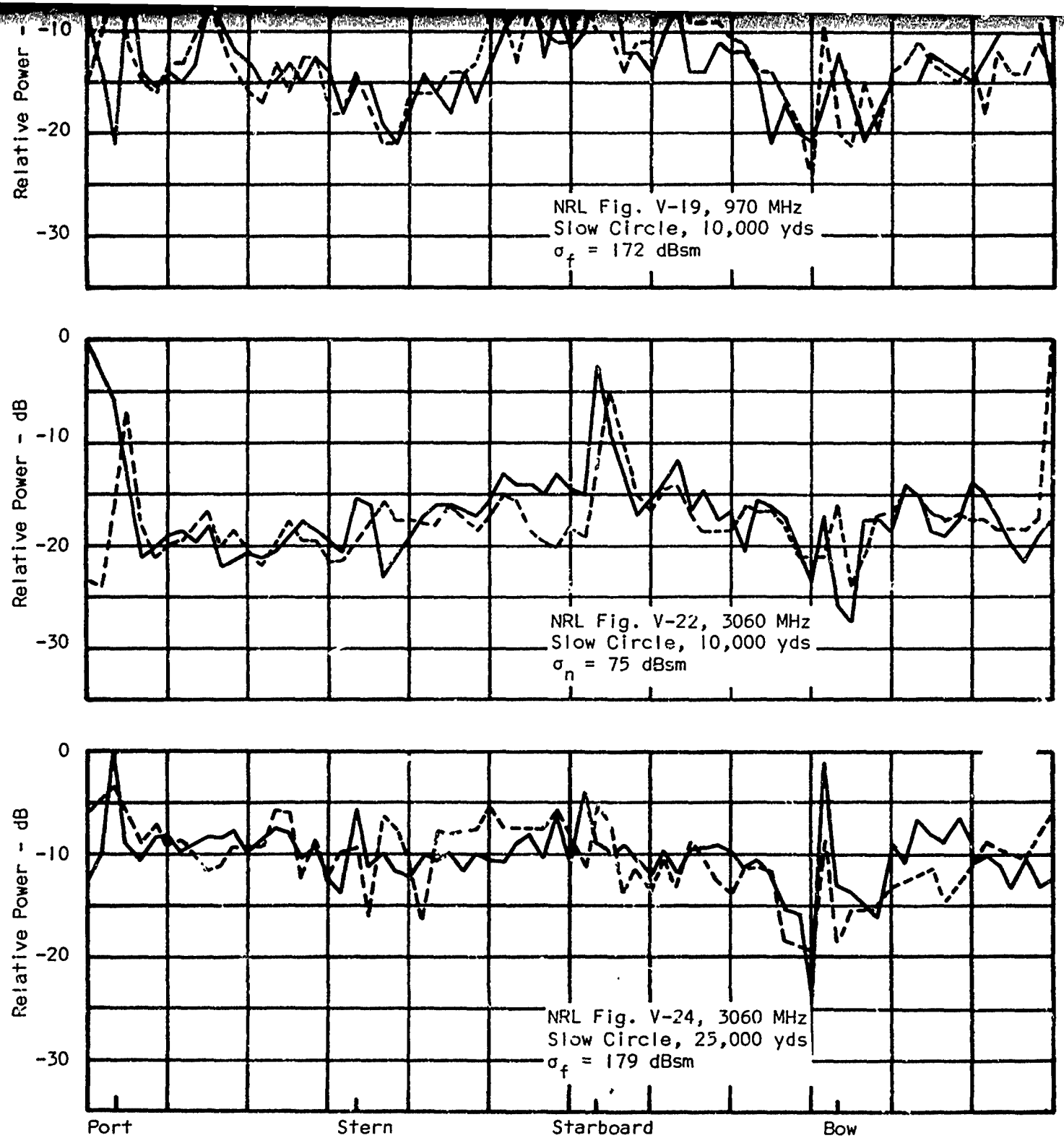

Variations of Return Power for Battleship USS Missouri (BB-63).

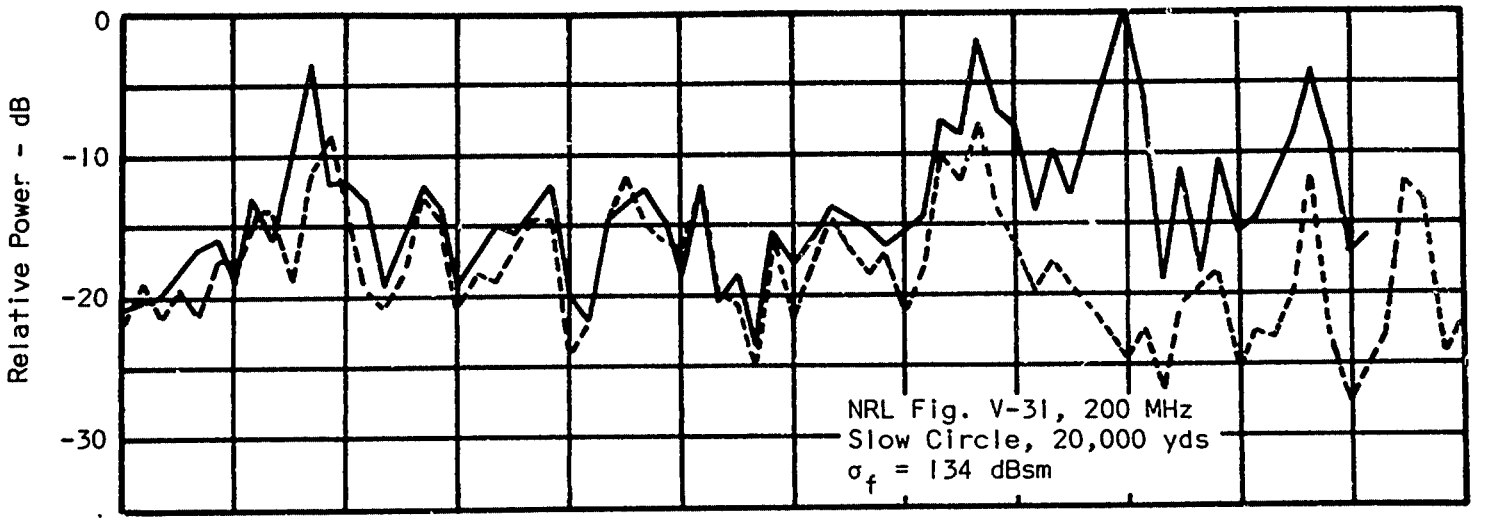
0
-10
-20
-30
Relative Power - dB
NRL Fig. V-31, 200 MHz
Slow Circle, 20,000 yds
σ_f = 134 dBsm

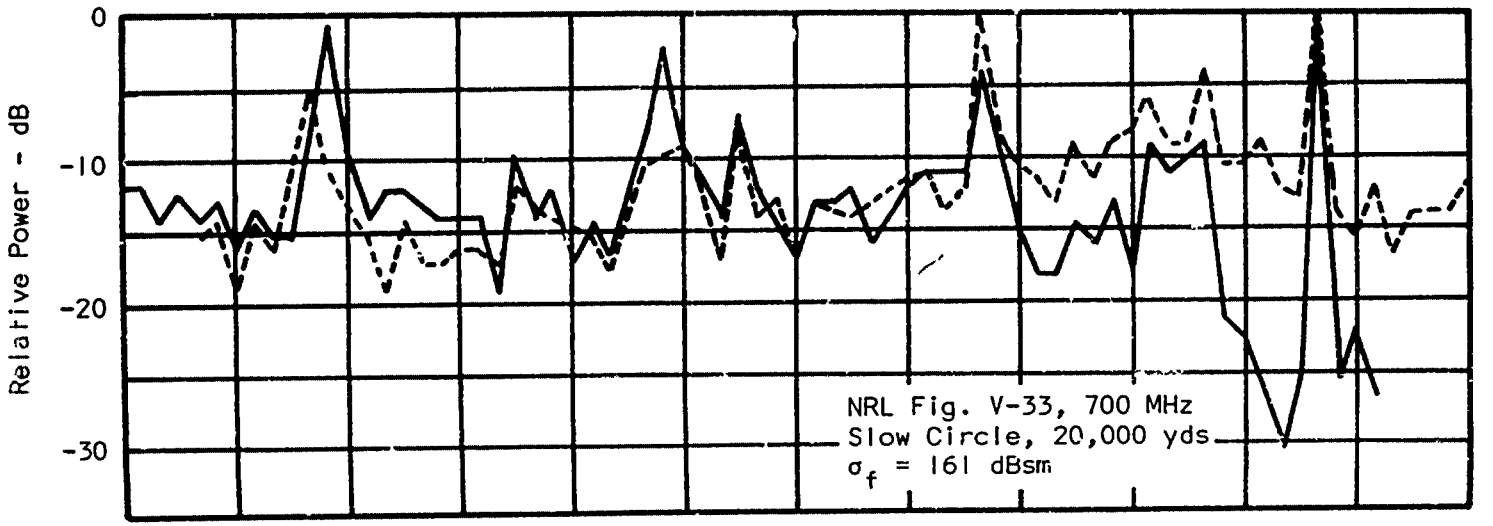
0
-10
-20
-30
Relative Power - dB
NRL Fig. V-33, 700 MHz
Slow Circle, 20,000 yds
σ_f = 161 dBsm


0
-10
-20
lative Power - dB

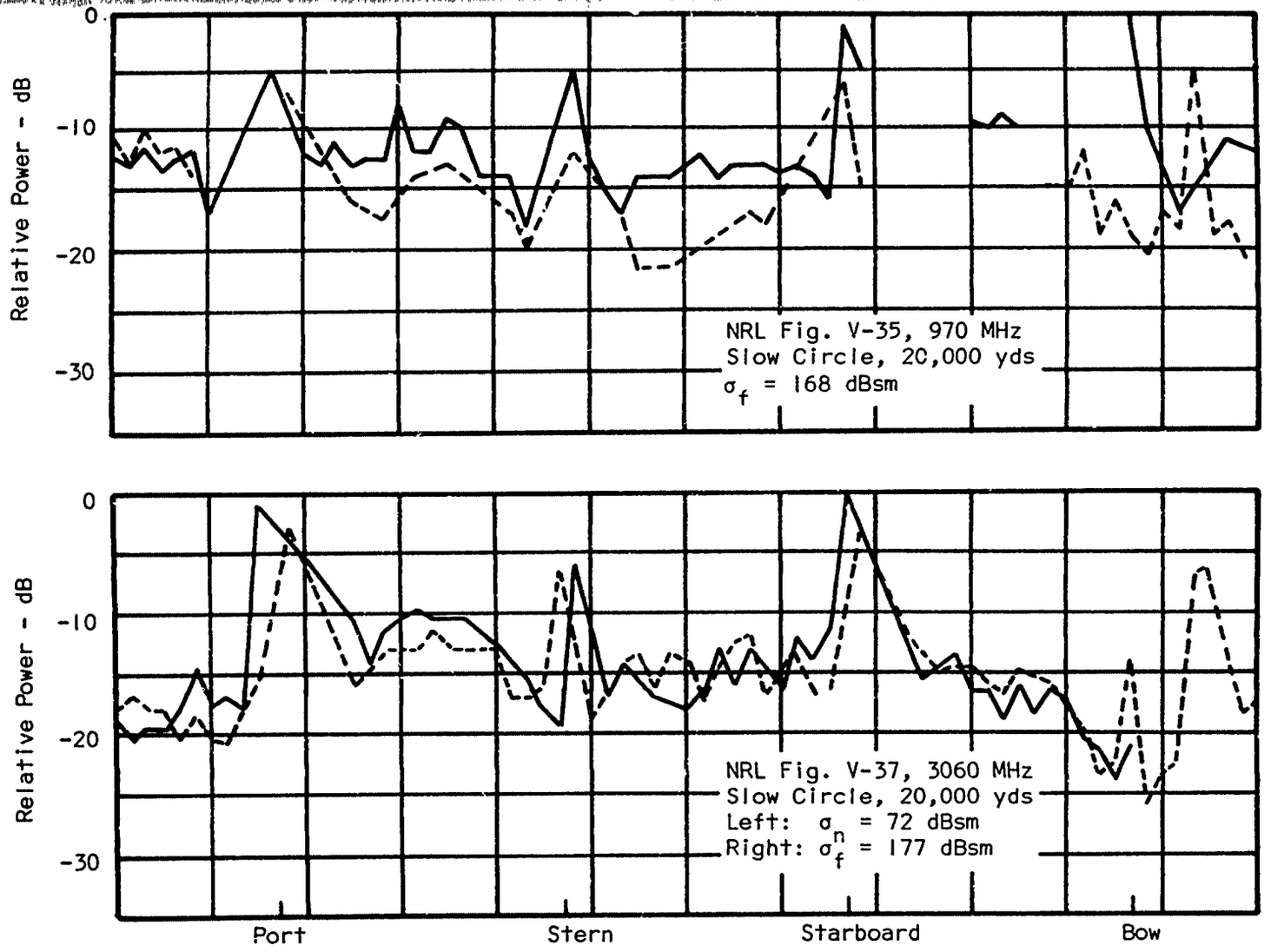

Figure 3. Aspect Variation of Return Power for Escort Carrier USS Croatan (CVE-25).

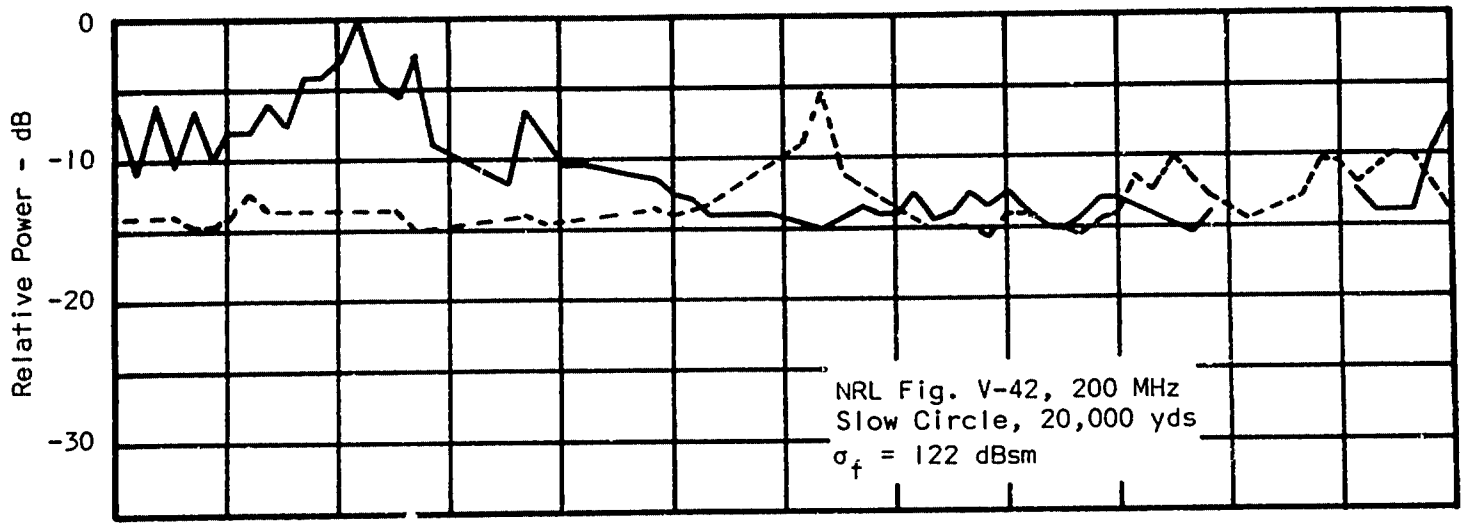
0
-10
-20
-30
Relative Power - dB
NRL Fig. V-42, 200 MHz
Slow Circle, 20,000 yds
σ_f = 122 dBsm

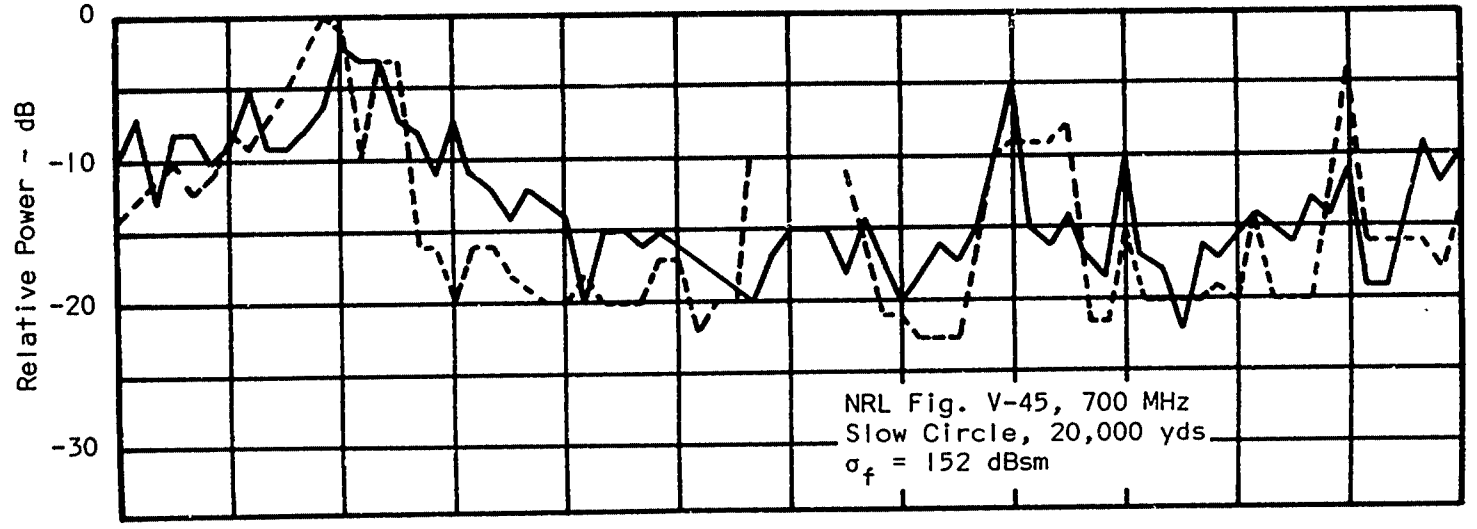
0
-10
-20
-30
Relative Power - dB
NRL Fig. V-45, 700 MHz
Slow Circle, 20,000 yds
σ_f = 152 dBsm

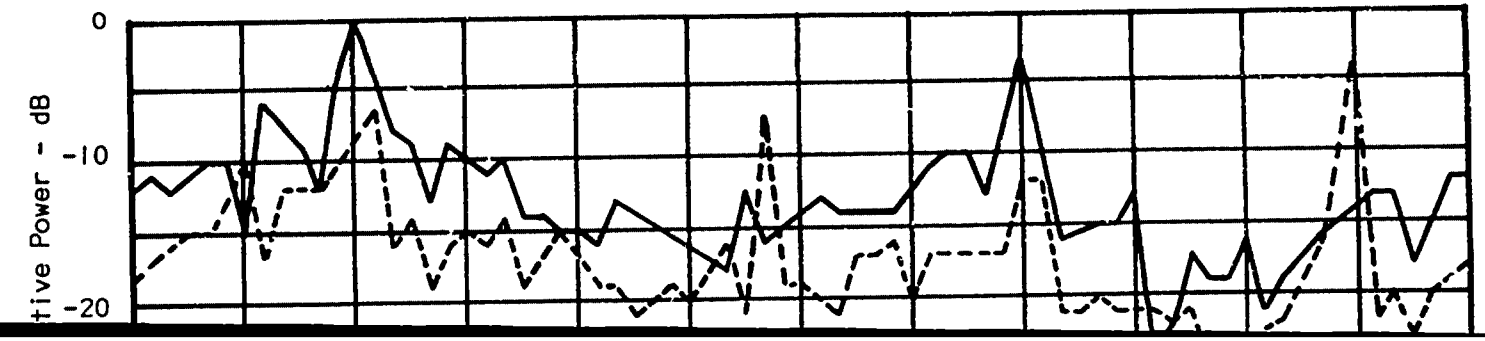
0
-10
-20
tive Power - dB

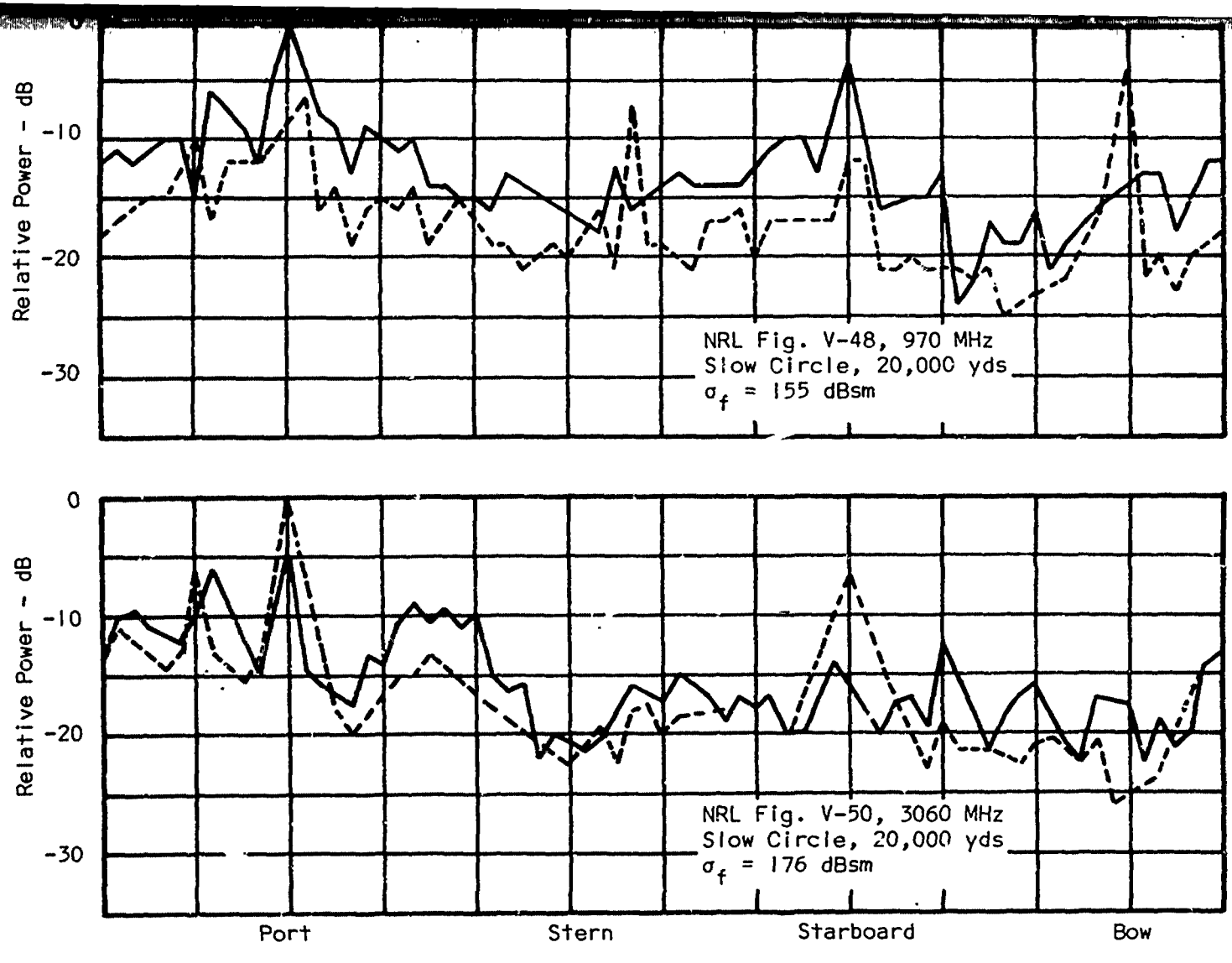

Figure 4. Aspect Variation of Return Power for Destroyer USS Moale (DD-693).

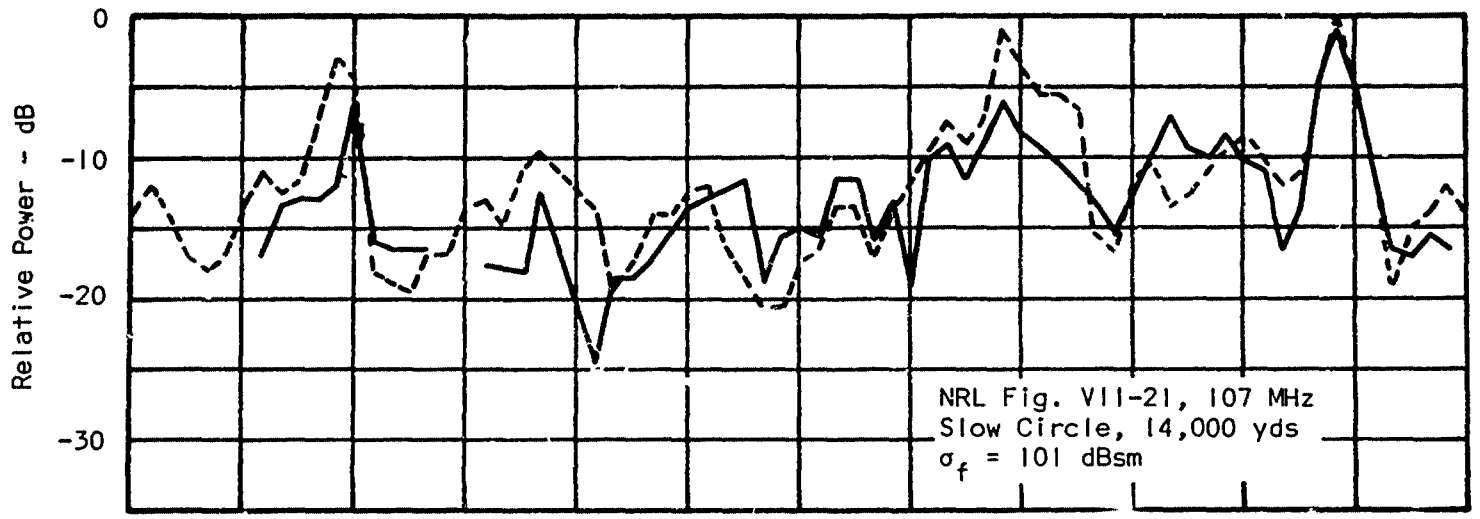
0
-10
-20
-30
Relative Power - dB
NRL Fig. VII-21, 107 MHz
Slow Circle, 14,000 yds
σ_f = 101 dBsm

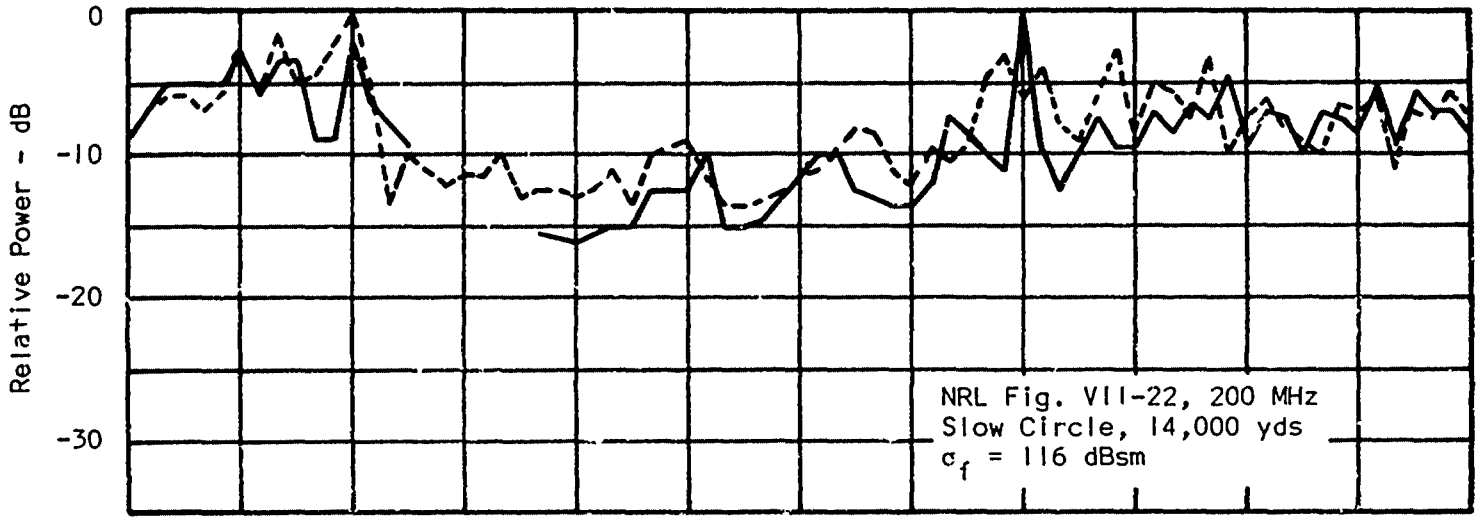
0
-10
-20
-30
Relative Power - dB
NRL Fig. VII-22, 200 MHz
Slow Circle, 14,000 yds
σ_f = 116 dBsm

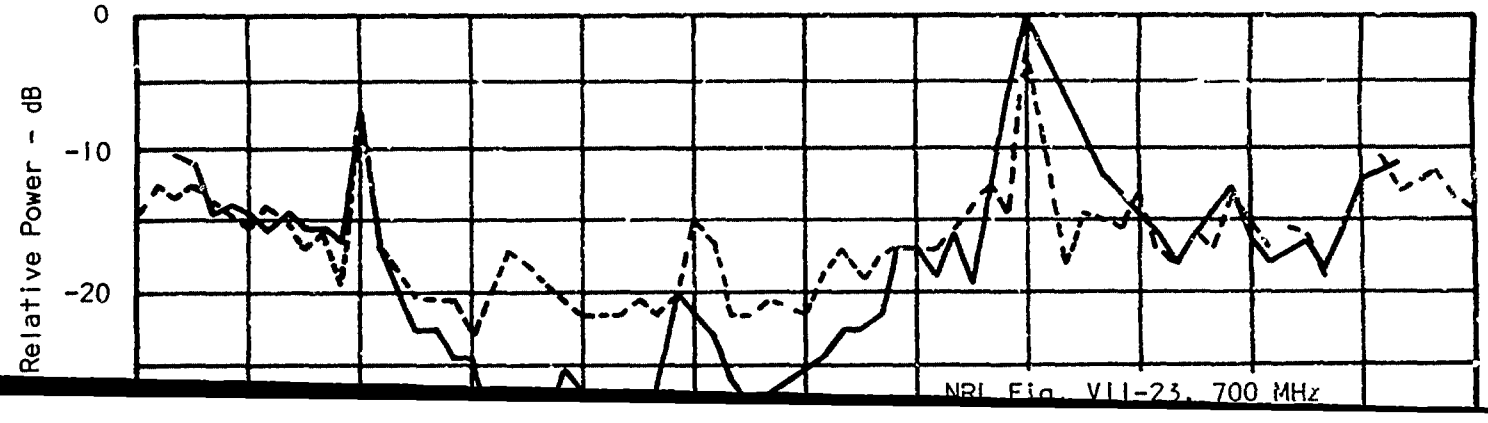
0
-10
-20
Relative Power - dB
NRL Fig. VII-23, 700 MHz

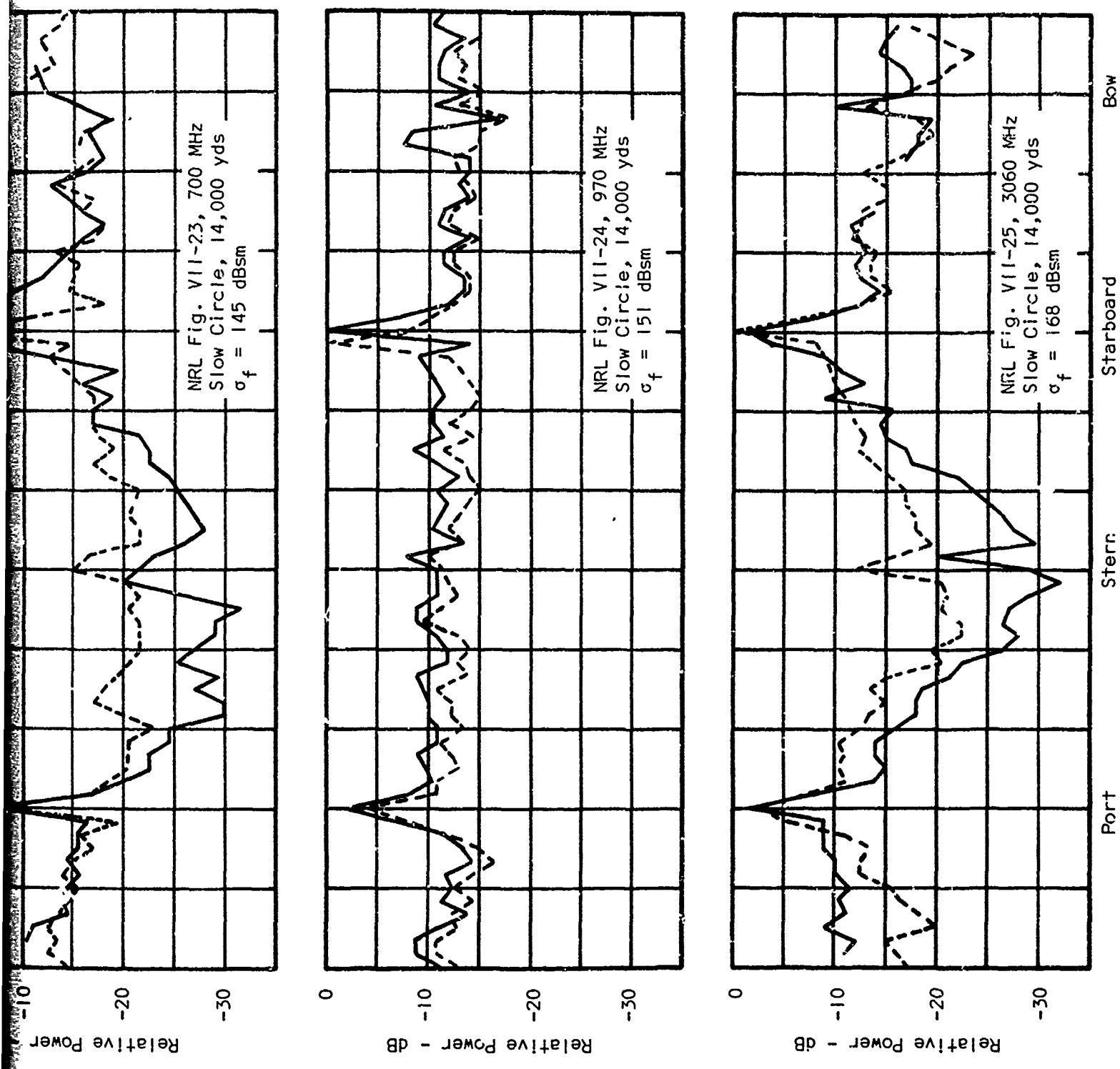

Figure 5. Aspect Variation of Return Power for LST-998.

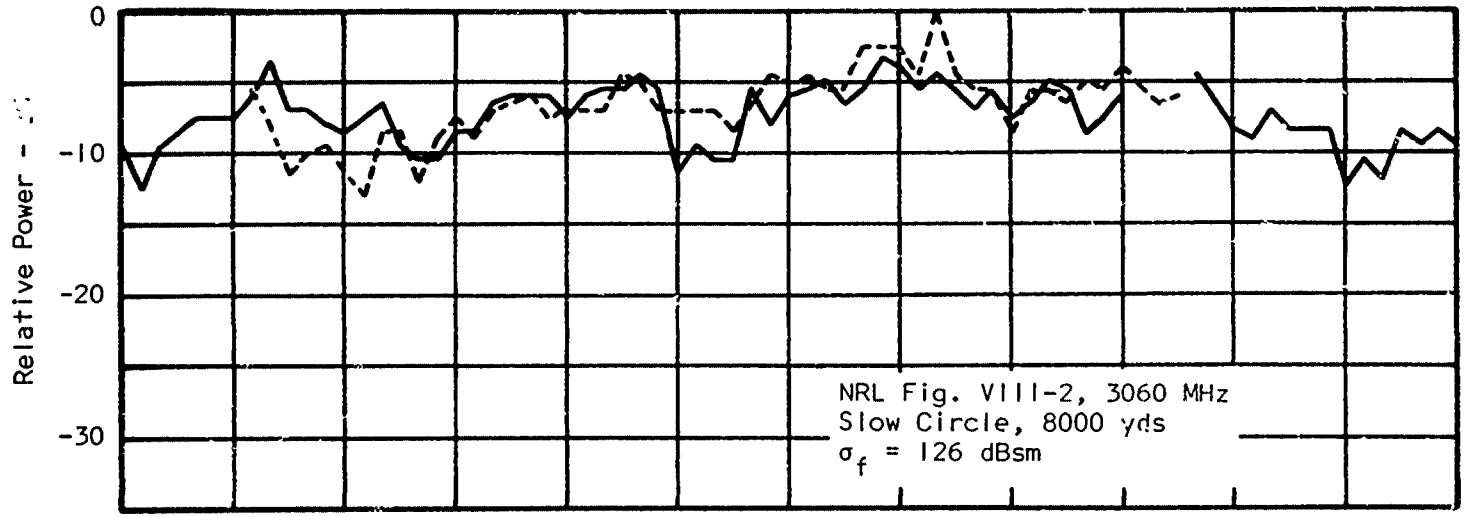
0
-10
-20
-30
Relative Power - dB
NRL Fig. VIII-2, 3060 MHz
Slow Circle, 8000 yds
σ_f = 126 dBsm

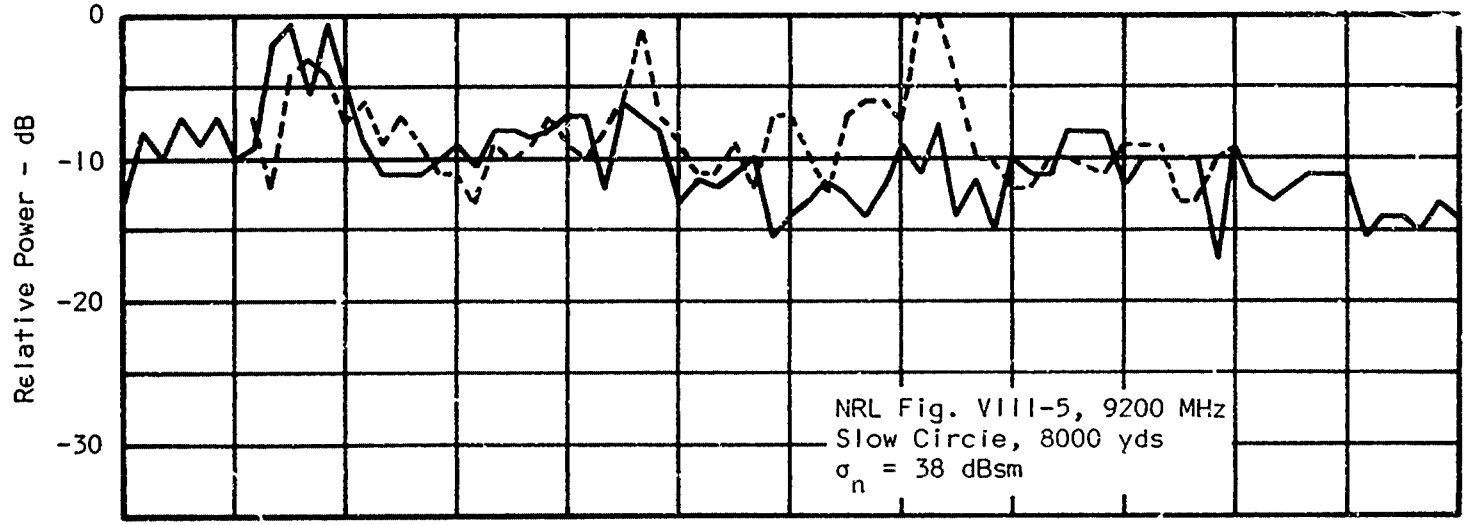
0
-10
-20
-30
Relative Power - dB
NRL Fig. VIII-5, 9200 MHz
Slow Circle, 8000 yds
σ_n = 38 dBsm

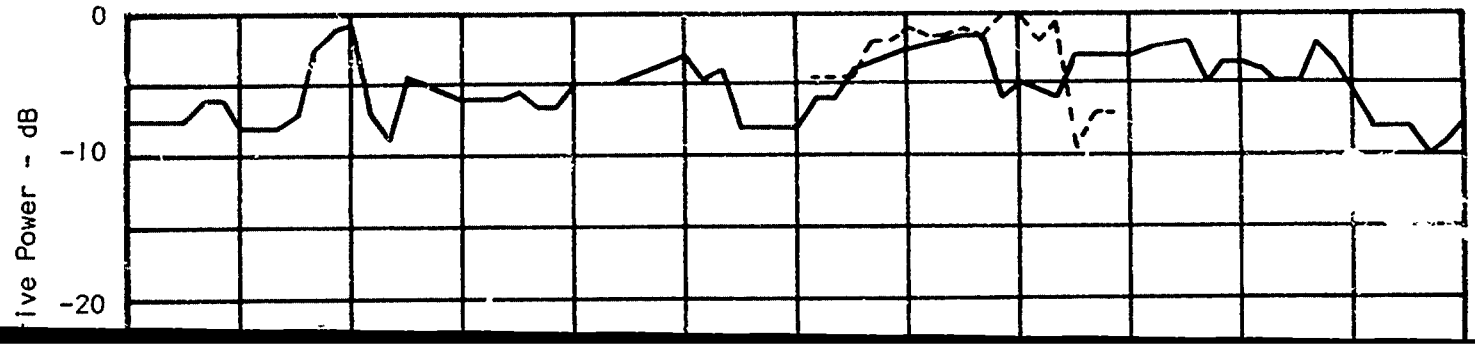
0
-10
-20
ive Power - dB

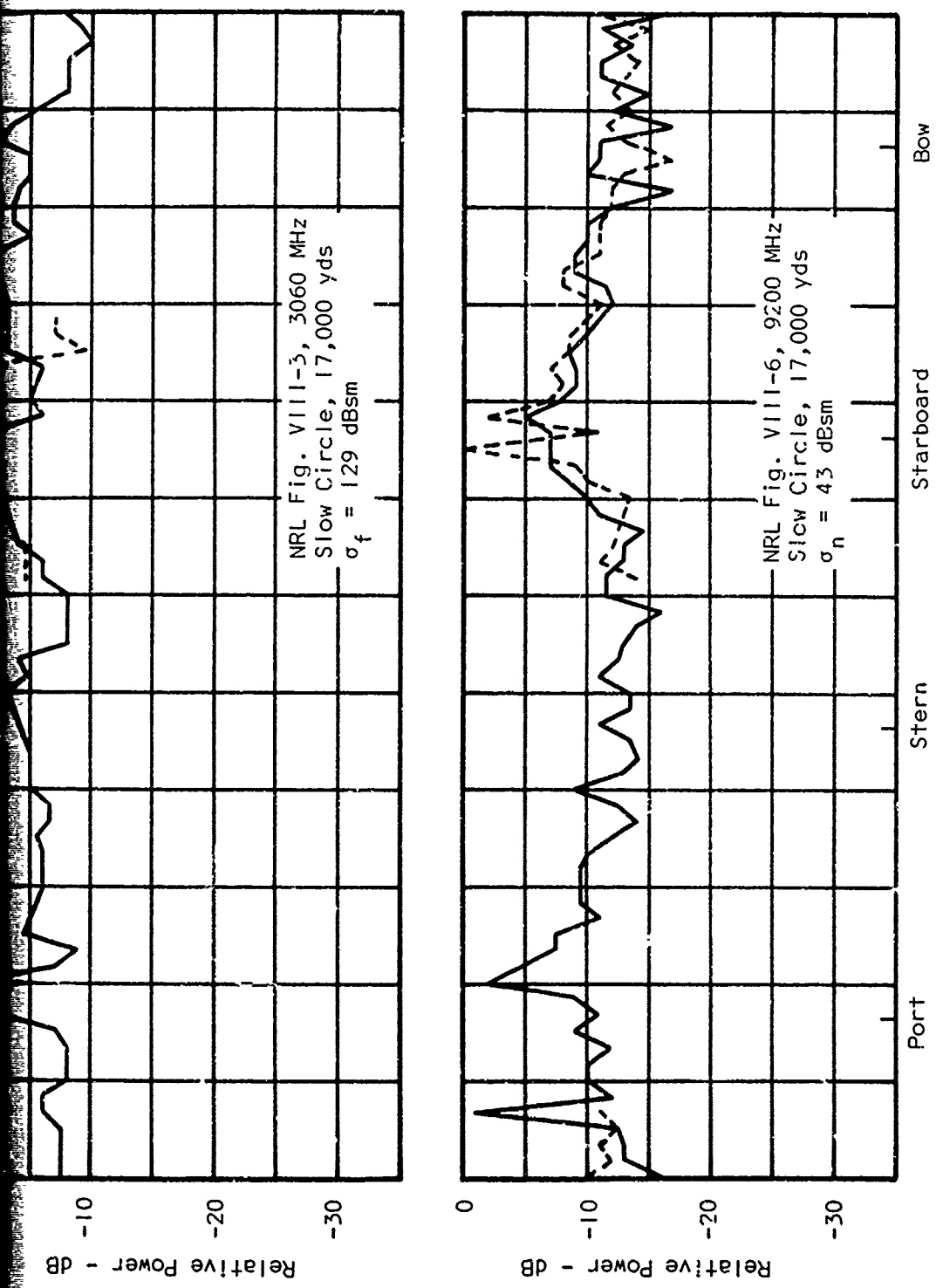

Figure 6. Aspect Variation of Return Power for PT-295.

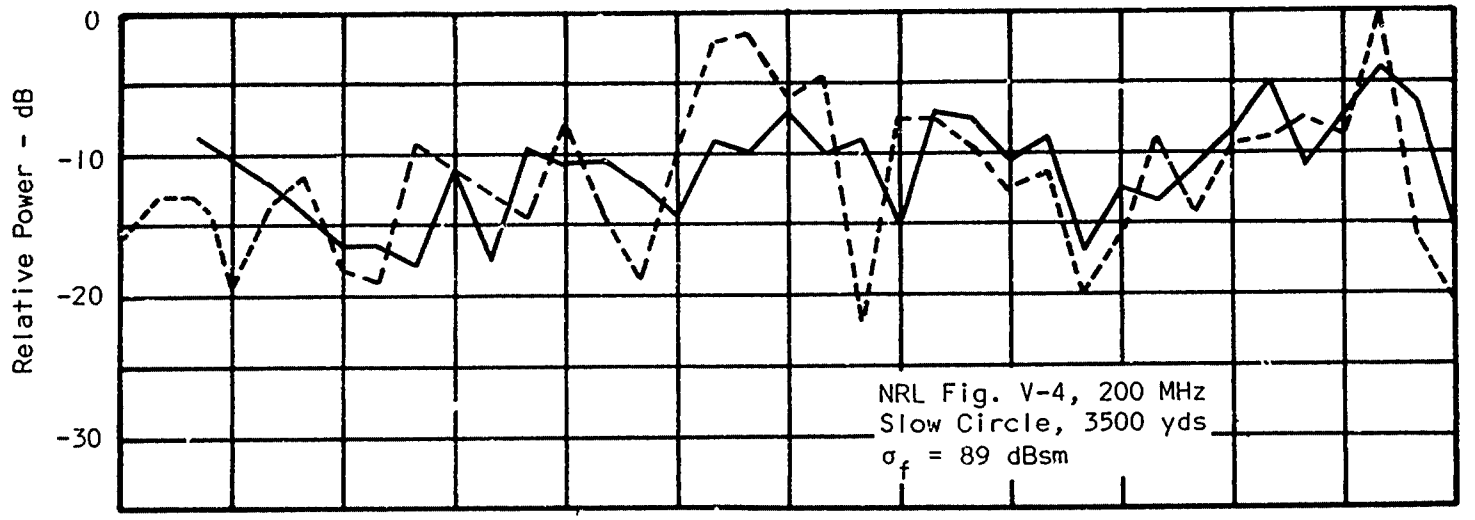
0
-10
-20
-30
Relative Power - dB
NRL Fig. V-4, 200 MHz
Slow Circle, 3500 yds
σ_f = 89 dBsm

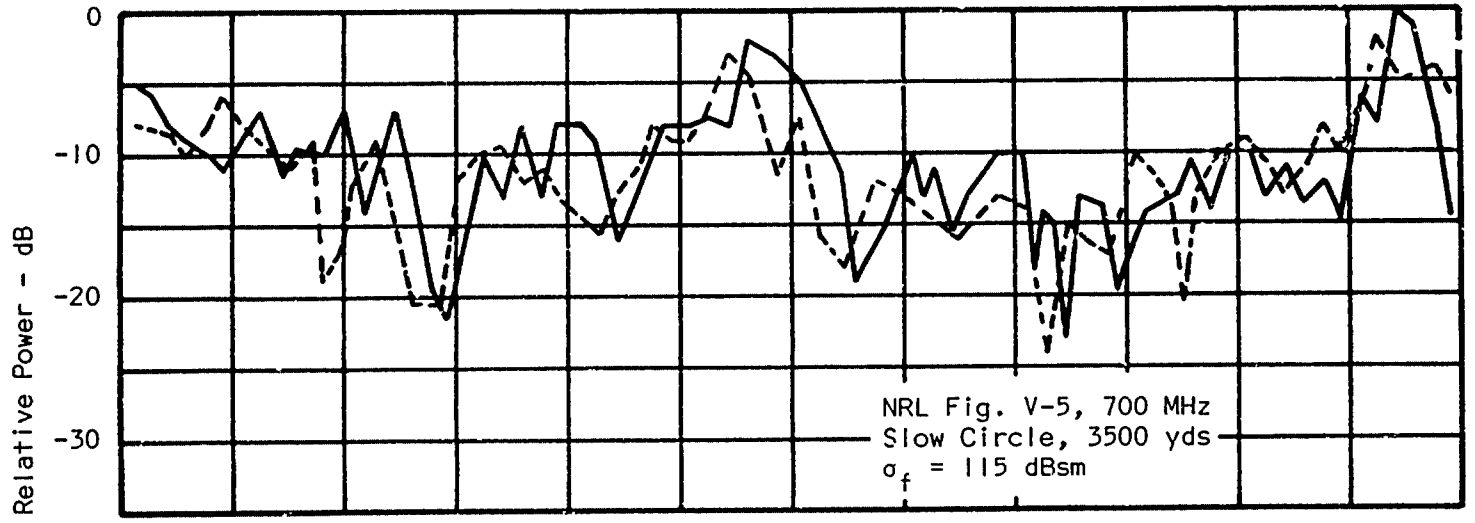
0
-10
-20
-30
Relative Power - dB
NRL Fig. V-5, 700 MHz
Slow Circle, 3500 yds
σ_f = 115 dBsm

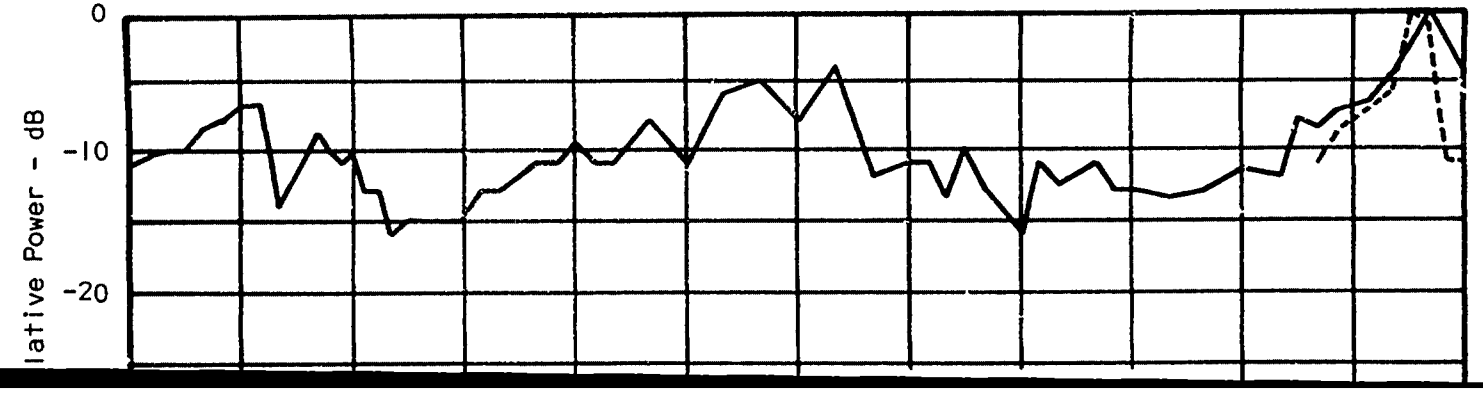
0
-10
-20
lative Power - dB

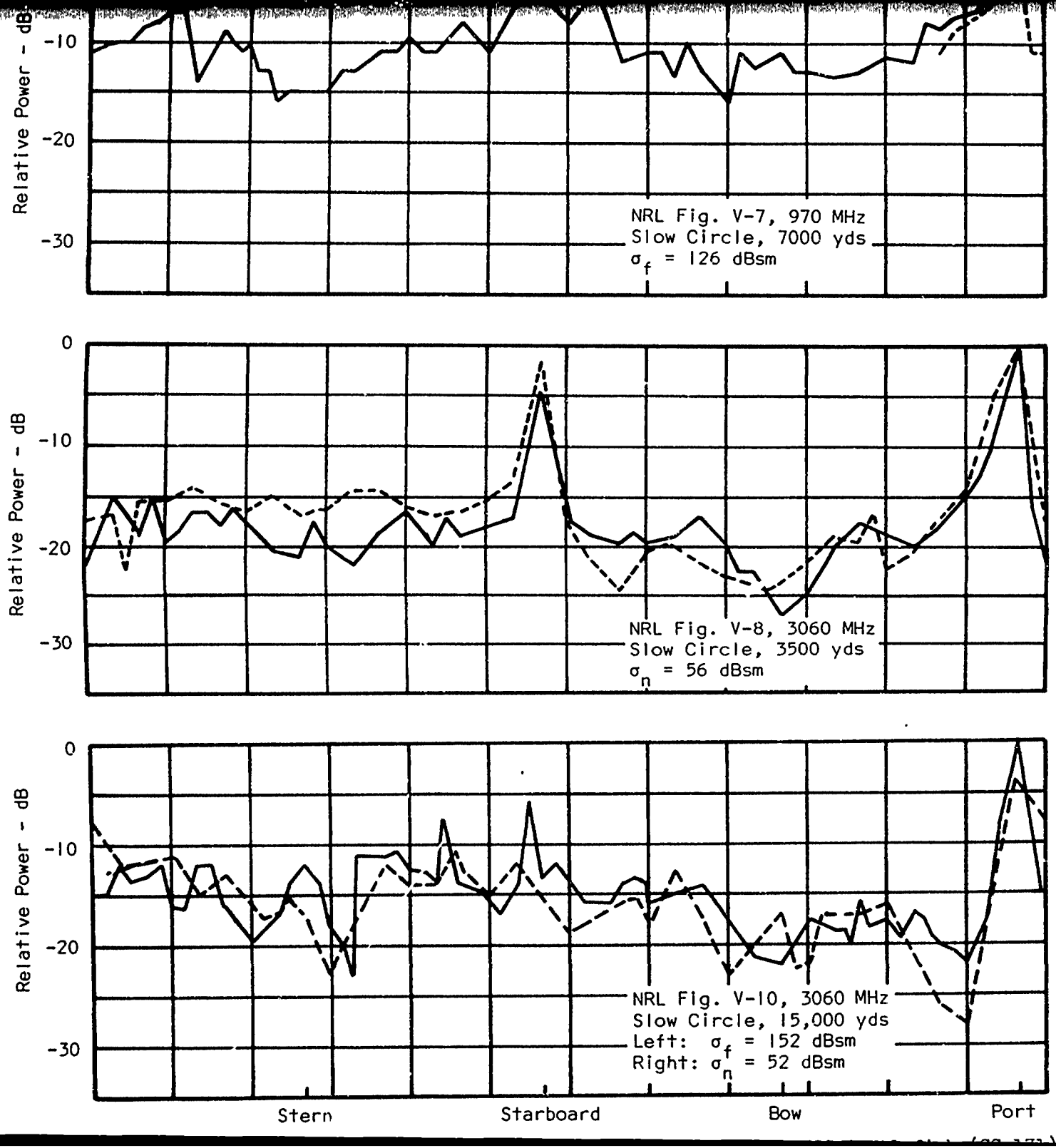
Relative Power - dB
-10
-20
-30
NRL Fig. V-7, 970 MHz
Slow Circle, 7000 yds
σ_f = 126 dBsm
0
-10
-20
-30
NRL Fig. V-8, 3060 MHz
Slow Circle, 3500 yds
σ_n = 56 dBsm
0
-10
-20
-30
NRL Fig. V-10, 3060 MHz
Slow Circle, 15,000 yds
Left: σ_f = 152 dBsm
Right: σ_n = 52 dBsm
Stern
Starboard
Bow
Port

radar was rotated while the ship was at anchor. The effect of return from this antenna upon the overall echo was indistinguishable from the ordinary fading of the ship.

Fig. 3 presents the aspect variation for the escort carrier USS Croatan (CVE-25). The range for these measurements was 20,000 yds, and all radars observed the target in the R^{-8} region except that one broadside peak at 3060 MHz was for the R^{-4} region. This ship produced secondary peaks at bow and stern aspects as well as broadside, attributed to the fact that the ship's SK radar antenna was pointed over the bow throughout the tests. The SK antenna is a flat-screen reflector approximately 17 ft square. Except for these secondary peaks, the variation with aspect is not as great as that observed for some other ships.

Aspect variation of the destroyer USS Moale (DD-693) at a range of 20,000 yds is shown in Fig. 4. For this ship, the lobe of the broadside peak becomes narrower as the frequency is increased. At 700 and 970 MHz the bow showed a secondary peak on one run at each frequency, but this effect was not strong on the other run. Fig. 5 presents data for the LST-998 at a nominal range of 14,000 yds. (The slow circle executed for these tests gave ranges of 12,900 to 15,700 yds, and the data were adjusted to compensate for this unusually large range variation.) All data are for the R^{-8} region and show peaks associated with broadside aspects. Although the form of variation in return differs for the five frequencies used, there is no evident pattern of behavior associated with frequency alone. That is, neither the widths of the broadside lobes nor the difference between maximum and minimum return seems directly associated with frequency change.

Fig. 6 shows the aspect variation for the PT-295 at frequencies of 3060 and 9200 MHz for slow circles at ranges of 8000 and 17,000 yds. The boat was in the R^{-8} region at 3060 MHz and in the R^{-4} region for 9200 MHz. There is very little aspect variation at 3060 MHz and only slightly more at 9200 MHz. Numerical values of cross-section are not greatly different for the two ranges.

The surfaced submarine USS Cuttlefish (SS-171) gave aspect variations in return as shown in Fig. 7. The top four plots show variations for four different frequencies; the range was 3500 yds except for the 970 MHz data which was taken at 7000 yds. The plot for 3060 MHz is for data in the R^{-4} region and shows an appreciably larger difference between broadside and non-broadside

aspects than do the other plots. In the bottom plot, the submarine was at 15,000 yds, which is near the transition point between R^{-4} and R^{-8} regions. The left side of this plot shows σ_f and the right side σ_n. It may be noted that the broadside peak return is larger in the R^{-4} region and the numerical cross-section value corresponds approximately to that given for measurements at 3500 yds.

2-4. Periscope Observations

Reference 15 describes observations of a periscope with exposed heights of 2 and 4 ft as observed by S- and X-band radars at two antenna heights, 11.4 and 50 ft. The target was in the R^{-8} region for these tests, and variation of return power with range was predicted according to a result in a study by Freehafer [16] (equivalent to Equation (82) in Section 6-5 of Kerr) using measured system characteristics of the radars. Data points which are the maximum returns in 15-second intervals show extremely close correspondence to the predicted curves. In particular, measured and calculated maximum ranges (to minimum detectable signal in noise) agree very well. Data were taken for ranges of about 2500 to 5000 yds with an antenna height of 11.4 ft, and from about 4000 to 10,000 yds with an antenna height of 50 ft.

For these results, the value of free-space cross-section is taken to be the normal-incidence cross-section of a cylinder of radius r and height h,

$$\sigma_o = 2\pi r h^2/\lambda \ .$$

By using data given in Reference 15, it was possible to determine that for the stated length of 4 ft, the S-band free-space cross-section σ_o was 2.7 m^2, and the X-band cross-section was 8.1 m^2. This leads to a calculated periscope diameter of approximately 2-1/8 inches.

The spread of points shown for the 4-ft observations is extremely low and all points fall within a few dB of the predicted R^{-8} line. Plots are not shown for the 2-ft length, but the variation is stated to have been large. It is indicated that the S-band observations fluctuated so much that they were unreliable. A possible explanation for this is that the cross-section of a vertical cylinder in the R^{-8} region theoretically will vary as h^6, so that a change of a few inches in exposed height will have a much more pronounced effect for a nominal exposure of 2 ft than it will for one of 4 ft.

III. AIRBORNE CROSS-SECTION MEASUREMENTS ON SHIPS AND SUBMARINES

Much of the calibrated cross-section data measured from airborne platforms has been obtained in recent years by the Naval Research Laboratory. Results of three of their programs are discussed below.

3-1. NRL 1962 Data

One of the most frequently quoted sets of airborne data on radar reflectivity of ships is that reported by NRL in 1962 [17]. The airborne X-band radar which was used had a pulse length of 0.3 μsec, a horizontal beamwidth of 5°, and a prf of 1000 pps. Vertical polarization was transmitted, and both vertically and horizontally polarized returns (i.e., VV and VH) were recorded on tape for later processing. System calibration was accomplished using 6-inch spheres dropped from the aircraft.

A loaded tanker was observed on one day, and a Navy radar picket ship (YAGR) of length 441 ft and width 57 ft was observed on another day. On some runs the antenna was manually pointed to track the target, while on others the depression angle of the antenna was fixed and the system measured sea return until the aircraft flew directly over the target so that the received echo then came from sea plus target. Because the illuminated area of the radar did not cover the entire ship for depression angles greater than 25°, a correction was made to the cross-section data, amounting to +3.6 dB at 45° and +6.7 dB at 90° for an aircraft altitude of 1280 ft. Table II reproduces data from Reference 17 and includes this correction which apparently assumes that the ship has uniform cross-section per unit area. This is not strictly the case, particularly for short radar wavelengths (see, for example, Fig. 16 in Section 7-4).

Data plots for the tracking runs in the original report showed received power in dBm vs. elevation angle, plus a calibration line. Received power vs. time was given for the fixed-angle runs. In order to make the plots easier to interpret, original data were obtained from NRL by the Applied Physics Laboratory (APL) and plots were made of cross-section vs. depression angle [18]. More plots are given by APL than were included in the NRL report, but no mention is made of corrections to the data such as that discussed above.

Four tracking runs were made on the tanker at broadside aspect, and Fig. 8 shows results from the APL report. Although it may be noted that the values

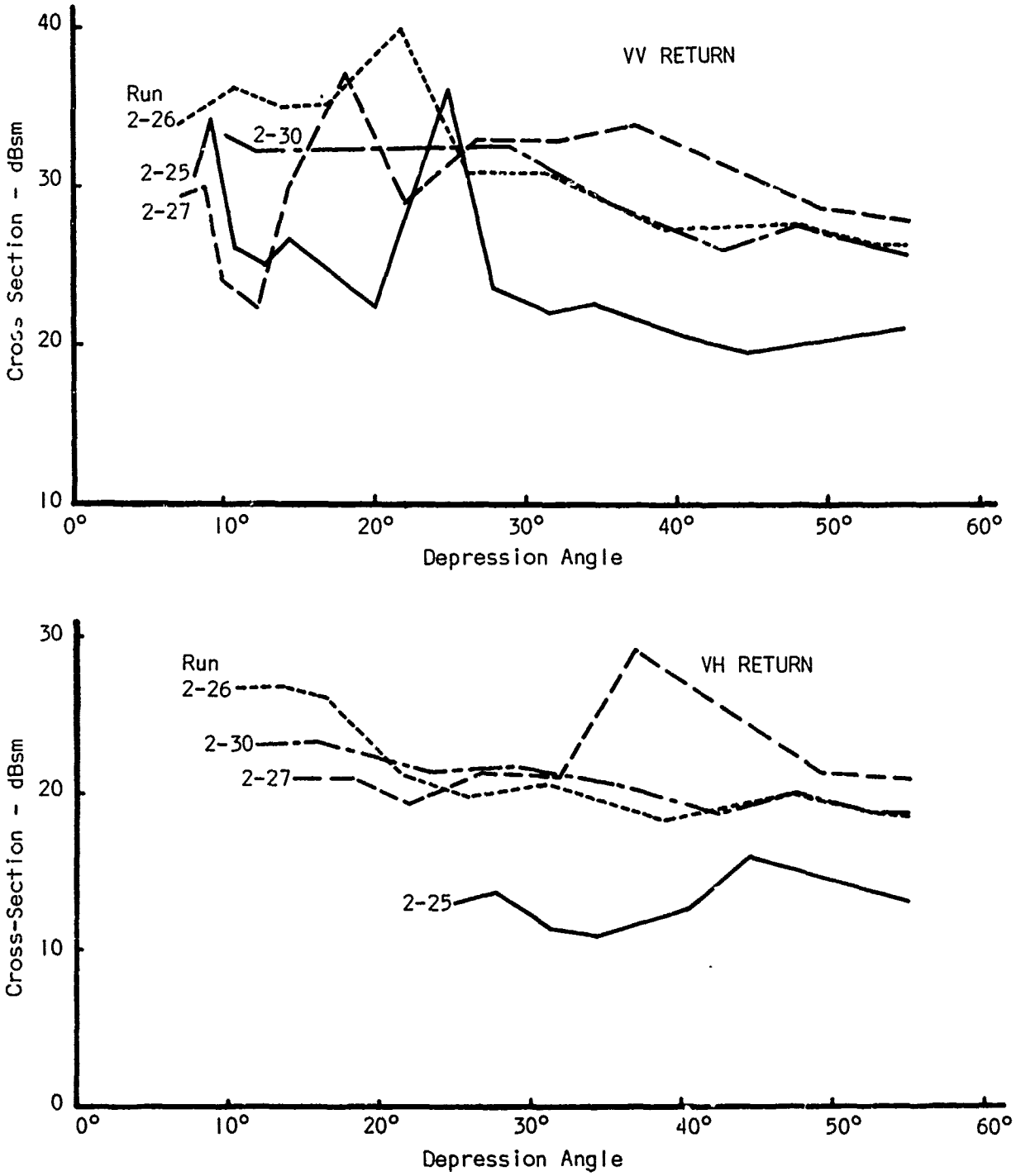

Figure 8. Median X-Band Cross-Sections (Direct-and Cross-Polarized) for Tanker at Broadside.

in Table II and Fig. 8 do not exactly agree, the main difference may be due to the correction mentioned above, although calibration differences may also exist between the two reductions of data.

Table II

Median Radar Cross-Sections (dBsm) for Tanker and Picket Ship at Four Depression Angles*

Run	Aspect	Depression Angle 5° VV	5° VH	10° VV	10° VH	20° VV	20° VH	45° VV	45° VH
Tanker:									
2-25	Beam	-	-	28	-	22	13	24	14
2-26	"	-	-	35	26	34	23	33	23
2-27	"	-	-	30	-	30	20	32	24
2-30	"	-	-	34	22	33	22	37	23
Picket Ship (YAGR):									
3-4	Bow	-	-	-	-	23	-5	18	2
3-6	"	-	-	25	3	19	1	14	-3
3-10	"	-	-	25	7	20	-4	19	4
3-33	Stbd. Bow	-	-	35	14	30	9	26	6
3-11	Beam	-	-	29	9	29	6	31	9
3-25	Stbd. Qtr.	34	-	30	7	25	4	34	8
3-27	" "	35	-	30	8	28	3	28	4
3-3	Stern	-	-	26	6	16	-5	18	-6
3-5	"	35	-	23	6	23	-6	18	-4
3-7	"	31	-	25	6	16	1	16	-7
3-24	Port Qtr.	35	-	27	9	22	3	17	5
3-32	20° Fwd. Port Beam	32	-	35	14	35	12	34	14
3-26	Port Bow	30	-	27	7	22	2	24	-4

*See text for explanation of possible + 13 dB correction to these values.

The curves of median cross-section vs. depression angle are seen to differ from run to run. As discussed in many other places in this report, this appreciable spread in results, even when highly smoothed data are being compared, is characteristic of ship cross-section measurements. This arises partly because of the inherent difficulty in replicating runs (aspect, sea conditions, system calibration, etc.), and partly because of the non-stationary nature of the process that is being measured.

Fig. 8 and Table II show that the cross-polarized return was typically down about 10 dB for the tanker and about 20 dB for the picket ship, which had the more complicated superstructure. For depression angles less than 55°, the target was detected in clutter with both VV and VH. At 90°, the target could be detected in the clutter only on VH; it is estimated that the increase in contrast with VH was about 10-15 dB over that with VV.

The Aerospace Corporation has made a particularly careful examination of the data in this NRL report, as well as additional data not given there [19]. They suggest that the cross-section values may be biased rather strongly toward the low side, and recommend an increase of 13 dB in the reported values. This total results from a +8 db correction if the sphere calibration is accepted as correct (Figure 3 of Reference 17), and a +5 dB correction due to the presence of multiplicative noise which affects the quantization calibration of the receiver. While this adjustment in the values of Table II and Fig. 8 (as well as others in References 17 and 18) cannot be made with absolute certainty, it would at least tend to place the cross-section values closer to those of other studies.

3-2. NRL 1965 Data

In July 1965, the NRL airborne four-frequency radar system was used off the coast of Puerto Rico to collect cross-section data, primarily on sea clutter but also on a ship [20, 21]. The radars operate coherently at P-, L-, C-, and X-bands, transmit with horizontal and vertical polarization alternately, and receive both, using one frequency or all four in rapid succession. Data were taken during runs of two types: with the antenna fixed in elevation angle and a pulse length of 0.25 μsec, or with the antenna tracking in elevation angle and a pulse length of 1.0 μsec. A 50-nsec range gate was used, and the peak return in the gate was digitized and recorded on magnetic tape.

The target ship for these tests was the Peacock, a converted wooden minesweeper of the Bluebird class having dimensions of 144 by 28 ft. A large metal rack extended 20-25 ft from the bow to hold camera equipment and probably contributed substantially to the return when the bow was illuminated. System calibration was obtained using 8-inch spheres dropped from the WV-2 radar aircraft. Pulse-to-pulse data were fed into a computer and cumulative distributions were determined for 1000-pulse samples (about 1.3 seconds at the prf of 778 pps). Median (50%), 10%, and 90% cross-section values are presented for various runs.

In the preliminary report [20], eight figures from one tracking run (25° off stern for C- and X-bands, and 25° off bow for P- and L-bands) present cross-sections for the ship and for the sea over the approximate elevation-angle range of 1.3° to 19° for VV and HH polarizations at all four frequencies. The ship shows considerable fluctuation in cross-section as the angle (time) changes, the return tending to decrease about 20 dB as elevation angle increases

from 1.3° to about 9° at C- and X-bands. At P- and L-bands the decrease is only about 5 dB, possibly since the lower frequencies were for an aspect which illuminated the metal bow structure more. Near grazing incidence (1.3° to 1.5°), typical median values are about 19 dBsm at C- and X-bands for 25° off stern, and about the same at P- and L-bands for 25° off bow. There does not appear to be a strong polarization dependence in the direct return, although the character of the curves differs somewhat for HH and VV at the same frequency. Median cross-polarized return is erratic, but is generally about 10 dB lower than direct. Tabulated figures for bow and beam runs show very little change in cross-section with elevation angles of 1° to 10°. Results from fixed-angle runs suggest that for some aspects the cross-section may first decrease with increasing elevation and then increase at an angle somewhere around 20°; however, the data are too sparse to make this a firm conclusion.

3-3. NRL 1966 Data

Additional data were taken with the four-frequency radar during May and June 1966. Targets included large and small cargo ships, small fishing trawlers, and a surfaced submarine. A preliminary report [22] contains some data on a cargo ship of dimensions 278 by 44 ft, and the submarine, which was 306 by 27-1/2 ft. For the flight pattern used, observations were for elevation angles of 16-22° and aspects from near stern-on through broadside to near bow-on. Median broadside cross-section for the ship was at least 60 dBsm (the system saturated), with other aspects nearer the bow and stern showing median cross-sections in the approximate range 20-30 dBsm. The submarine was viewed at elevations angles of 10-15° and showed much less of a broadside peak than did the ship. Median cross-section was about 23 dBsm at broadside, with aspects nearer bow and stern showing wide variations but mostly being in the range 10-20 dBsm.

(This page intentionally left blank.)

IV. OBSERVATIONS OF OTHER TARGETS

4-1. Wakes

The wake produced by a vessel moving through the water may be detectable by radar either as increased return from the rough surface of the disturbance itself, or as decreased return from a smoothed area in a region of clutter. The detection of wakes will be affected primarily by the same factors which affect the detection of small targets or sea return: wavelength, polarization, antenna height, resolution, etc.

In 1944, the MIT Radiation Laboratory developed a K-band (1.25-cm) radar which had an azimuth beamwidth of 0.8° and a pulse length of 0.15 μsec. A report on this system [23] shows PPI displays of various harbor areas which include ships, buoys, a submarine net, etc. In one case, a large V-wake is clearly seen behind a destroyer at a range of about 3/4 mile. Transverse striations in the wake which the appearance of a well-defined wave structure are not explained in this report, whose only text outlines equipment characteristics.

Coherent X-band Doppler spectra of snorkel wakes were obtained by the University of Illinois in studies on snorkel detection in clutter [24] (see also Section 6-3.3). The wake echo was found to be spread in frequency much like the sea clutter, having an average spread at half power of 80 to 90 cps (2-1/2 to 3 knots). It showed on the average a mean displacement from the sea clutter of about 2-1/2 to 3 knots, usually being shifted with respect to the sea clutter in the same direction as the direct echo from the snorkel.

For the underwater-exhaust type of snorkel, about 60% of the total echo power was in the snorkel echo, and about 40% in the wake echo. Presence or absence of the search periscope appeared to make no difference in the division of power or in the total power. For the overwater-exhaust snorkel, about 95% of the total echo power was in the direct echo, and only about 5% in the wake echo. Some inconclusive evidence was noted that the search periscope added considerable power in this case. Six detections of an attack periscope showed an average of 40% power in the direct echo, 60% in the wake echo. In only two detections did the direct echo exceed the wake echo in power.

In the case of a non-coherent radar, the fluctuating return from the wake, bow wave, hull turbulence, or other water disturbance would be added in with any target return in the same radar cell of resolution (see, for example, Fig. 16). The general effects would be to add to the overall cross-section and to

increase the rate of fluctuation of return, the degree of these effects depending on the relative magnitudes of target and wake returns.

4.2. Buoys

Quite a variety of radar-reflecting sea buoys are in general use, but nearly all are based on some combination of dihedral or trihedral reflectors. According to a survey made by Trinity House [25], by far the majority in use or being experimented with involve some combination of trihedrals, frequently in clusters or other groupings. Dihedral reflectors are not infrequently included also. Of those described, most in actual use have an approximate cross-section for a single reflector ranging from 50 to a few hundred square meters, but a few are described as significantly higher. Reflectivity optimization must of course be modified by practical considerations of design and the desire to furnish a suitable daymark as well as radar appearance. A trihedral cluster mounted on top of a buoy may be subject to damage when laying or lifting the buoy. The dihedral-trihedral reflector, while not so efficient a reflector as normally designed, is easier to construct and can easily be built into the superstructure of a buoy.

The simple dihedral reflector with common axis vertical has a very narrow beamwidth in the vertical plane which is undesirable for use in a seamark, where it is subject to tilting which can greatly reduce the effective cross-section. (Dihedrals are quite satisfactory, however, for stationary land markers, provided they are accurately mounted.) If the trihedral reflector with triangular plates is mounted with base horizontal, the other plates give dihedral reflection in the horizontal plane that is 1-1/2 times the on-axis trihedral cross-section, but is subject to the disadvantage of the narrow vertical beamwidth of the simple dihedral. When such a mounting is tilted, there is a gap of about 10° between the dihedral polar diagram and that of the trihedral reflection, so this mounting gives rather erratic echo area. When tilted with the axis horizontal, the trihedral reflector gives a very broad vertical beamwidth (about 45°) which is desirable for seamark mounting. Probably the best results are obtained with a combination of trihedral reflectors mounted horizontally or vertically in a fashion so as to approximately level out the maxima and minima of coverage. Interference lobes and other propagation effects must be considered in predicting maximum detection range on a buoy [26].

Several buoy types with dihedral or trihedral reflectors were studied by the U.S. Coast Guard [27]. The design adopted for standard service for 8-ft buoys was the 8 x 26 (RR), which incorporates a simple vertical dihedral reflector with plates 2.1 x 2.6 ft, giving a nominal maximum cross-section of some 7000 m^2.

The Naval Research Laboratory has examined the polarization properties and cross-sections of three standard types of radar navigational buoys [28]. The radar used was an X-band system capable of transmitting with vertical, horizontal, left-circular, or right-circular polarization, and of receiving and recording all four components simultaneously for any transmitted polarization. Three buoys were examined at a range of about 3400 yds: Coast Guard 8 x 26 (RR), the same as that described above; Coast Guard 1st Class (RR); and Coast Guard 3rd Class (RR). Results were obtained in the form of cumulative echo-area distributions for VV, HH, RR, RL, LL, and LR operating modes. (HV and VH modes were said to show "no" cross-polarized return.) Table III summarizes the median (50%) points from the curves.

Table III

Median Cross-Sections for Three Coast Guard Buoys

Buoy	Median Cross-Section in Square Feet					
	VV	HH	RR	LL	LR	RL
8 x 26 (RR)	4000	5900	7300	2100	420	1750
1st Class (RR)	7200	13000	7000	9700	900	3600
3rd Class (RR)	700	300	100	200	150	370

It is of interest to note that for no polarization does the 50% point for the 8 x 26 (RR) buoy approach its nominal maximum echo area of 7000 m^2 (76,000 ft^2). Examination of the distributions themselves shows that, with any polarization, the buoy under these experimental conditions had an echo area of about 76,000 ft^2 only some 1% or 2% of the time or less. Presumably this result implies that the dihedral reflecting surfaces are tilted enough most of the time as to greatly reduce the net echo area. The NRL experimenters measured the loss in received signal as the elevation angle of a diplane buoy is varied with the radar beam bisecting a dihedral corner. A 2.5° tilt was found sufficient to reduce the return 10 dB to some 7600 ft^2, not far from the 50% values observed with some polarizations. (It should be noted that the NRL observations were made under conditions such that the top of this buoy would be well above the first maximum of the transmitter's lobe structure for ideal sea reflection.)

Power spectra were determined from the NRL data. For all polarizations, these show significant power only at frequencies below 1 cps, a result which would be a function of the water conditions existing at the time of the runs. In most instances, power is more concentrated at lower frequencies with same-sense return than with opposite-sense return.

Polarization work on buoys was also done in brief experimentation by the Admiralty Surface Weapons Establishment (ASWE) [29], using a modified Decca 424 radar. They examined a number of marine targets and compared the relative response using circular, horizontal, and vertical polarization. (Although not stated, their circular polarization was apparently same-sense.) Several different types of buoys were included, and showed losses with circular relative to horizontal ranging from 2.3 dB on a "can buoy" to 14.0 on a "conical buoy with radar reflector." This result agrees qualitatively with the NRL work shown in the table above, for which same-sense circular polarization usually gave lower echo area than did horizontal. The ASWE measurements on four types of buoys showed vertical polarization gave response ranging from 2.2 dB above to 1.2 dB below horizontal response.

4-3. Ice

While a few studies have been made on the various forms of sea ice as targets for radar, it appears that no calibrated cross-section measurements have been performed on such targets.

Le Page and Milwright have described observations and experiments undertaken during an extended voyage in an ice-breaker along the coast of Labrador and into Hudson Bay [30, 31]. While they were not equipped to make cross-section measurements, they did take useful quantitative data. Their radar observations were made with a Type 268 marine radar, characterized by a wavelength of 3 cm, a power output of 27 kW, half-power beamwidths of 2.5° in the horizontal plane and 20° in the vertical plane, and a pulse length of 0.75 μsec. The radar observations were supplemented by sextant observations and photographs to furnish information on the size and shape of the observed ice bodies, and by psychrometer and temperature observations at two or three elevations to furnish information on propagation conditions.

For a number of icebergs, the projected area was determined from photographs and plotted against the range at which the berg gave an echo 20 dB above receiver noise. A best-fit curve was obtained by least squares assuming an R^{-4} law. When this is compared with the curve representing the theoretical

response of a metal sphere, it is found that the icebergs have a projected area 60 to 70 times that of the metal sphere giving equal echo amplitude. This result cannot be taken as equivalent to a calibrated measurement of cross-section for an iceberg of specified shape, but it serves to indicate that the berg is a rather poor radar target.

Shape is a factor of some importance in determining the return from floating ice. The typical berg is angular in structure and normally will present to a viewing radar a rough, irregular form, likely to contain flats, corners, or other forms that furnish relatively high backscatter. Rather different is the "growler," a smaller floating ice formation which is characterized by a rounded, smooth upper contour, possibly as the result of having "turned turtle." Growlers offer lower return, due both to their smaller size and to their smooth shape.

In calm seas, the Type 268 radar furnished a detection range of about 15 to 20 miles on large bergs, down to 2 miles on small growlers. Under calm conditions, it appears likely that a growler or berg large enough to represent a danger to a ship would be detected by radar at a safe range. Under conditions of rough sea, where clutter may extend to much greater ranges, it is quite possible that growlers of a dangerous size might go undetected by radar.

Le Page and Milwright had little experience with field ice, but did encounter broken hummocked ice once, for which they state the detection range to be approximately 3 miles.

Observations on sea ice were also made by Perry during a voyage to Port Churchill on the shore of Hudson Bay [32]. Perry used a Decca Type 12 radar, said to furnish a radar horizon of 9.3 nmi for the ship in light condition (antenna height 60 ft) and 8.3 nmi in loaded condition (antenna height 48 ft), but not otherwise specified.

Perry furnished largely qualitative observations with results agreeing in general with those of Le Page and Milwright. He states that the detection ranges of bergs of various sizes compare quite favorably with those from land of similar height. He emphasizes the importance of shape or slope, but notes that virtually every berg is likely to display some formation giving good return. His observations on growlers also agree: in a calm sea, the detection range was 2 to 3 miles, but he also notes that dangerous growlers may well be lost in clutter during heavy swell or rough sea. Perry indicates that land ice, while it might be a poor target if possessed of a smooth featureless slope, will

generally, from his experience, have ridges or hummocks giving some return. His minimum detection range was 4 miles. He states that floes or field ice, if smooth, will give a return very similar to occasional sea-clutter paint from a calm sea. Even the edge of the pack may not be observed in smooth water.

Neither Le Page and Milwright nor Perry experienced any example of abnormal propagation conditions leading to unusually short detection ranges. Both mention the concept that a cold air pocket to leeward of a berg may have significant effect on radar visibility in that direction, and both express skepticism as to its validity. Perry, in particular, states that he never observed deterioration of the echo that might be associated with this cause, even in cases where bergs were circumnavigated.

4-4. Splashes

Although many reports consider the detection of shell or mine splashes for various purposes, fairly few quantitative data exist (for example, References 33 and 34). Most available information is summarized in other Georgia Tech reports [35, 36, 37], and this section will be based on that material.

Numerous factors affect the formation of a particular splash, many of which are experimentally uncontrollable. Among these factors are: the physical size, weight, and shape of the impacting object; the entry angle and associated horizontal and vertical components of impact velocity; surface condition and depth of the water; and, in the case of a mine, the aspect of the wedge nose and presence or absence of a parachute. At non-ricocheting entry angles, shells produce fairly uniform splashes, as contrasted with the variation observed for parachute-type mines. Despite the variability, splashes have certain fundamental physical and radar-reflection characteristics which may be described in general terms.

Observations indicate that a shell or mine splash generally takes the visual form of an approximately elliptical column of water and spray which grows very rapidly to its maximum height and then decays to a small residuum of spray and surface "boil." Usually growth occurs in somewhat less than a second [38] but may take several times as long. The second stage of splash life is characterized by churning of the water column and a transformation into spray which takes up to several seconds if the splash is large. The dissipation of the spray and the surface boil may take several more seconds if calm wind and sea conditions prevail. Height and width of splashes are usually in the

range 20-100 ft, but are highly variable depending upon the object and its impact conditions. Overall visual durations of mine and shell splashes as measured from the beginning of a water disturbance to loss of visibility of the spray (or boil) lie predominantly in the range 1-10 seconds.

Amplitude variations of the radar return from a splash follow approximately the same pattern: short rise time, a fluctuating middle period, and a decay time somewhat longer than the rise time. However, the radar observations differ from the visual observations in that the radar echo seems both to rise to its maximum and then to decay somewhat more slowly than do the visual dimensions. Although no explanation is readily available for the slower growth behavior, it appears that the slower decay is caused by the spray and fine mist which present a fairly good radar target (at appropriate wavelengths) even after the main water column has fallen. The total time that the radar signal is above the noise level will depend on the receiver sensitivity and gain, since both the rise and the fall of radar cross-section occur with finite slopes. There is also some wavelength dependence which tends to extend the duration slightly for shorter wavelengths, although at least part of this may be the effect of the wavelength dependence of the illumination (i.e., interference lobes). Whether or not the surface boil is seen and the signal duration thereby further lengthened depends upon the incidence angle.

Simultaneous observations of mine splashes with K- and X-band rapid-scan radars were made by Georgia Tech and Yale University in 1952. Neither radar was calibrated for cross-section measurements, but B-scope film records were made and the azimuth blip size is roughly related to cross-section. Exposure time varied during the tests, so the number of samples integrated on the film frames was not constant. By normalizing to the maximum width observed during the complete splash history, some comparisons were possible. Results on splashes having durations of about 4 and 8 seconds are shown in Fig. 9.

No significant difference in splash durations was seen between the K-band FEAR and X-band AN/MPG-1 radars. This is a rather interesting result since it is known that the signal sensitivity levels of the radars were different and the gain of the FEAR was purposely varied over a wide range. A possibility is that the sensitivity was relatively low for both radars, especially the K-band one, so that only the high cross-section portion of the splash was detected and the K-band "tail" was below the system threshold.

As shown in Fig. 9(b), and in other plots not reproduced here, the frame-to-frame fluctuations in blip size are much more pronounced on K-band (1.25 cm).

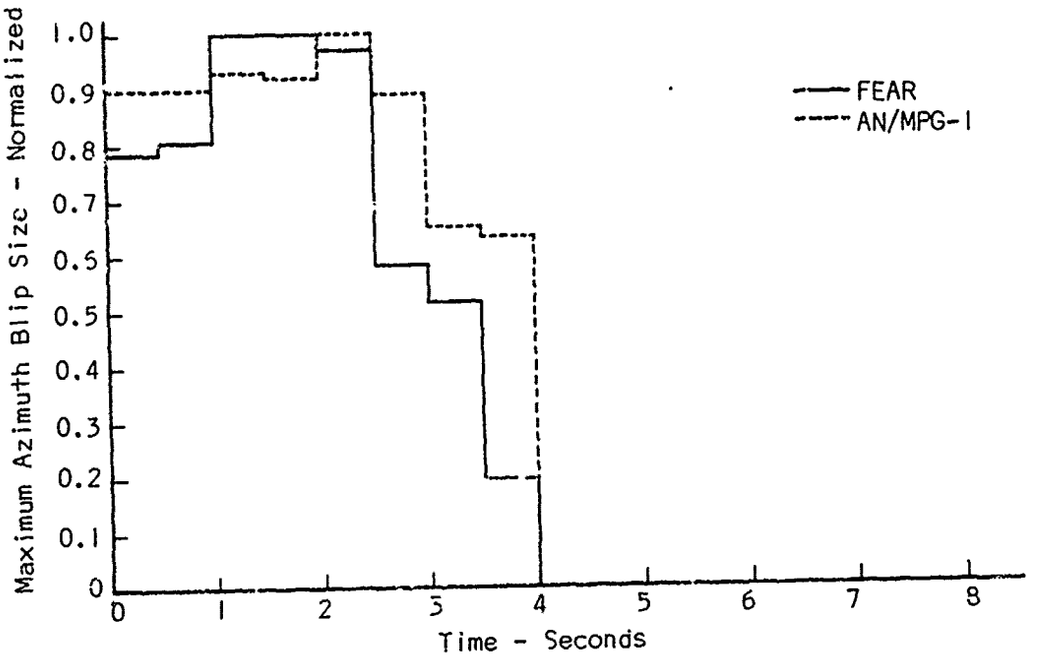

(a) Short-Duration Splash with Integration Period of 0.5 Second (Drop 4, 30 January 1952)

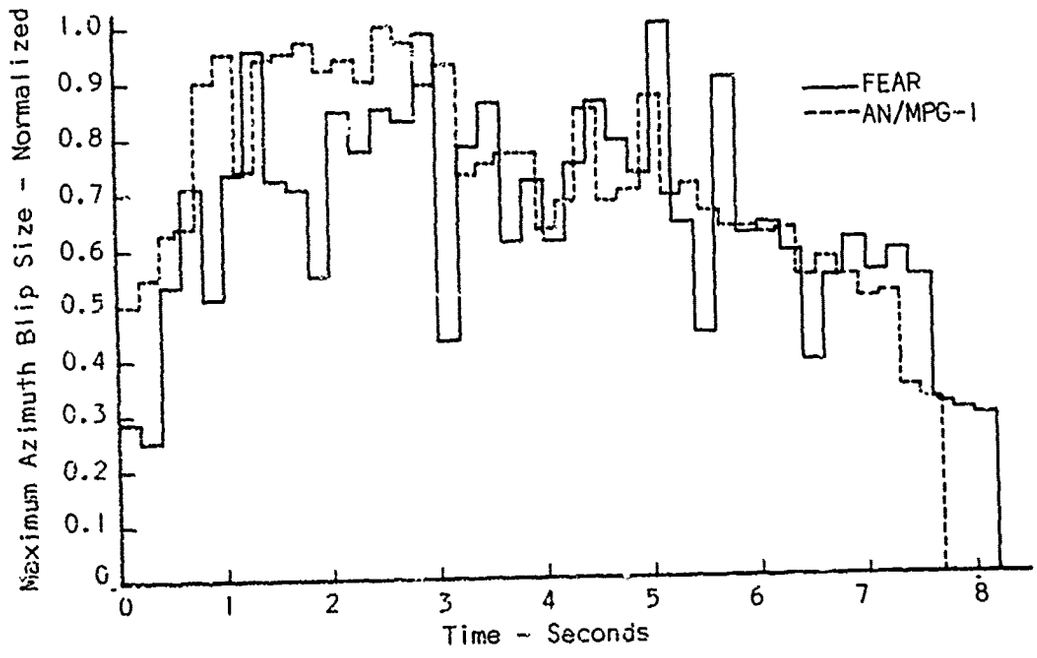

(b) Long-Duration Splash with Integration Period of 0.2 Second (Drop 3, 6 February 1952)

Figure 9. Time Variation in Normalized Maximum Azimuth Blip Sizes of Splashes.

This would be expected if the splash return has fluctuation properties describable by a set of incoherent random scatterers. After the main water column has degenerated into primarily spray, such a condition very likely exists. As a reasonable guess, it appears that the magnitudes of effective cross-sections as seen by both K-band and X-band radars with low antenna heights are roughly comparable through most of the life of a splash, although the fluctuation rates differ.

Observations were made in 1955 by the Naval Proving Ground (now Naval Weapons Laboratory) using a low-sited S-band radar with a beamwidth of 2.3° and a pulse length of 0.3 μsec [37]. Pen recordings were made of the voltage output of the AGC circuit, which had a time constant of 0.057 second; system calibration was accomplished with a sphere target. Several mines were tracked as they were dropped from aircraft and subsequently impacted in the Potomac River; shell-splash data were obtained by pointing the radar at the predicted impact position. Fig. 10 shows examples of these recordings (note that time increases from right to left).

Figs. 10(a) and (b) illustrate the non-uniform splash returns produced by two 1000-lb parachute mines dropped under approximately the same conditions. The splash cross-section in (a) reached a maximum value of about 7 m^2, and was greater than 3 m^2 for much of its life of 2.2 seconds; in (b), the maximum was about 30 m^2 (the non-linear calibration makes large values difficult to read accurately), with over 10 m^2 exhibited for most of the lifetime of 3 seconds. The maximum return from the mine in flight is somewhat over 35 m^2 in (a) and somewhat less than this value in (b). These figures compare favorably with a calculated maximum broadside cross-section of 40 m^2 for a cylinder 18.6 inches in diameter and 66.6 inches long at a wavelength of 10.7 cm. The recording of Fig. 10(c) is from a 2000-lb free-fall mine and effects of passage of the unit through vertical interference lobes may be seen at the right end of the strip. Splash return exceeds 50 m^2 at its maximum and is about 10 m^2 for much of the duration of 5.6 seconds. Note that clutter was also present in the region of impact.

Figs. 10(d) and (e) illustrate cross-section behavior for two 3"/50 shell splashes and the general round-to-round reproducibility of such splashes is evident. Cross-section in each case was about 15 m^2 at the maximum, and exceeded 7 m^2 for much of the splash life of 2.8 seconds. Peaks in return from the projectiles as they passed through the interference lobes may also be seen in these records.

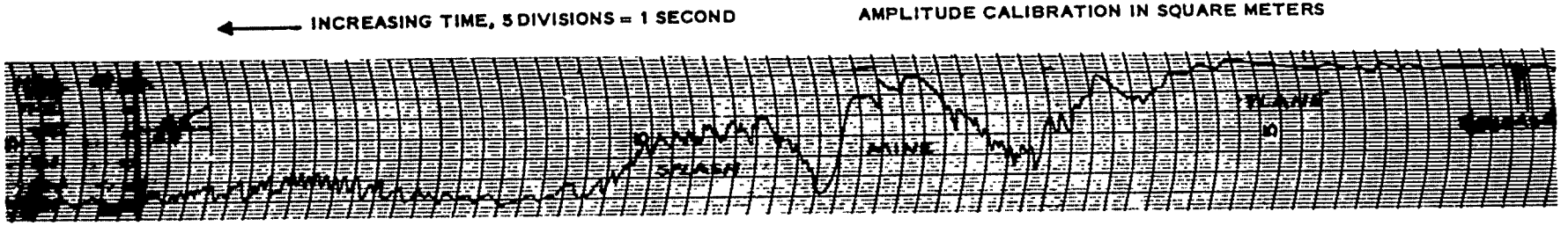

(a) Splash from Mk 36-1 Mine Dropped from 580 feet at 240 Knots (Drop 8, 23 March 1955)

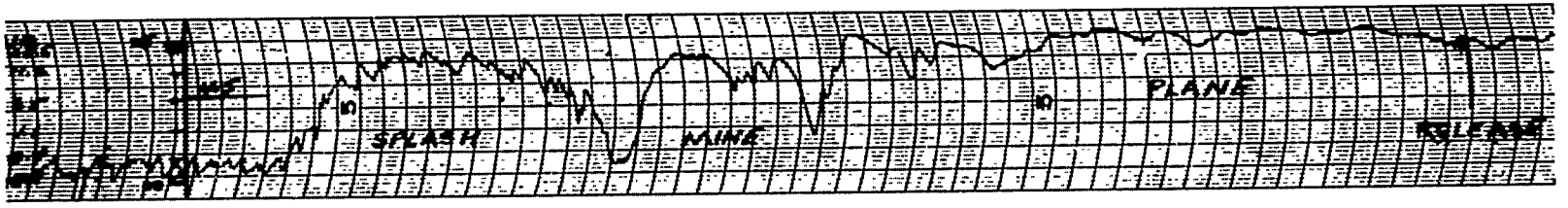

(b) Splash from Mk 36-1 Mine Dropped from 490 Feet at 250 Knots (Drop 9, 23 March 1955)

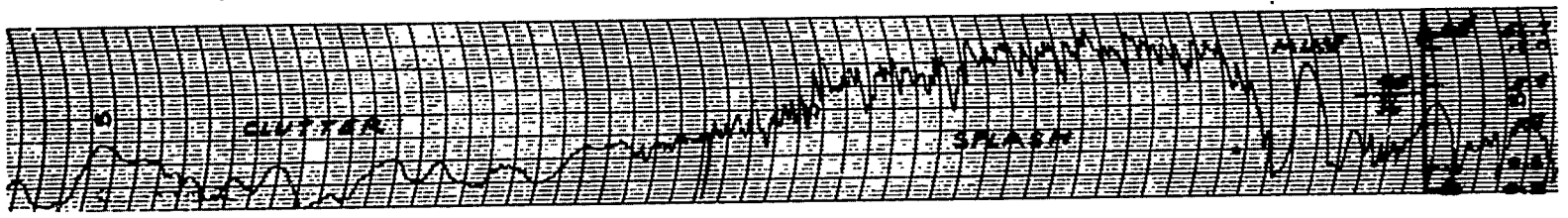

(c) Splash from Mk 39-0 Mine Dropped from 5000 Feet at 153 Knots (Drop 7, 24 March 1955)

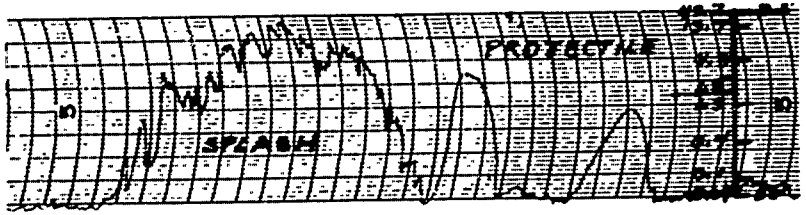

(d) Splash from 3"/50 Shell
(Round 37, 24 March 1955)

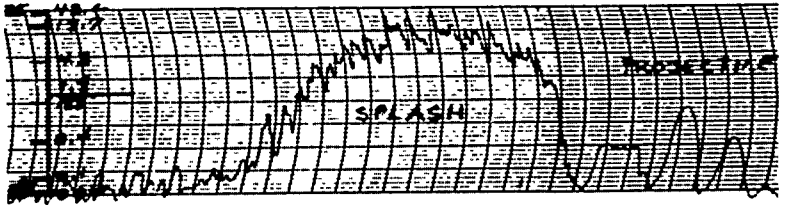

(e) Splash from 3"/50 Shell
(Round 38, 24 March 1955)

Figure 10. S-Band Cross-Sections vs. Time for Mine and Shell Splashes.

The S-band effective cross-sections discussed above are for an antenna height of about 25 ft. Assuming an incoherent scatterer model for a splash [34; see also Section A-2], the cross-section would be about 6 times the free-space value if the water (or spray) column extended above the maximum of the lowest interference lobe; this interference effect is important in considering splash detection. Quite small splashes (from 50-caliber and 20-mm weapons) have been detected at several hundred yards using low-sited K- and X-band systems of low to moderate system sensitivity, and individual impacts of rapid-fire 5-inch rockets were detected at ranges of several thousand yards.

(This page intentionally left blank.)

V. RANGE VARIATION OF RETURN POWER

As discussed in the Appendix, to a first approximation the return power of an object above a reflecting surface will decrease with increasing range as R^{-4} out to some transition range, and then as R^{-8} for longer ranges but not so far that the earth's curvature has a major effect. In a broad sense, this behavior has been confirmed experimentally; however, departures from the approximate theory are also common.

5-1. Experimental Data

Figs. 11 and 12 illustrate some World War II experimental data obtained by the British using high-sited S-band radars having low resolution [39, 40]. Each data point is the maximum return in a 20-second interval and is thus likely to be on the high-return tail of the statistical distribution of returns (see also Section 2-2). Dashed lines on the figures represent theoretical range variation using incoherent theory (see Eq. (A-14)), assuming that the phase of the resultant of the direct and indirect rays illuminating the target is linearly proportional to height. In computing the phase for different heights as a function of range, spherical-earth methods have been used, and the curves have been adjusted for variation in effective earth's radius (i.e., different propagation conditions) in order to give the best fit.

In Fig. 11, the WDMV Llys Helig, a former pleasure yacht, was tracked stern-on from about 9,000 to 65,000 yds by a CHEL radar with an antenna height of 530 ft. The best fit was obtained using a target height of 22.8 ft and an effective earth radius of 7200 miles (4/3 earth radius for "standard" propagation is 5280 statute miles). These measurements were made on a calm day and stratification of the atmosphere may have existed. Data points tend to lie above theoretical for ranges just shorter than that corresponding to the knee of the curve, but for still shorter ranges, they tend to fall below. While obscured by the scatter in the data, there is at least a suggestion of an oscillatory behavior of the range variation in the R^{-4} region.

The target for the data of Fig. 12 was a four-stack destroyer, the HMS Lancaster, and the radar was the CA No. 1 Mk II (Star) with an antenna height of 470 ft. The destroyer was tracked stern-on from about 6,000 to 60,000 yds, and the theoretical curve chosen as best fitting the data is for a target height of 46.6 ft and an effective earth radius of 5000 miles (approximately standard). Weather on this day was windy, and propagation was generally

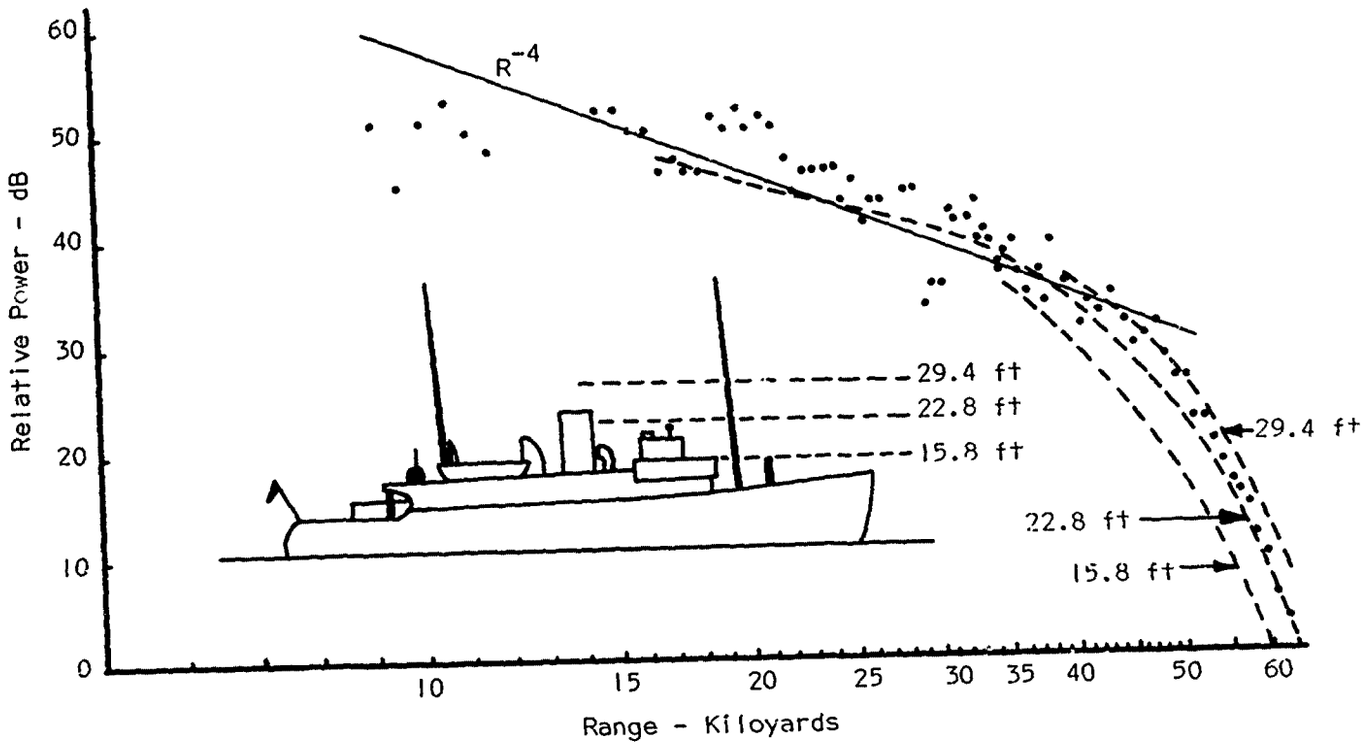

Figure 11. Range Variation of Return Power for WDMV Llys Helig Stern-On (CHEL Radar, Antenna Height 530 Feet).

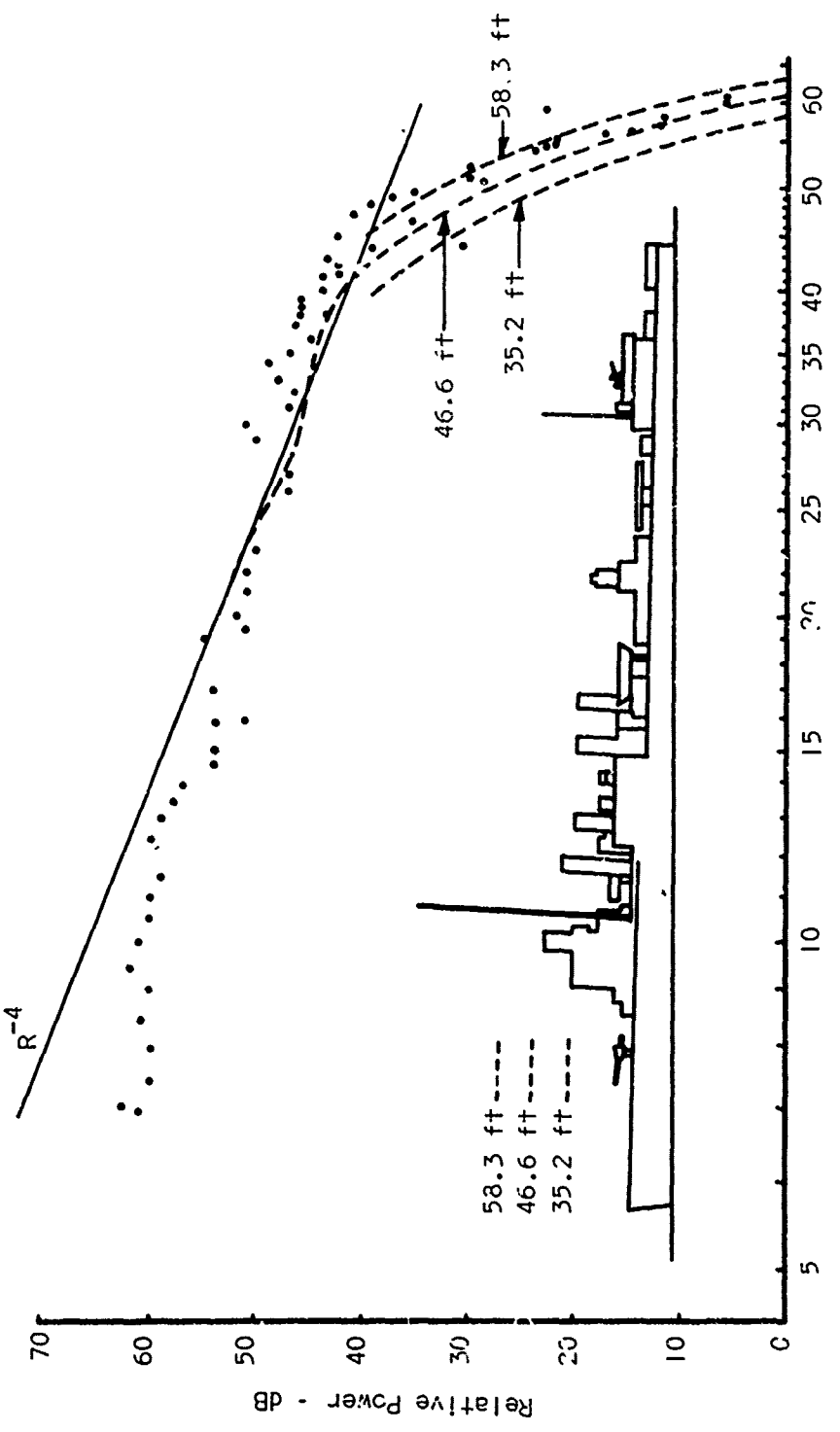

Figure 12. Range Variation of Return Power for Destroyer HMS Lancaster Stern-On (CA No. 1 Mk II (Star) Radar, Antenna Height 470 Feet).

observed to be normal. Here, again, the experimental points tend to lie above the theoretical curve ranges near its knee, next to show an oscillatory behavior, and then tend to fall below the curve at shorter ranges.

Power vs. range plots available elsewhere (for example, References 7, 9-13, 15) show the same general characteristics as those of Figs. 11 and 12. Data points frequently are scattered, and considerable leeway is offered in fitting theoretical curves. While data for lower frequencies do not clearly exhibit it, S- and X-band data fairly often have the oscillatory pattern illustrated here. We believe that this is indicative of a major contribution by a sensibly flat scattering center elevated above the surface, but the data are too sparse to make this much more than a conjecture. Also seen in these illustrations is a drooping of return power at long ranges such that the data points fall below an R^{-8} relationship.

The tendency for short-range data to fall below the R^{-4} line fitted to points closer to the transition range has been explained as being due to a number of possible causes. Among those most plausible, one is that the target (or the sea at the point of reflection of the indirect ray) is not illuminated at the maximum of the antenna vertical beam pattern. A second one is that the reflection coefficient of the sea departs from "perfect" (i.e., -1) as the angle of incidence departs from grazing; this may be caused by roughness, by polarization (Brewster angle) effects, or by the divergence of rays reflected from the spherical surface. Still another effect which may occur when peak returns are being considered is that, as the range becomes short enough, there is sufficient phase error across a coherent scatterer that the effective return is reduced [5, 41].

5-2. Conjectured Form of Variation

Consideration of theoretical and experimental aspects of the problem have led us to make some general conjectures about the variation of return power with range; the basic scheme is illustrated in Fig. 13. The reader is strongly cautioned against drawing more than a qualitative feeling about the situation from this figure, since some of the variations it illustrates may not be correct for all experimental conditions and others are based purely on speculation. Also, the various regions shown may overlap or be entirely absent.

Fig. 13 shows the variation of the logarithm of received power vs. the logarithm of range. Starting at extreme range, the return power increases with decreasing range as the target rises higher in the lowest interference lobe of

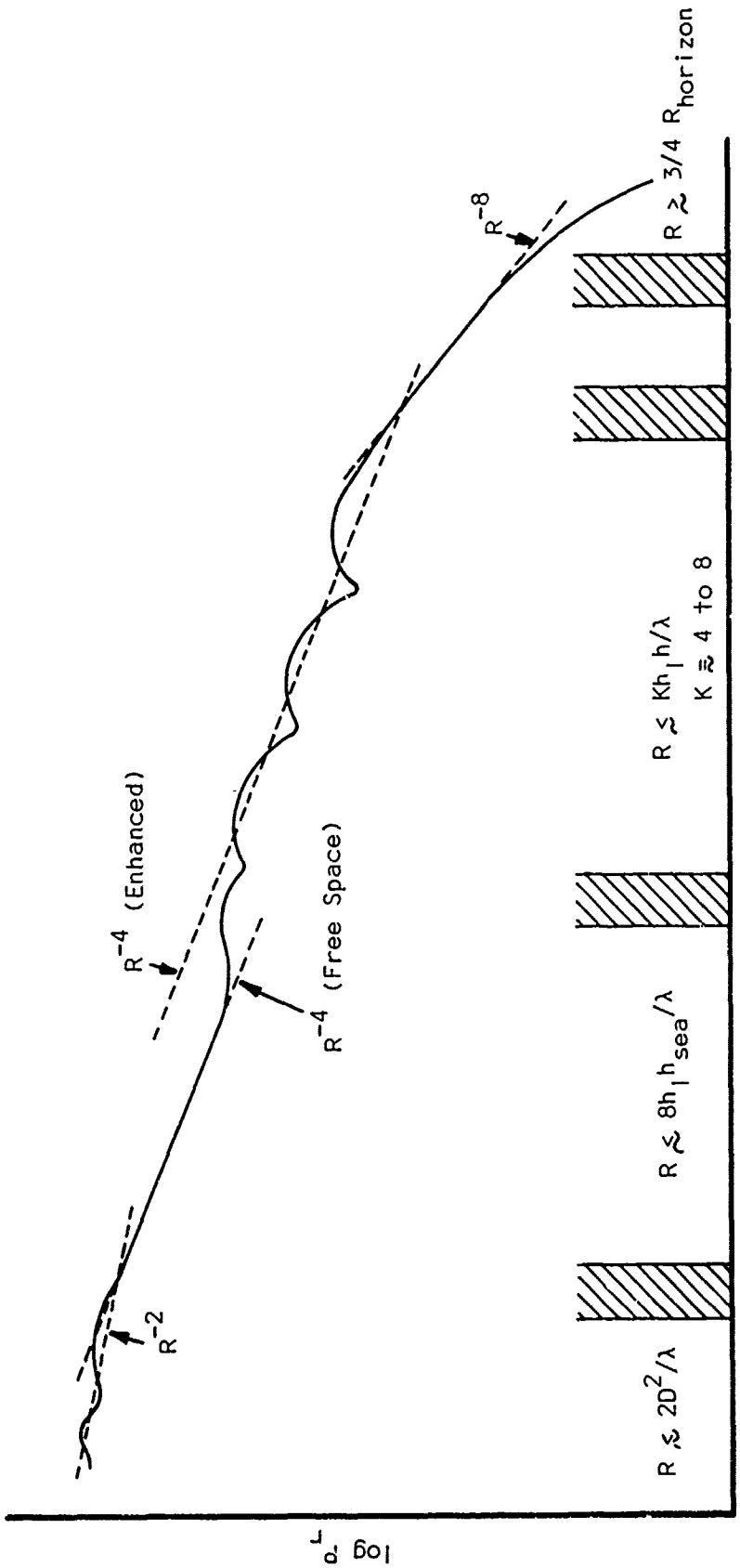

Figure 13. Conjectural Range Variation of Peak Received Power for an Elevated Coherent Scatterer.

the height-varying field. This corresponds to the direct illumination region just inside the radar horizon of the spherical earth, or in the diffraction region beyond the radar horizon; here, the variation of return would not be well-approximated by a straight line and under standard propagation conditions would vary faster with range than R^{-8}. For ranges less than, say, about three-fourths that of the radar horizon, the curve might be approximated by an R^{-8} line. Finally, a transition region is reached where the effective target height is approximately the same as the height of the maximum of the lowest interference lobe. Return power falls below the R^{-8} line in this region as variation with range became less. The approximate range of the transition is $(Kh_1 h/\lambda)$, where K is of the order 4 to 8, but the variation changes slope gradually so the transition range is not a well-defined point.

As range continues to decrease, the return power may be expected to oscillate above and below a trend line behaving as R^{-4}. The amplitude and form of these oscillations will be influenced by the particular data being plotted, and by the character of the dominant scattering centers of the target. For example, if peak data were being plotted for a target consisting of an elevated coherent scatterer of reasonably small vertical extent, then the oscillations might have large amplitude and show rounded peaks with somewhat cusped nulls, as plotted in the figure. Incoherent scatterers would be expected to show smooth peaks and nulls of smaller amplitude.

The target will be viewed at non-grazing incidence as range decreases further, and surface roughness of the water may cause sufficiently diffuse scattering of the indirect ray as to destroy the interference pattern. Although this would not take place at any specific range, it should begin to occur approximately according to the Rayleigh roughness criterion, or at a range of about $8h_1 h_{sea}/\lambda$ (see Section A-1). Thus, whereas at ranges somewhat greater than this transition region, the return is presumably enhanced by the increased illumination provided by the interference lobes, inside the transition region lack of the indirect radiation path will cause the return to be about that governed by the free-space far-zone cross-section of the target. (Note also that vertically polarized radiation having an incidence angle in the vicinity of the Brewster angle would not produce a strong indirect ray.) At quite short ranges, the elevation angle at which the target is viewed changes significantly with range, and any dependence of target scattering properties with elevation angle will also affect the return.

Again considering peak returns and a dominant coherent scatterer, further decrease in range will eventually bring us to a point where the phase error across the scatterer becomes appreciable and the effective cross-section is decreased. Although subject to much interpretation [42], the range where this might begin to matter is on the order of $2D^2/\lambda$, where D is the maximum dimension of the scatterer. As range continues to decrease, return from a coherent scatterer in the Fresnel region will once more exhibit oscillatory behavior [5] about a line varying approximately as R^{-2} [41].

(This page intentionally left blank.)

VI. STATISTICAL DESCRIPTION OF RETURNS

In this chapter we discuss the statistical description of the moment-to-moment fluctuations in the returns from sea targets. These fluctuations may be described by a probability distribution of return power, plus a measure of the frequency of fluctuation--either the power spectral density or the autocorrelation function. In present usage, the probability distribution is frequently characterized by a single number, its median value.

In discussing sea-target return, many writers have assumed, at least implicitly, that they are dealing with a stationary process having unchanging statistical properties. This is usually in error--the nature of the return from a typical sea target may change greatly from one period of time to another. Return from a ship, for example, at one aspect may resemble that from a collection of random scatterers, whereas at a different aspect the return may be dominated by reflection from a single large element. This changing character of the return from a sea target should be borne in mind in considering the experimental evidence discussed below, most of which has involved only rather limited observations on a small number of targets.

Radar return from a typical sea target undergoes extremely large variations from moment to moment. These variations arise from several causes, but the most important is the incessant motion of the target, which is continually changing its aspect and thereby the relative phases between scattering elements. As aspect changes, the three-dimensional cross-section pattern of the target is swept past the line of sight in a complex and irregular manner. For large sea targets this pattern has an extremely fine lobe structure so that even a moderate angular motion can produce amplitude scintillations having relatively high frequency, as well as large dynamic ranges.

Aside from aspect changes, amplitude fluctuations can also arise from changes in the effective size of the target. For example, changes in the exposed height of a periscope or snorkel might be expected to cause fluctuations. Atmospheric propagation can also vary from moment to moment, and this too can give rise to fluctuations in amplitude. Under circumstances such that radiation reflected from the sea surface plays a significant role in the return signal, the continually changing scattering properties of the surface will introduce amplitude fluctuations. In particular, the interference lobes of the illuminating field may change with respect to the scattering pattern of the target;

this may be a slow change for a surface radar, or a rapid change for an airborne radar.

6-1. Probability Distributions

It was sometimes assumed in the earlier days of radar that complex targets such as aircraft or ships could be represented by a random collection of scattering elements (for example, see Kerr, p 545). The return would therefore evidence a Rayleigh amplitude distribution. Such a model is quite likely to be a good one for ships at some aspects, but not at others.

If the return is dominated by a single scatterer, or by only two or three scatterers, the assumptions of the Rayleigh model do not apply. This might well be the situation for bow, stern, and broadside aspects. Actual data have frequently shown an excess of high cross-section values relative to a Rayleigh curve which would fit the rest of the points. It has been suggested that the log-normal distribution may apply for such cases, and there appears to be some evidence that experimental data on ships fit the two-parameter log-normal distribution better than the one-parameter Rayleigh distribution (see Section 6-3.1). If, however, the data for a restricted region of target aspects which exhibited these high values were mixed in with data for aspects which did not, the overall data would then also show a high-cross-section tail. The form of distribution is particularly important in cases where it affects detection probabilities.

In our opinion, a single distribution to represent all target aspects is unlikely to represent any specific aspect well. Unless all aspects of the target are equally likely in an operational situation, the statistics of the most likely aspects would appear to be most important. As far as we can determine, little investigation has been made of this subject. Also, most checks on the type of distribution which fits the data have been made on the basis of curve fitting. We have found no cases where the quality of fits to different distributions were compared using statistical criteria.

6-2. Doppler Spectra

In a coherent radar the return signal is compared with a sample of the transmitted signal with phase preserved. Any radial velocity v of the target produces a frequency shift in the return signal which may be detected by the coherent system. This Doppler frequency shift f_D is proportional to target velocity and inversely proportional to transmitted wavelength,

$$f_D = 2v/\lambda \ .$$

If the target were only a point, the Doppler spectrum would consist of a line at f_D. However, for targets which consist of a number of scattering centers, each element having relative radial velocity will contribute to a spread in the Doppler spectrum about the frequency corresponding to average radial velocity. (The Doppler spread is not necessarily symmetrical.)

In the case of a non-coherent radar, any shift in frequency due to average radial velocity would not be detected if the target were a point. For a complex target, the frequencies related to the various scattering centers beat together in the final detector to give an echo spectrum also.

Consider now two identical spheres a distance d apart with the line of centers making an angle θ from the normal to the radar line of sight and rotating with an angular velocity ω about the center of gravity. The difference in Doppler frequency between these two scatterers is given by

$$\Delta f_D = (2d\omega/\lambda) \cos \theta \ .$$

The Doppler spread of this two-element target is thus proportional to the distance between scatterers, their angular velocity, the radar frequency, and the gross target aspect. Since the radar cross-sections of the two elements are equal, the resultant cross-section will vary between zero and four times the value of a single element, corresponding to the individual returns being exactly out of phase or in phase, respectively.

As an alternative to representing the fluctuation rate as a power spectral density (Doppler spectrum), the autocorrelation function may be used. Although the two representations are related to one another through a Fourier transform pair, in practice one form or the other is usually preferred for studying specific experimental data. While experimental probability distributions of cross-section are fairly frequently obtained, Doppler spectra or autocorrelation information are considerably less common.

6-3. Experimental Data

6-3.1. Ships

An early study of ship return was done by the Radio Research Laboratory of Harvard University during World War II [43]. Their primary interest was in the possible difference in the amplitude fluctuations of return from a ship and those from a corner-reflector decoy. Observations were made at 3000 MHz and 700 MHz using horizontal polarization on targets consisting of a large

corner-reflector cluster mounted on a float, a balloon-supported meteorological reflector, and a variety of naval surface craft, including a battleship.

Wide variations in the return were noted on all targets, and no criterion was found for distinguishing them by visual observation of the A-scope display. The amplitude fluctuations of the returns were also photographically recorded at 24 frames/second; in all, some 30,000 frames were analyzed. Generally speaking, plots of pip height vs. frame number (time) such as that of Fig. 14, discussed below, changed character with time for the same target. This emphasizes the point made at the beginning of this section: that such returns cannot always be regarded as coming from a stationary process.

Simple observation of the plots did not show cyclic behavior such as might be expected due to ship roll. The 3000-MHz returns on the battleship were subjected to periodogram analysis seeking periodicity associated with the roll (known to be nominally 17.6 seconds under the specified loading); results were largely negative. Another approach was to fold the plots over against themselves, and seek positions of close alignment where the pattern of a section of trace would appear to reverse itself and might be associated with reversal in the attitude-time history at moments of extreme roll.

A number of examples of rather close similarity in such patterns were found for the battleship at 700 MHz as shown along the right side of Fig. 14. This is taken as strong qualitative evidence that the return does exhibit a repetitive pattern associated with the roll of the ship when the overall aspect is suitable for the pattern to be produced. An average period of 15.4 seconds calculated from these records compares with the nominal figure of 17.6 seconds cited above (the actual period at the time of observation was not known).

Distributions were obtained of signal amplitude, as measured by pip height. Linear plots of these for the float target and the battleship show general agreement with the Rayleigh distribution, but it appears doubtful if any difference between Rayleigh and log-normal would be distinguishable from these data.

The return from several ship targets was studied in more recent work by the Naval Research Laboratory using a shore-based polarization research radar [44]. Their system was an X-band pulse radar, capable of transmitting with right- or left-circular, horizontal, or vertical polarization, and of simultaneously receiving all four components. Data presented include sample time plots of amplitude, power spectra, and photographs showing amplitude density distributions

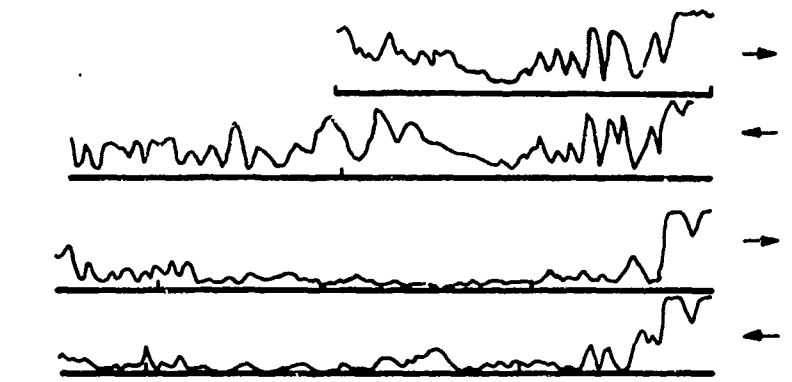

(a) 16,000 Yards

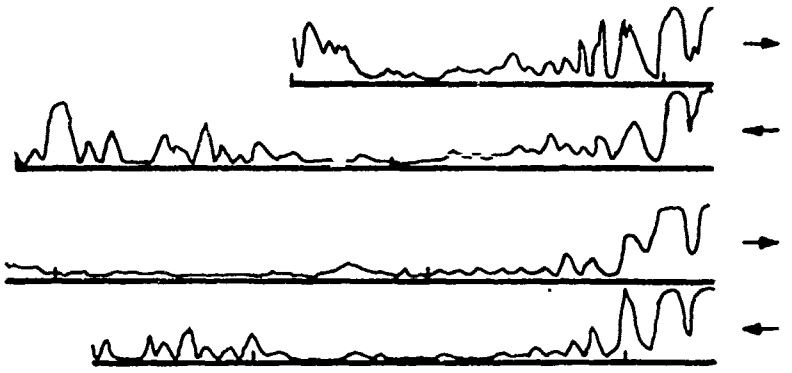

(b) 17,600 Yards

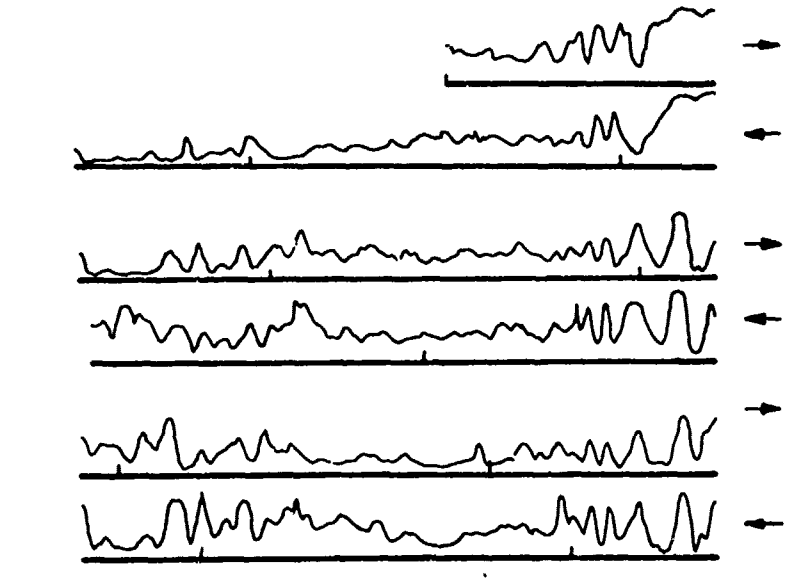

(c) 21,200 Yards

Figure 14. Repetition in Pattern of Pip Height vs. Time for Battleship at 700 MHz Using SCR-296 (Tick Marks are at 100-Frame Intervals, 24 Frames/Second).

obtained with a gray wedge analyzer. Data are given for a tanker, a freighter, a fleet tug, and a barge.

The time plots show very clearly the non-stationary nature of the returns. For example, the tanker return shown in Fig. 15 displays at times a complex, spikey signal resembling random noise in the plots, and at other times a very smooth, slowly varying signal having no sharp fluctuations. Based on the polarization information, NRL suggests that the slowly varying returns are from the large dihedral between deck and superstructure which was visible for the existing aspect angle. Note that here the radar frequency is about 10 GHz rather than 700 Mhz as for Fig. 14, and that very high fluctuation rates are present some of the time.

The non-stationary character of the returns is also indicated by the sample gray-wedge photographs from different portions of a run. Most of these show rather smooth density distributions, which presumably correspond to segments of the return that arise from a considerable number of contributing target elements. Others, however, show definite spikiness, such as would be associated with discrete reflectors.

The several power spectra included show a maximum of significant power that varies from as low as 4 cps to as high as 25 cps. The lower value was obtained with vertical polarization transmitted and received on the freighter and measured in a time interval of 5 to 10 seconds. The value of 25 cps was obtained on the barge in a time interval of 5 to 10 seconds when transmitting right-circular polarization and receiving left-circular.

Comparison of returns in the four-channel receiver when transmitting circular polarization indicated that at some times the ship targets gave a reversal of polarization associated with a single reflection. At other times, the same-sense return contains significant amplitude, implying that a double-bounce mechanism which produces two polarization sense reversals is prominent.

Data from the airborne measurements on the converted minesweeper Peacock described in Section 3-2 allowed statistical analysis, and NRL has prepared cumulative probability distributions on the ship when it was the dominant target during a run at fixed depression angle. These may be compared with other distributions obtained for sea clutter alone which, when plotted on Rayleigh paper, gave fairly straight lines, indicating reasonable fit to a Rayleigh distribution. The Peacock data, however, show larger departures from linearity, which seems to indicate less likelihood of being Rayleigh distributed. The

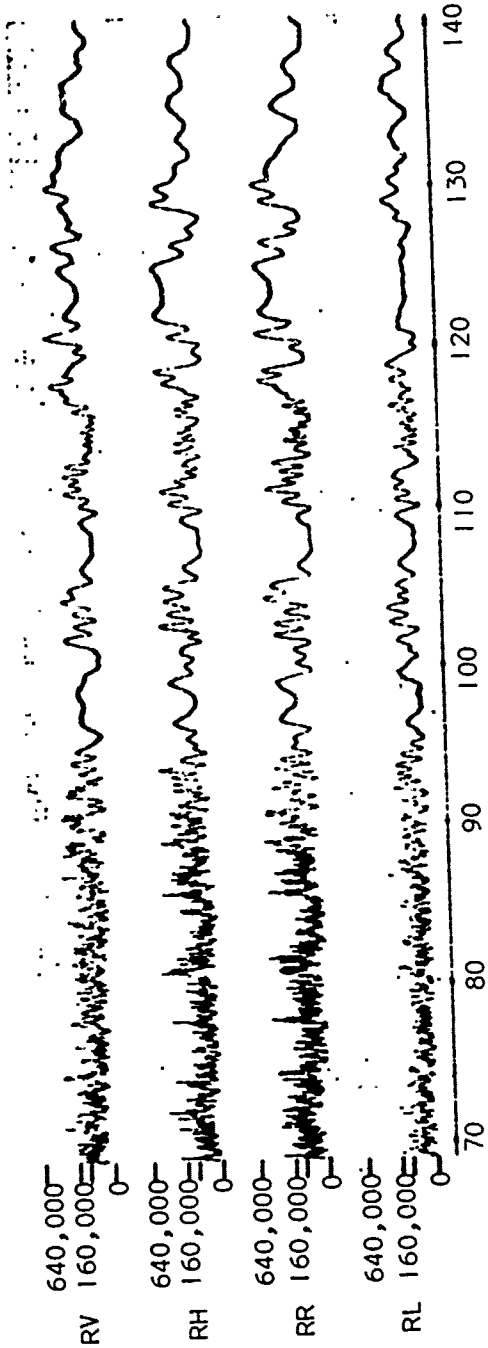

Figure 15. Time History of X-Band Return from Tanker at 16,000 Yards, Showing Non-Stationarity.

samples given are for different polarizations and frequencies and are therefore too limited for making very definite conclusions.

Later observations were made with the same radar on a large cargo vessel (see Section 3-3). Plots of 2-second data runs at 788 pps were made on log-normal probability paper. The resulting plots are interpreted as indicating a good fit to log-normal distribution over the central part, but with deviations at the tails, for P-, L-, C-, and X-bands. It is stated that other work by Harrison at Aerospace [45] also indicates that distributions of ship returns agree well with log-normal. For the reasons discussed in Section 6-1, we believe that more data are to be desired for different target aspects before the question of whether or not there is a "best fit" can be decided.

6-3.2. Submarines

In addition to the NRL data on the cargo vessel discussed in the preceding paragraph, data points for 4-second runs on a submarine were plotted and showed a more radical departure from the log-normal fit. When replotted on Rayleigh paper, the interpretation is that a better fit was obtained. It is suggested, however, that this result may be due to the fact that the submarine is a fairly small target in a large illuminated area so that the sea-clutter may dominate and hence bring about the tendency to exhibit Rayleigh statistics. Again, the lack of exact fit to either distribution is apparent and the question of which one (if either) is preferred cannot be considered as settled.

6-3.3. Snorkels and Periscopes

A coherent radar was used by the University of Illinois in studying the detection of snorkels and periscopes in sea clutter [24, 46, 47]. Frequency spectra were analyzed for 52 snorkels and 6 attack periscopes detected in low sea states with an X-band coherent radar. It was found that echoes from snorkels and periscopes consist of a direct echo and a wake echo. The direct echo is narrow in frequency, less than 10 cps or 1/3 knot. It usually shows no observable frequency modulation due to target acceleration, but characteristically shows strong intensity fluctuations of 2 or 3 cps, which set a limit on signal coherence. The direct echo is normally displaced from the sea clutter spectrum by its velocity component in the direction of the radar, as is the wake echo (see Section 4-1).

6-3.4. Small Craft

The radar reflection properties of small landing craft were studied by the Naval Research Laboratory in the early 1950's [48, 49]. The craft involved

were: LCM, LCVP, LVT, LCPR, and an LCPR camouflaged with Harp absorbing material. Cumulative distributions were obtained for the cross-sections of the boats under different sea states. In the main, these distributions display a better fit to the Rayleigh line for weak echoes (high probabilities) than for strong echoes (low probabilities), with the stronger returns tending to occur more often than would be predicted by the otherwise corresponding Rayleigh curve. These features are independent of sea state and range. The distributions are consistent with the picture of the targets as involving a large number of scattering elements at most aspects, but having a dominating single scatterer at certain aspects. The boxlike form of landing craft, (as compared with most other vessels), would lead one to expect strong dominant flat-plate returns at beam, bow, and stern aspects, and these echoes are possibly the cause of the departure from Rayleigh statistics shown by the distributions.

Observations were also made on four sizes of rafts--ten-man, seven-man, four-man, and two-man. Resulting distributions of these data points in general displayed a much better fit to the Rayleigh statistics than did those of the landing craft.

Spectra of the amplitude fluctuations were obtained for bow runs of the landing craft: for Sea States 1 through 4 for the LCPR, and Sea State 1 only for the others. Amplitudes of equally spaced pulses were obtained from the pulse-by-pulse recordings, plotted, converted to a voltage, modulated on a carrier and recorded on tape, and finally the frequency structure extracted from a tape loop by spectrum analyzer. Their accuracy is limited, and only the trends of the spectra are regarded as meaningful. In general, there was a steady increase in fluctuation amplitude with increasing sea state. All the spectra show a more-or-less uniform decrease of amplitude with increasing frequency. The maximum extent of significant energy varies from about 4 to 20 cps.

The University of Illinois has measured the Doppler spectra of two small boats: a 30-ft craft and a 40-ft craft [50]. Half-power widths were of the order of 70-100 cps, and the spectra showed some fine structure.

(Both at X-band.)

(This page intentionally left blank.)

VII. OTHER TARGET PROPERTIES AND MISCELLANEOUS TOPICS

7-1. Bistatic Scattering

Complete specification of bistatic scattering properties for a target would involve defining a pattern of scattered energy for all possible directions of incidence, in sharp contrast to the single direction of the monostatic case. Obviously this is likely to be too complicated to be practical for a complex target such as a ship on the sea. Any meaningful statement concerning bistatic scattering must, at the least, specify both direction of illumination and direction of viewing (relative to target aspect), not merely the single bistatic angle between these two directions as is commonly done.

Moreover, since transmitter-target and target-receiver paths are non-coincident, a different pattern propagation factor F will apply for each path. That is, the definition of bistatic cross-section must involve a factor having the form $F_a^2 F_b^2$ rather than F^4 as in the monostatic case, as well as take into account the proper bistatic scattering of the target (elements or overall) for the four possible propagation paths. When done completely, this leads to the rather complicated expression given by Durlach [4] as his Equation (31).

A few qualitative general comments can be made about bistatic scattering from ship-like targets. To begin with, it is apparent that any flat surface which is large in terms of wavelength will produce strong reflected energy in the specular direction, and very little in non-specular directions. Some ships evidence a relatively large and uncluttered flat deck surface in the horizontal plane; the carrier is of course the prime example. Even when a single open deck is not present, there may be a number of smaller flat horizontal surfaces--deck sections, roofs of superstructure elements, etc.--each of which is of dimensions large compared to wavelength. In this case, the various surfaces may together produce appreciable specular forward scatter.

The question of whether or not strong bistatic scattering in the specular direction from horizontal surfaces can be observed is largely determined by the contrast with sea clutter. Generally, when illumination and observation angles lie close to grazing and the bistatic angle is near 180°, forward scatter from the sea is apt to be strong even for quite a rough sea, and the target forward scatter is likely to be indistinguishable from the clutter. Similarly, when illumination and viewing directions are both near vertical and the bistatic angle is small, sea clutter is also apt to be strong, and again the specular

return from horizontal target surfaces is unlikely to be distinguishable. (Note that increasing roughness of the sea causes decreasing sea return at vertical incidence.) Considering illumination and viewing angles not too close to either horizontal or vertical conditions, sea clutter in the specular direction might be expected to be relatively small (depending on surface roughness), and the possibility of observing the strong specular return from a horizontal target surface would appear to be greatest.

Vertical flat surfaces on ship-like targets will give rise to similar strong specular return for illumination and observing directions in the horizontal plane. In this case, the effects of sea clutter will depend on the particular geometry involved and there may or may not be good target contrast. To the extent that the reflecting surface approximates a flat plate in form, one would expect a pattern of lobes surrounding the specular direction and normal motions of a ship under way would be expected to bring about large fluctuations in received signal strength for bistatic observations.

Even when a bistatic viewing direction does not have a specular orientation relative to a flat surface, significant return is likely to occur from a target as complicated as a ship, arising from various scattering elements by single- or multiple-bounce modes. If important target elements take the form of dihedral or trihedral corner reflectors, they would not be expected to contribute to any but extremely small bistatic angles if the corner angles were exactly 90°. However, bistatic scattering will take place when the corner angles depart slightly from 90° and this is the more likely situation for a complex target.

Experimental data on bistatic scattering are very sparse and conditions are usually not fully specified in terms of illumination and viewing angles. Some observations were reported by Massachusetts Institute of Technology during World War II on the contrast between sea targets and clutter at S- and X-bands [51]. Their interest was in the possibility of attacking ships with homing missiles, either active or semi-active, and an airborne search gear (ASG) illuminated small cargo vessels at incidence angles between 2.2° and 10.7° above the horizontal. A probe aircraft flew over the target with a receiving antenna trained on the target by optical means.

Detailed results were not given on S-band, but in general, significant return with the low illumination angles mentioned was found in a wide angular sector on the same side of the target as the illuminator and up to 40° in elevation. Above about 40°, return was weak, and no return was detected at

angles lying between 10° on illuminator side of the vertical and 20° above horizon on opposite side. At near-grazing angles opposite the illumination, good return was obtained from the target (presumably at or near the specular direction), but lack of contrast with the strong sea clutter for these angles would make it useless for tracking.

At X-band, similar results were obtained. For lower viewing angles, the cross-sections of various ships were greater than that of the sea surface, but at higher angles the ships were lost in clutter. Roughly speaking, the cross-over occurred at viewing angles of about 40° to 60°.

7-2. Wavelength Dependence of Cross-Section

There does not appear to be a strong wavelength dependence for ship cross-sections as measured with relatively low resolution systems. While a strong wavelength dependence on the order of λ^{-4} or λ^{-5} is given for the NRL low-angle data [8-13], this is for σ_f (see Section 2-2) and includes the effect of F^4, which itself has a λ^{-4} dependence in the commonly used approximation for the R^{-8} region--namely, $(4\pi h_1 h/\lambda R)^4/9$. Since F^4 does not have an explicit wavelength dependence in the R^{-4} region, the wavelength dependence of a target would best be examined using R^{-4} data rather than R^{-8} data. Note, however, that reflection from the sea varies with wavelength and thereby affects F^4.

From the discussion above, we can infer that the overall (unresolved) target at elevation angles near grazing probably has weak wavelength dependence, perhaps on the order of λ^0 or λ^{-1}. Recent airborne measurements at somewhat higher elevation angles [21, 22] have led NRL to the conclusion that there is generally about a λ^0 dependence. The data points are scattered, but there is probably some variation in dependence associated with target azimuth.

Although there does not appear to be a very strong wavelength dependence when a complex target such as a ship is viewed as an unresolved target, the individual scattering centers should exhibit the usual behavior associated with their geometrical shape. Simple targets such as periscopes would be expected to preserve such dependence also. The particular attribute used to characterize the distribution of data would probably have a further effect on the wavelength dependence observed. That is, it may matter whether the peak, median, or some other value is used for exploring dependence; to our knowledge, this possibility has not been investigated.

7-3. Polarization Dependence of Cross-Section

Although few available data are suitable for assessing any polarization dependence of sea targets, a few general comments are possible. Most polarization data have been concerned with possible differences between VV and HH returns. Recent NRL airborne measurements on ships [21] indicate that there may be some differences which are also both wavelength and aspect dependent. The data are too few to draw more than preliminary conclusions, particularly if differences of around 5 dB are discounted as probably within the spread of experimental data.

Other data (see Section 3-1) indicate that cross-polarized (VH) return is down about 10 dB from direct polarized (VV) return at X-band for moderate elevation angles and a partially resolved target [17]. The da are too few to associate any dependence on aspect.

As in the case of wavelength dependence, it should matter whether or not the target was resolved into elemental scattering centers which might themselves exhibit polarization dependence. There is also a potentially strong polarization dependence within F^4, particularly when reflections off the sea take place at angles near the Brewster angle. The point here is that we are dealing with an overall situation involving both target and sea, and measurements are not usually made which allow the effects of each to be separated. At any rate, practical usage would always involve the combination of sea and target.

7-4. Effects of Frequency Agility

A-scope observations of ships were made by Georgia Tech under this program, using a radar located at Boca Raton, Florida. Southbound targets of opportunity were available a few miles off the coast, and were viewed by an X-band radar operating either with fixed frequency or with frequency agility. For the work reported here, the radar had a horizontal beamwidth of 0.8°, horizontal polarization, a pulse length of approximately 0.2 μsec, a logarithmic receiver with an IF bandwidth of 10 MHz, and transmitted at a prf of 3600 pps with a peak power of 250 Kw. In the agility mode, frequency was changed in forty 5-MHz steps. The antenna is 80 ft above the sea, and observations were made near grazing incidence.

Fig. 16 shows an unloaded tanker about 750 ft long for two aspect regions. The three A-scope samples in each photograph differ in time by only a few seconds, and show about 36 pulse returns each. The top-left photograph is at

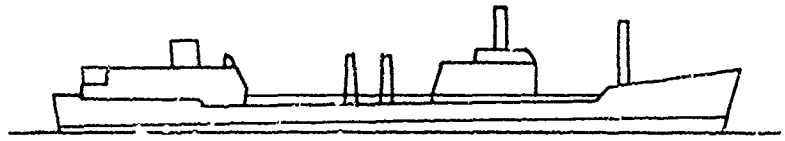

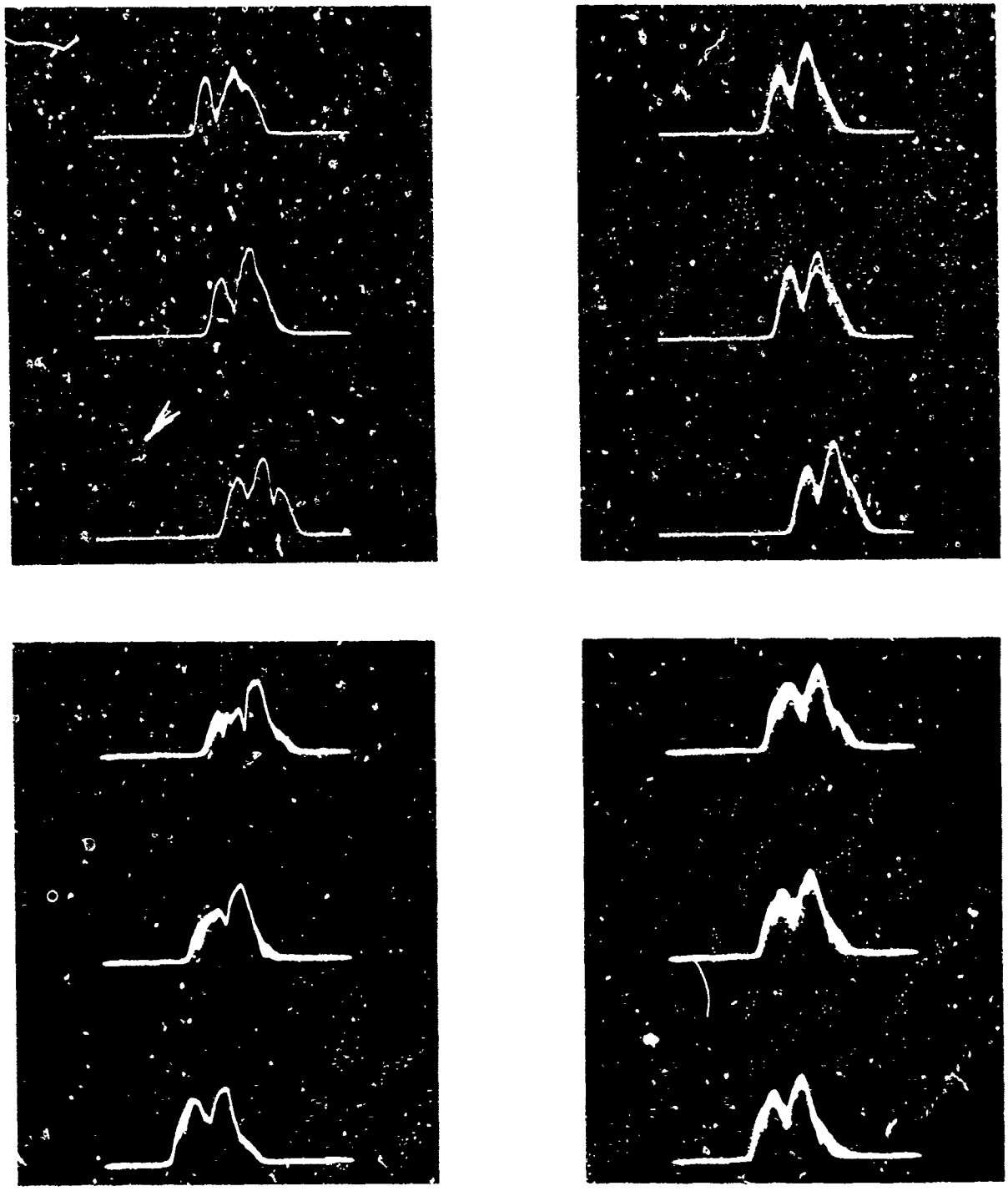

Figure 16. X-Band Radar Return from Unloaded Tanker Near Bow-On Using Fixed Frequency (Left) and Frequency Agility (Right). Top: 25° Off Bow; Bottom: 21° Off Bow..

fixed frequency for an aspect about 25° off the bow. The drastic differences in structure among the samples are characteristic of changes in the interference between various elements of a complex target; here, the changes have occurred in the few seconds between samples. On the other hand, there is little difference in the return for the 36 pulses in each sample; that is, the returns are not decorrelated in 1/100 second, but are decorrelated in a few seconds. The top-right photograph was taken about a minute later at nearly the same aspect, but now using frequency agility. Here, the individual radar returns are more nearly statistically independent and the partially resolved target shows two clearly identifiable peaks spaced about 290 ft apart, a figure which may be compared with an approximate projected distance of 315 ft between the two major blocks of the tanker superstructure at this aspect.

The lower photographs in Fig. 16 show fixed and agile samples at an azimuth of 31° off the bow. Here the distance between peaks is about 300 ft in the agile samples, corresponding to the same approximate figure for the blocks of superstructure. Return from the bow wave shows up clearly in the fixed-frequency samples as spreading of individual pulse returns, the variation implying many independent samples in the observation time of 1/100 second.

These and other similar observations provide evidence that the major portion of the return at low elevation angles is associated with features of the ship's superstructure. When the azimuth angle is such that major blocks of superstructure are separated by distances greater than the range resolution of the radar, they produce peaks in the return. These are generally identifiable with short observation times when frequency agility is used to obtain many independent samples.

It might be thought that results equivalent to the use of frequency agility could be obtained with longer sample times at a fixed frequency, thus permitting the target to take on different spatial orientations and produce enough independent samples to show a "stable" structure. For most practical situations, however, this is not true. The reason is that gross changes in aspect can occur before the relative phases between interfering elements of the target have taken on a sufficient number of combinations of values to build up a reasonably good statistical description of the return structure. For targets with very short decorrelation times (high frequency components in the variation of return), this would not be the case and fixed frequency would give

results similar to those with frequency agility. For example, note the region of return from the bow wave mentioned above.

A further point of interest is that the fewer the number of contributing scatterers within a pulse length, the less difference there will be between samples obtained with fixed and agile frequency. Thus, for a single target there is no difference, while return from two equal scatterers will vary between zero and four times that from a single target, accordingly as the two returns are exactly out of phase or in phase. Targets involving many scattering elements can also show very large spreads in return power which may or may not evidence the peaked statistical distributions that give a "non-smeared" pattern in the return structure. The differences in character between regions of the overall return for fixed and agile observations are therefore related to differences in scattering behavior caused by the physical structure of corresponding regions of the target.

7-5. Glint

Glint (also called angular scintillation, or wander) is the variation in angle experienced by a radar tracking a non-point target. It has been described as the variation in the angle of arrival of the waves reflected off the target. Although many studies have been made of the glint effect for aircraft targets, few such studies have been made for sea targets.

Observations of glint were made during World War II by the Admiralty Signal Establishment on a four-stack destroyer, HMS Lancaster (sketched in Fig. 12) [52]. A Type 274 S-band radar was set up with an antenna 105 ft above sea level. The Lancaster steamed a figure-eight course at approximately 10,000 yds range, the rate of turn being approximately 0.85° per second. Moderate variations in the apparent direction of the target were observed to occur: the maximum variation was about 5 minutes of angle, corresponding to 40 ft at the target, whose length was 309 ft. (Here the vessel's foremast, which was optically observed, is taken as the reference point.) These observations, together with theoretical considerations, led to the conclusion that errors in bearing large enough to bring the radar line of sight outside the target may occur. Errors are greatest when the target is viewed within $\pm$ 45° of broadside, and least for bow-on or stern-on aspects. Angular bearing errors are expected to be largest when the target is changing aspect very slowly, and when the magnitude of the return is low.

More recent studies [53] have indicated that glint may be reduced by using frequency-agile radars. Although system details are not given in the paper, the work was presumably done at X-band and observations are reported on two freighters.

One ship had a high bow, with major blocks of superstructure slightly forward of amidships and at the stern. This target subtended an azimuth angle of about 16 milliradians at the radar. With fixed-frequency operation, the bearing to the target varied over about 13 milliradians, and showed a fairly uniform distribution having a standard deviation of 2.8 milliradians. With frequency agility, the distribution was much more peaked, extended over about 7 milliradians, and had a standard deviation of 1.4 milliradians.

The other ship subtended an azimuth angle of about 11 milliradians, and produced bearings which varied over some 12 milliradians with fixed frequency. The distribution was slightly skewed toward the bow, and had a standard deviation of 3 milliradians. With agility, the distribution was again more peaked, extended over about 4 milliradians, and had a standard deviation of 0.7 milliradians.

7-6. Camouflage of Submarines, Snorkels, and Periscopes

A World War II study at Harvard [54] examined the possibility of using shielding screens of wire mesh to camouflage surfaced submarines. The general aim was to eliminate specular reflection and to minimize the non-specular, diffracted return. Theoretical estimates suggested that cross-section could be greatly reduced by a bell-shaped screen. A patent (U.S. No. 2,801,411) was issued on this construction.

Although no experimental studies on this screen are described in the original report, tests [55] on a prolate ellipsoidal snorkel shield showed it to be "very effective" in reducing the echo received by ship and airborne radars at low angles. Concurrent tests on a dummy periscope covered with Harp absorber gave inconclusive results, primarily because of the excessive tilting of the dummy target.

In other World War II work, the MIT Radiation Laboratory experimented with camouflaging a 1/3-scale model submarine by the use of Harp [56]. The model was tested at a range of 1750 yds using an S-band radar. Observations were made of the hull alone, the conning tower alone, and the fully assembled model, with and without coating of Harp. For the hull alone, the broadside return was reduced about 10 dB by the material, but little decrease was obtained on

the conning tower. The latter result was due to the fact that the material was effective only for near-normal incidence, and hence would not work well in the high curvatures involved in the conning-tower application. For the fully assembled model, the reduction was about 5 dB.

7-7. Propagation Effects

That propagation has a profound effect on the power returned from a surface target has long been noted. One manifestation of better-than-normal propagation is an increase in the range at which the range variation changes from R^{-4} to R^{-8}. A classic example of this is shown in Figure 1-5 of Kerr, and essentially all experimental investigators have noticed the effect with low-sited radars (for example, References 9-13, 15, 39, 40). It might be noted that the same elevated refractive-index discontinuity which traps microwave radiation and increases the range of a low-sited radar, would also serve as a reflecting surface to a radar above it, but in a manner so as to decrease the illumination at the surface and lessen the range capability for surface targets.

A somewhat more subtle effect has been observed which may affect detection of small surface targets having highly directive reradiation patterns, such as a periscope or snorkel [57]. Here, a fairly rapid variation of refractive index very close to the surface can cause a tilt in the phase front of the illuminating radiation so that the rays strike the target at a different angle of arrival from that predicted by purely geometrical considerations. A second effect of such a refractive-index variation is to compress the lobes of the interference pattern, the lowest lobe being affected most.

Although it is beyond the scope of the present report to discuss propagation effects in detail, they cannot be ignored in many practical situations. Both meteorological conditions, such as those mentioned above, and the curvature of the earth will have a strong influence on the maximum range of detection. Other propagation effects enter into the problem and should be considered in systems analysis, particularly if sophisticated radars are involved.

7-8. Desirable Features of Future Experimental Work

In future cross-section measurement programs which would be directed toward expanding general knowledge on sea targets as well as determining specific characteristics for systems purposes, we believe that the following features, while probably not all attainable for each program, would be

particularly important.* Note also that extensive data on a few targets might be more useful than fragmentary data on many targets. (1) Pulse-to-pulse recordings should be made with systems having at least 50-dB dynamic range in order to obtain meaningful statistical data, and data runs should be replicated to establish run-to-run variations. (2) Target-aspect effects should be investigated by having, insofar as possible, only one target angle (say, azimuth or elevation) vary at a time, with enough data taken to build up a picture of the variation of cross-section over the full hemisphere. (3) A range of target dynamic conditions should be investigated with respect to different combinations of target speed, sea state, etc., to establish the effects of wake, sea return, etc. (4) Effects of radar resolution on large targets should be taken into account in deciding what characteristics are to be measured and the results then interpreted in view of what was actually observed. (5) When possible simultaneous measurements should be made in more than one frequency band, and effects of changes in parameters such as polarization, resolution, frequency agility, etc., should be investigated on a time-shared basis. (6) Overall system calibration should be made using a free-space sphere target, and fixed targets on the sea would be useful in establishing the effects of changes in pattern propagation factor F for adjustment of data. (7) Ancillary information on weather, sea state, target heading and aspect, etc., should be available for interpreting measured data, as well as A-scope photographs and drawings or photographs of the target.

While there are many radar systems which might be used, each of the following has features known to be particularly applicable to such measurements. For further information the references should be consulted. (1) NRL airborne four-frequency radar [59]. (2) NRL Chesapeake Bay tracking radar facility [60]. (3) University of Texas Defense Research Laboratory airborne radars [61, 62]. (4) Tracking radars on the Advanced Range Instrumentation Ships (ARIS) operated by the RCA Service Company [63]. (5) Transportable shore-based radar operated by North American Aviation, Inc., Tulsa [64]. (6) Experimental Navy radar at Boca Raton, Florida, operated by Georgia Tech [65]. It would be particularly valuable in future work to make simultaneous measurements with shore-based and airborne radars in order to cover a wide range of elevation angles on the target and to allow intercomparison of statistical data from fixed and moving platforms.

*A number of these points are the same as those made previously by the Aerospace Corporation [58].

VIII. CONCLUSIONS AND RECOMMENDATIONS

In this report we have attempted to present a broad overview of the state of knowledge concerning the radar reflectivity of targets on the sea. Targets of many forms have been treated briefly; these include small, relatively simple targets such as periscopes and [illegible]vels, and very large, complex targets such as ships. Several approximate theories which have been advanced to explain the radar return of sea targets have been compared, and additional work on the present program has indicated the serious limitations inherent in the commonly used coherent (flat plate) model. Experimental data have been discussed and suggestions made for interpreting older (World War II) cross-section values for possible use in present-day systems studies. Based on the totality of theoretical and experimental evidence available to us, we have conjectured the form of the variation of return power with range.

The single most important underlying feature of all the discussions in this report is that the effective radar cross-section of a sea target is modified from its inherent ("free-space") cross-section by the presence of the sea in a manner that may or may not be determinable. The use of the pattern propagation factor F allows us conceptually to think of effective cross-section σ as the product of F^4 times the free-space cross-section σ_o. Ideally, we should be able to determine the F^4 which prevailed during an experimental measurement of σ, remove it to obtain σ_o, and then apply another F^4 to establish the appropriate effective σ for systems analysis. That this cannot be done precisely is very clear; the only data that are available usually have F^4 inextricably bound into the results and this fact must be appreciated.

Two of the striking features of experimental data on sea targets are the extremely large temporal fluctuations in return power and the wide differences between smoothed results of different experimenters who have measured cross-section. It is suggested that the existence of this variability is genuine and is as important to the systems designer as the knowledge of a single-number estimate of cross-section. Full statistical information on all targets of interest and the associated environmental conditions is not likely to be available soon. Meanwhile, estimates of inherent target properties, F^4 for appropriate combinations of geometry and radar parameters, and the general character of the variations to be expected in effective cross-section will have to be used.

There appears to be some possibility that our theoretical understanding of the problem can be improved with the hope of predicting at least gross values of cross-section for targets of interest. The gathering of extensive experimental data on a very few targets (rather than a little data on many targets) is suggested as being basic to an eventual understanding of the problem, and such a step is recommended. Additional studies to develop mathematical models of the scattering process for targets on the sea should accompany such work.

APPENDIX

THEORETICAL ASPECTS OF REFLECTION BY TARGETS ON THE SEA

In this Appendix we will summarize the general characteristics of several approximate theories which have been used for targets on the sea, supplemented by the results of some additional work performed on the present program. Since fairly detailed treatments of the basic points are contained in several readily available references, much of the development will be merely sketched. The reader is referred to Kerr [3], Durlach [4], and Katzin [5] for additional information; all three references should be consulted since their treatments emphasize different points. Our summary most closely follows Sections 2-2, 2-13, 5-4, and 6-5 of Kerr.

A-1. Reflection from the Sea Surface

A-1.1. Reflection Coefficient

A fundamental consideration in treating the reflectivity of targets on the sea is that both direct illumination and indirect illumination via reflection off the surface are involved. The reflection coefficient Γ of a smooth, plane surface can be expressed as

$$\Gamma = \rho e^{-j\varphi} \quad , \tag{A-1}$$

where ρ = magnitude, and

φ = phase shift on reflection.

The coefficient Γ is thus complex and depends on many parameters, among them being wavelength, grazing angle, and polarization. Usually the polarization dependence is treated by defining two coefficients, Γ_H and Γ_V, for horizontal and vertical polarization, respectively.

For a smooth, flat sea surface and for horizontal polarization, $\rho \approx 1$ and $\varphi \approx \pi$ for all grazing angles and all commonly used radar wavelengths.

For vertical polarization, $\rho \approx 1$ and $\varphi \approx \pi$ only for very low grazing angles and, as the grazing angle is increased, φ decreases and becomes essentially zero at vertical incidence. Concurrently ρ decreases until $\varphi = \pi/2$ and increases thereafter. The angle for which $\varphi = \pi/2$ and ρ is at a minimum is frequently called the pseudo-Brewster angle.

A reflection coefficient as defined above for a smooth plane surface is not completely suitable for treating reflection from the surface of the sea. Where long path distances are involved the curvature of the earth can have a significant effect on the apparent reflection coefficient. Rays reflecting from a convex surface diverge after reflection, causing an apparent lowering of the magnitude of the reflection coefficient. This effect is commonly accounted for by multiplying ρ by a divergence factor $\mathcal{D}$ which takes on only real values between zero and one (for a detailed discussion of the divergence factor, see pp 113-115 of Kerr).

Roughness of the sea surface due to waves and swell can also lower the effective magnitude of the reflection coefficient by scattering radiation in non-specular directions. The Rayleigh roughness criterion from optical theory is commonly used to determine the maximum surface irregularity that will not significantly lower the reflection coefficient (Kerr, p 411). This theory states that if the surface irregularities introduce path-length variations substantially less than one wavelength ($\lambda/4$ is frequently assumed), then the surface will reflect essentially as a smooth surface. For a ray incident at a grazing angle of ϵ on a surface with maximum peak-to-trough variations of h_{sea}, this requires that

$$h_{sea} \sin \epsilon \leq \lambda/8 \quad . \tag{A-2}$$

Any time that Eq. (A-2) is satisfied, the surface can be assumed to be

essentially smooth. Note that even a surface with quite large waves or swells will still appear smooth for sufficiently small grazing angles or long wavelengths.

For a given h_{sea} and λ, there is an angle ϵ below which all of the reflected energy can be assumed to be concentrated in a specularly reflected wave. If the grazing angle is many times larger than this angle, then the specularly reflected wave may disappear entirely with the reflected energy being scattered diffusely over the hemisphere above the surface.

The effect of roughness on the magnitude of the reflection coefficient has been accounted for by use of a roughness factor $\mathcal{R}$ having values between zero and one [66]. The overall reflection coefficient of the sea may therefore be taken to be

$$\Gamma = \mathcal{D}\,\mathcal{R}\,\rho e^{-j\varphi} \quad . \tag{A-3}$$

A-1.2. Geometry of Reflection

The geometry of the general case of specular reflection from a spherical earth is illustrated in Fig. A-1. Assume that a radar at height h_1 above

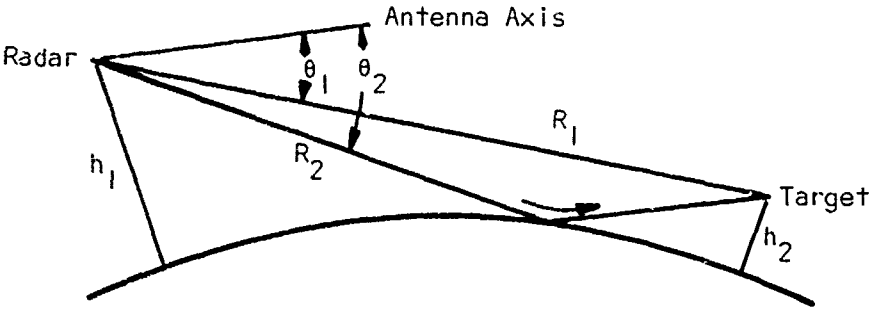

Figure A-1. Spherical-Earth Geometry.

a spherical earth is illuminating a target at height h_2. The field at the target due to the direct ray alone can be represented as

$$E_d = E_o f(\theta_1) e^{-jkR_1} \quad , \tag{A-4}$$

where E_o = magnitude of the free-space field at the target if the antenna axis were pointed directly toward the target,

$f(\theta_1)$ = antenna gain function for the direct ray,

R_1 = direct path length, and

$k = 2\pi/\lambda$.

Using Eq. (A-3), the field at the target due to the indirect ray can then be expressed as

$$E_i = \mathcal{D}\mathcal{R}\rho E_o f(\theta_2) e^{-j(kR_2 + \varphi)} \quad . \tag{A-5}$$

The total field is given by $E = E_d + E_i$, hence

$$E = E_o\left[f(\theta_1)e^{-jkR_1} + \mathcal{D}\mathcal{R}\rho f(\theta_2)e^{-j(kR_2 + \varphi)}\right] . \tag{A-6}$$

Because of reciprocity, energy scattered by the target back toward the radar will traverse the same two paths, and be subject to the same reflection effects and antenna gains as was the illuminating energy. Thus the received field at the radar will be proportional to E^2 as defined by Eq. (A-6), and the power received will be proportional to E^4. Note that the possibility of interference between direct and reflected rays, which leads to the usual interference lobes, is inherent in Eq. (A-6).

A parameter which has been widely used in studies of the effect of surface reflection is the pattern propagation factor F. This factor is defined to be the ratio of the magnitude of the actual field at the target

to the magnitude of the field which would exist if the target were in free space and the antenna pointed directly at it; hence

$$F = \frac{|E|}{|E_o|} \quad . \tag{A-7}$$

With F thus defined, the power received from a point target can be obtained by multiplying the usual free-space radar equation by F^4,

$$P_r = [P_t G^2 \lambda^2 \sigma_o / (4\pi)^3 R^4] \, F^4, \tag{A-8}$$

where the symbols have their usual meanings except that σ_o is emphasized as being the free-space radar cross-section.* Use of F then permits the radar cross-section as defined for free-space situations to be retained.

Any attempt to measure cross-section of a target on the sea actually results in measuring an effective cross-section $\sigma = F^4 \sigma_o$. An estimate of σ_o could be obtained from such a measurement provided F were known with reasonable accuracy. This concept is quite valid if the target is a point target, and the geometry, propagation conditions, etc., are accurately known. Considerable difficulty has been encountered, however, in trying to apply the concept to extended targets; this problem is discussed in more detail later in this Appendix.

A-3b. Consequences of Multipath Propagation

As shown in Fig. A-1 and expressed mathematically in Eq. (A-6), the target is illuminated along two different paths when surface reflection is involved. Energy may travel to the target on either the direct or indirect

*The symbol σ used here should not be confused with the symbol σ_o or σ^o used for radar cross-section per unit area in studies of sea and ground return.

(surface-reflected) path, and may also return to the radar over either path. If the direct path is indicated by D and the indirect path by I, there are four possibilities for two-way transmission: DD, DI, ID, and II. These paths are illustrated in Fig. A-2.

Since the paths are of different lengths, it follows that return pulses from a single target point will not all coincide in time at the receiver. Referring to Fig. A-2, it can be seen that the four paths have only three different path lengths: path DD is the shortest, path II is the longest, and the two paths DI and ID have the same length intermediate between the other two. Due to these differences in path lengths, the radar actually receives three different pulses separated in time.

If the difference in path length between direct and indirect paths is denoted by ΔR and the velocity of propagation by c, then the pulses traveling the DI or ID paths will lag behind the pulse traveling the DD path by $\Delta R/c$, and the pulse traveling the II path will lag by $2\Delta R/c$. In many practical cases, the pulse length τ will be long compared to $\Delta R/c$ and the three return pulses will overlap considerably as shown in Fig. A-3(a). In this situation, interference can occur between energy transmitted along the different paths and the concept of lobe-type illumination is valid.

In another case, the pulse length τ can be less than the time difference $\Delta R/c$ and the radar then receives three pulses separated in time as shown in Fig. A-3(b). This effect is usually important only when the grazing angle is not too small and the target height is at least moderately large. For example, a grazing angle of 10° and a target height of 50 ft will give a time difference $\Delta R/c$ of about 30 nsec. It should be noted that, while the DD ray is not affected by the surface reflectivity, the magnitude of the DI and ID rays will be multiplied by $|\Gamma|$ and that of the II ray by $|\Gamma|^2$.

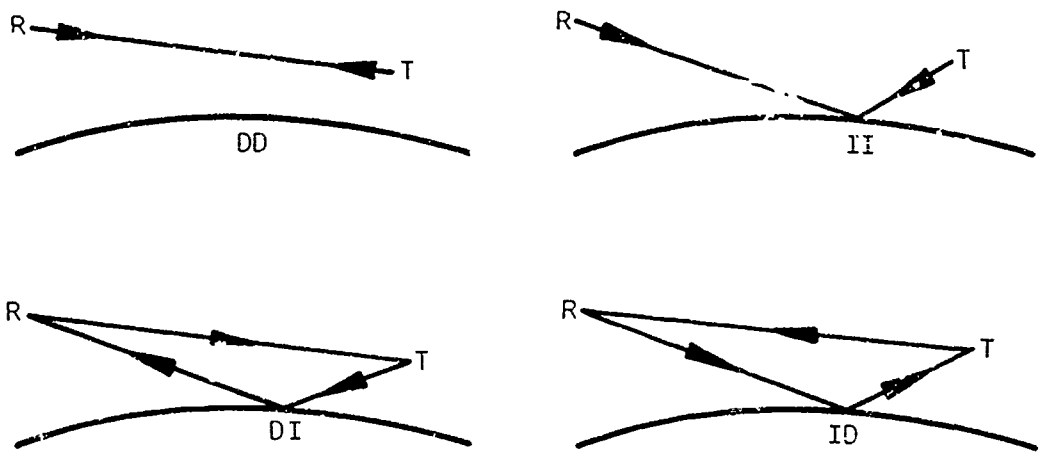

Figure A-2. Four Possible Radar-Target Paths when Surface Reflections are Involved.

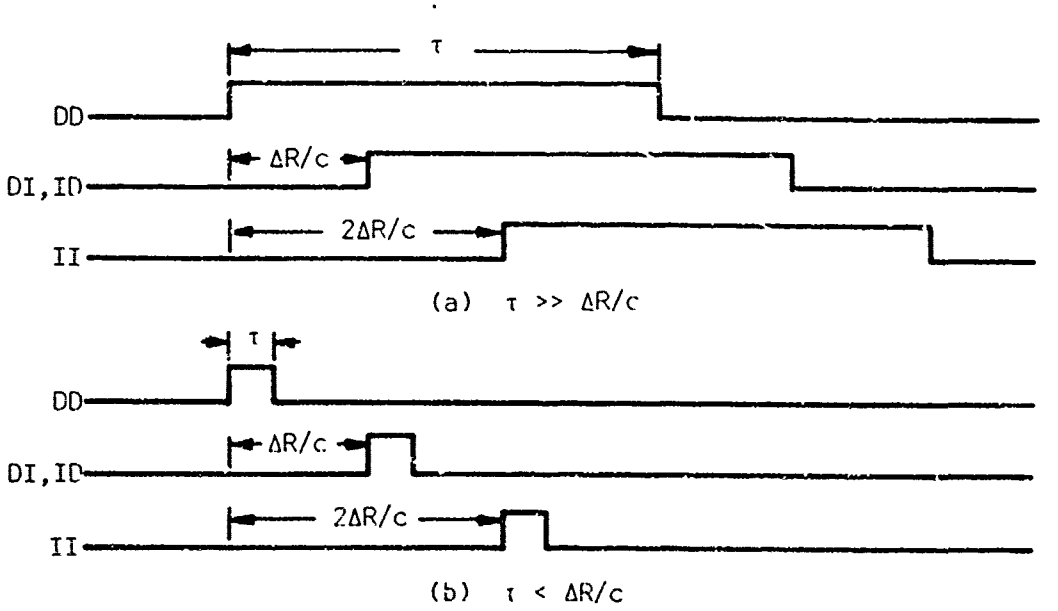

Figure A-3. Time Relationships of Multipath Received Pulses for Long and Short Pulse Lengths.

It is frequently assumed that the reradiation pattern of the target has a large enough lobewidth that both direct and indirect paths are equally illuminated by the reflected energy. For some geometries this requires a very wide lobewidth which is not compatible with an efficient scatterer. Should a scatterer have a diffraction minimum in the direction of one path or the other, the effect of that path would be diminished. A target such as a dihedral or trihedral corner reflector with corner angles of exactly 90° is a highly efficient retrodirectional scatterer but very little energy is reflected in other directions, with the result that the DD and II paths might exist but not the other two.

A-2. Extended Vertical Targets at Low Grazing Angles

Several approaches have been taken in solving the problem of a target extending upward from the surface and (usually) having uniform free-space cross-section as a function of height. Much of this work has been carried out using several simplifications, among them being the assumptions of a flat earth ($\mathcal{D} = 1$), a smooth surface ($\mathcal{R} = 1$), perfect reflection ($\rho = 1$ and $\varphi = \pi$ so that $\Gamma = -1$), and maximum antenna gain on both paths ($f(\theta_1) = f(\theta_2) \approx 1$). These assumptions are particularly applicable for low grazing angles and horizontal polarization. With these assumptions, Eq. (A-6) can be rewritten as

$$E = E_o \left[e^{-jkR_1} - e^{-jkR_2} \right] \qquad \text{(A-9a)}$$

$$= E_o e^{-jkR_1} \left[1 - e^{-jk\Delta R} \right] , \qquad \text{(A-9b)}$$

where $\Delta R = R_2 - R_1$.

It will be convenient in the work that follows to approximate R_1 and ΔR as is done in Section 2-2 of Kerr for the case of h_1 and h_2 small compared

to R. The results are

$$R_1 \approx R[1 + (h_2 - h_1)^2/2R^2] \quad \text{and} \tag{A-10}$$

$$\Delta R \approx 2h_1h_2/R \quad . \tag{A-11}$$

Strictly speaking, F as defined in Eq. (A-7) is a scalar quantity and would be the magnitude of the bracketed factor in Eq. (A-9). While the use of F^4 as a scalar in Eq. (A-8) is entirely satisfactory when both σ_o and F^4 refer to the overall target, we shall see that F itself must be treated as a phasor in arriving at an average F^4 for an extended target which itself involves phase (i.e., a coherent target).

First, let us consider a point target where only the magnitude of F is important. As given in Section 2-2 of Kerr and elsewhere, the conditions assumed above lead to

$$F_o = 2\,|\sin \Delta/2| \quad , \tag{A-12}$$

where $$\Delta = k\Delta R = 4\pi h_1 h_2/\lambda R \quad ,$$

and the subscript has been added to identify the F applicable to this particular target form. The effective cross-section of a point target can then vary between 0 and 16 times its free-space value according to the variation in

$$F_o^4 = 16 \sin^4(\Delta/2) \quad . \tag{A-13}$$

In considering an extended target, one model has been taken to be a collection of independent random scatterers [34, 39, 67], either uniformly distributed with height or having some simple weighting function. The effective F^4 for this incoherent target model is found by averaging F_o^4 over the

target height h, using the appropriate weighting for vertical distribution of cross-section. Once again, only the magnitude of F is important. For the case of uniform height distribution of scatterers, the integration is simple and

$$F_1^4 = 16 \int_0^h \sin^4(2\pi h_1 h_2/\lambda R)\, dh_2 \;\div\; \int_0^h dh_2$$

$$= 6 - \frac{8 \sin \Delta - \sin 2\Delta}{\Delta}$$

$$= 6 \left[1 - \frac{\sin \Delta\, (4 - \cos \Delta)}{3\Delta}\right] , \qquad \text{(A-14)}$$

where now the h_2 in Δ is replaced by h and F_1^4 is actually an average over h.

Another frequently used model is that of a "coherent" flat plate extending upward from the surface. Since scattering can be treated on the basis of either electric or magnetic fields, we will use here the result for the magnetic field from Section 6-5 of Kerr. For a target consisting of a flat plate of width b extending between heights h_a and h_b, the magnetic component of the field at the radar is given by

$$H = (-jH_o b/\lambda R) \int_{h_a}^{h_b} e^{-j2kR_1} \left(1 - e^{-jk\Delta R}\right)^2 dh_2 , \qquad \text{(A-15)}$$

where H_o is the strength of the incident magnetic field. Substituting the approximations of Eqs. (A-10) and (A-11), this can be written as

$$H = (-j4H_o b/\lambda R)\, e^{-j2kR(1 + h_2^2/2R^2)} \int_{h_a}^{h_b} e^{-jkh_2^2/R} \sin^2(\Delta/2)\, dh_2 . \qquad \text{(A-16)}$$

We may note here that the integrand of Eq. (A-15) is the same as the bracketed factor of Eq. (A-9a) and, hence, its magnitude is F. However, here the phase factor appears under the integral sign and we should now interpret F as being a phasor. In the customary treatment of the vertical plate in Section 6-5 of Kerr and elsewhere [6, 68], the phase factor in the integrand of Eq. (A-16) is neglected. (This is equivalent to assuming that the phase of the resultant of the direct and indirect rays is uniform over the extent of the target.) Under these assumptions, Eq. (A-16) can be evaluated between the limits $h_a = 0$ and $h_b = h$ to obtain

$$H = [2H_o bh/\lambda R][1 - (\sin \Delta)/\Delta] \quad . \tag{A-17}$$

The effective cross-section is then

$$\sigma = 4\pi R^2 \, |H/H_o|^2 = 4\sigma_o[1 - (\sin \Delta)/\Delta]^2 \quad , \tag{A-18}$$

where σ_o is the normal incidence, far-field cross-section of a flat plate,

$$\sigma_o = 4\pi(bh/\lambda)^2 \quad .$$

Since $\sigma = \sigma_o F^4$, then

$$F_2^4 = 4[1 - (\sin \Delta)/\Delta]^2 \quad . \tag{A-19}$$

We have carried out another analysis of this problem in which the phase of the direct ray was assumed to be uniform over the vertical extent of the target, but the variation in phase of the reflected ray was retained. In this approach to a coherent target, the analysis amounted to evaluating Eq. (A-15) with the only approximations being that the direct-wave phase term, e^{-j2kR_2},

was dropped and the approximate expressions for R_1 and ΔR given by Eqs. (A-10) and (A-11) were used. The results give

$$F_3^4 = 1 + \frac{\sin 2\Delta - 4 \sin \Delta}{\Delta} + \frac{3 \cos 2\Delta - 16 \cos \Delta + 13}{2\Delta^2}$$

$$= 1 - \frac{2 \sin \Delta (2 - \cos \Delta)}{\Delta} + \frac{(3 \cos \Delta - 5)(\cos \Delta - 1)}{\Delta^2} \quad . \qquad \text{(A-20)}$$

A-3. Comparison of Results for Extended Vertical Targets

The assumptions and approximations used in this analysis have given us results which are particularly easy to compare, since each form of F^4 obtained is a function only of the dimensionless parameter Δ. Plots of Eqs. (A-13), (A-14), (A-19), and (A-20) are shown in Fig. A-4 and each form of F^4 increases rapidly as Δ increases from zero. (Note that an increase in Δ may be interpreted as an increase in radar or target height, or as a decrease in wavelength or range. In any case, an increase in Δ implies an increase in the number of interference lobes of the illuminating field which are subtended by the target.)

Although F_o^4 for the point target oscillates between values of 0 and 16, each of the other target models exhibits oscillations of diminishing amplitude about an asymptotic value of F^4 as $\Delta \to \infty$; $F_1^4 \to 6$, $F_2^4 \to 4$, and $F_3^4 \to 1$. (The asymptotes of the two latter forms are suspect, as discussed below.) Considering the behavior as $\Delta \to 0$, we note that the curve of F_o^4 remains above the other curves, that F_1^4 remains above F_2^4 and F_3^4, and that the latter two merge and finally follow one common curve.

To a good approximation, all the curves of F^4 as $\Delta \to 0$ can be represented as being of the form $K\Delta^4$. Because of the R^{-1} factor contained in Δ, this approximation gives an additional factor of R^{-4} in the modified radar equation, Eq. (A-8). This then leads to the prediction of an R^{-8} dependence between received power and range, as is discussed by many authors.

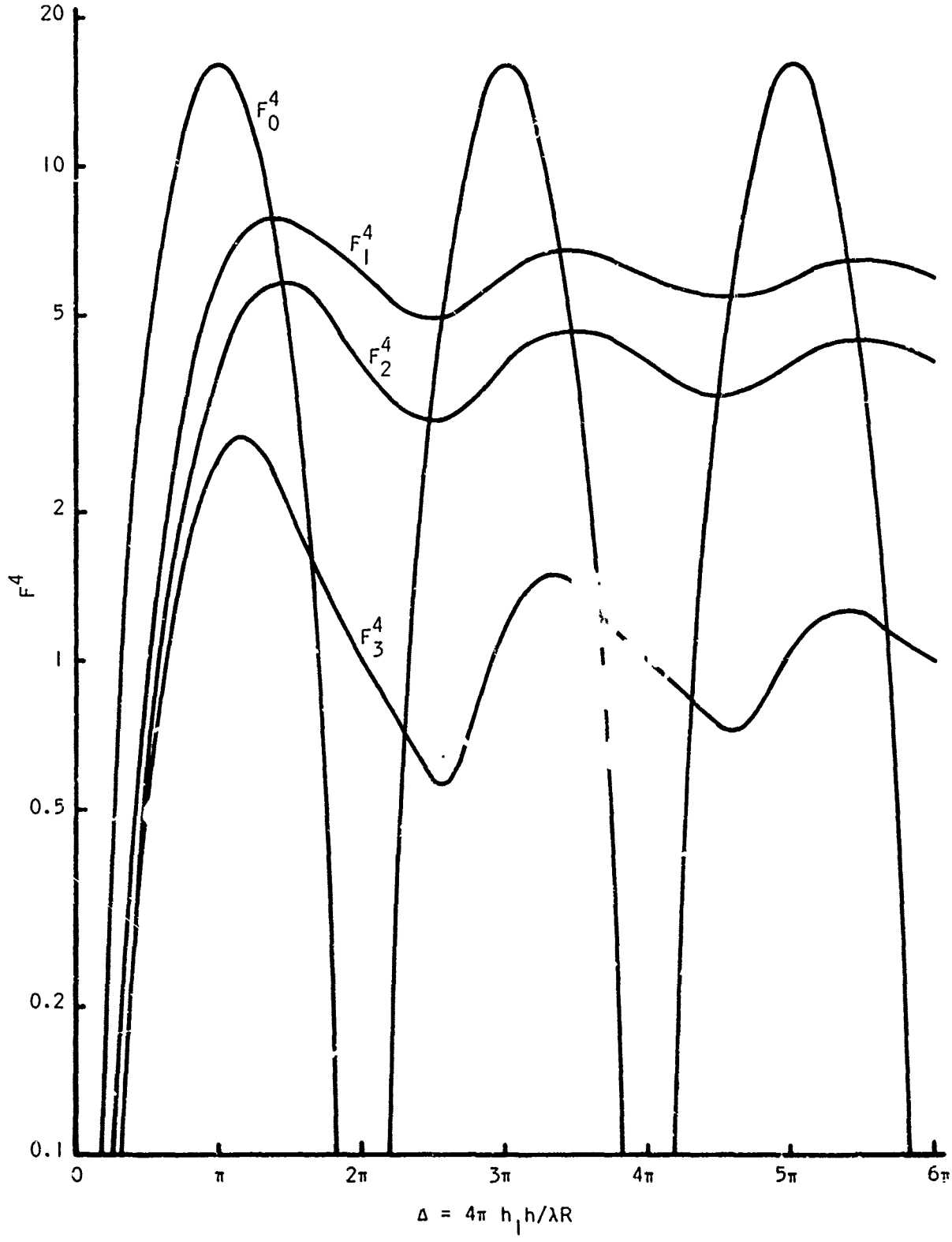

Figure A-4. Variation of F^4 vs.Δ for Point Target and Incoherent and Coherent Models of an Extended Vertical Target.

It has become customary to associate the term "transition range," designated R_t, with the range at which the value of F^4 using the small-Δ approximation is equal to its asymptotic value. (We may note that it is in this very region that the approximation departs most from the actual curve.) This then is taken as the point where the decrease in return power vs. range changes from an R^{-4} behavior to R^{-8}. Table A-I presents the values of F^4 as

Table A-I

Characteristics of F^4 for Various Target Models

Model	Approx. $\Delta \to 0$	Asymp. $\Delta \to \infty$	$\lambda R_t / h_1 h_2$
F_o^4 Point	Δ^4	none*	4*
F_1^4 Incoherent	$\Delta^4/5$	6	5.37
F_2^4 Coherent (uniform phase of resultant illumination)	$\Delta^4/9$	4	5.13
F_3^4 Coherent (uniform phase of direct illumination)	$\Delta^4/9$	1	7.26

*Peaks are tangent to $F_o^4 = 16$; R_t taken to be where $\Delta = \pi$.

$\Delta \to 0$ and $\Delta \to \infty$, together with the resulting values of R_t for the four forms of F^4 derived above.

We wish to point out here that the value of R_t is strongly affected by the choice of model used. For the point model the transition range is taken to be that at which the target height equals the height of the maximum of the lowest interference lobe and this gives the lowest value for R_t of the various models considered. Since gross approximations are necessary in defining target scattering properties, the point-target estimate is perhaps as useful as any. Effective target height (which directly affects transition range) is particularly difficult to establish for extended targets. Also earth curvature and

propagation conditions strongly affect R_t. We note further that the existence of an R^{-8} region and a consequent R_t is the direct result of having an interference lobe in the illuminating field. The specific value of the exponent (-8) is the result of the approximation to F^4 and should not be expected to give a curve exactly matching experimental data.

A-4. Further Investigation of the Flat-Plate Model

Since the two methods of approximating F^4 for a coherent flat plate gave such different results, some further investigation was undertaken. The F_3^4 approximation given by Eq. (A-20) should provide the more accurate result, provided that phase variations in the direct wave could be neglected, an assumption which would only be valid if the direct wave were normal to the surface and the plate did not exceed a certain size. Investigation of the maximum plate size for which the assumption was valid revealed that the values of h_1, h, λ, and R had to be such that essentially only one or two lobes of the interference pattern could be on the plate. Any time these parameters were such that more lobes were subtended by the plate, phase variations in the direct wave were too large to be neglected. This implies that the tendency toward an asymptote which requires many lobes to be on the plate is simply a mathematical fiction with no physical significance. This limitation does not apply to F_1^4 since random phase has been assumed and we have averaged out all phase effects.

Since the approximations leading to F_2^4 were obtained from even more gross assumptions on phase uniformity, it appears that the same statement applies and that asymptotes to both F_2^4 and F_3^4 are meaningless. Another way of saying this is that by the time more than one or two interference lobes are on the plate, the plate size has become so large that we must consider Fresnel (near-field) rather than Fraunhofer (far-field) diffraction.

In still further analysis, the integral shown in Eq. (A-15) was evaluated for $h_a = 0$ and $h_b = h$ with all phase information retained. This requires use of Fresnel integrals with the only approximations introduced being those of Eqs. (A-10) and (A-11), which are very good wnen h_1 and h_2 are small compared to R. Evaluating the return and dividing by the free-space return of the same target when viewed at normal-incidence gave

$$F_4^4 = \left| \frac{F'[2(h - h_1)/\sqrt{\lambda R}] - 2e^{-j2\pi h_1^2/\lambda R} F'[2h/\sqrt{\lambda R}] + F'[2(h + h_1)/\sqrt{\lambda R}]}{2F'[h/\sqrt{\lambda R}]} \right|^2 , \quad \text{(A-21)}$$

where $F'(x) = C(x) - jS(x)$,

and $C(x)$ and $S(x)$ are the usual Fresnel integrals.

A program for the Burroughs B-5500 computer was constructed to evaluate Eq. (A-21). Of course, the computations had to be made for specific values of h_1, h, λ, and R since the generality of being able tc express F^4 in terms of the single dimensionless parameter Δ is lost when all the phase information is retained. (The Russian work of Section A-7 uses natural units--Kerr, pp 96-98.)

Some examples of the variation of F_4^4 as a function of h are shown in Figs. A-5, A-6, and A-7, along with F_2^4 and F_3^4 computed for the same parameters. It should be recognized that these are only samples and do not show all the variations that can occur. In fact, these studies show that the curves of F_4^4 vs. h vary widely with the particular values of h_1, λ, and R; there does not exist a "typical" curve which is characteristic of all those that can occur.

In comparing the three curves shown in each of the figures, it should be noted that F_4^4 is normalized in a slightly different manner than the other two. Both F_2^4 and F_3^4 were normalized by dividing the radar return from the target in the presence of reflection by the free-space, <u>far-field</u>, normal-incidence return

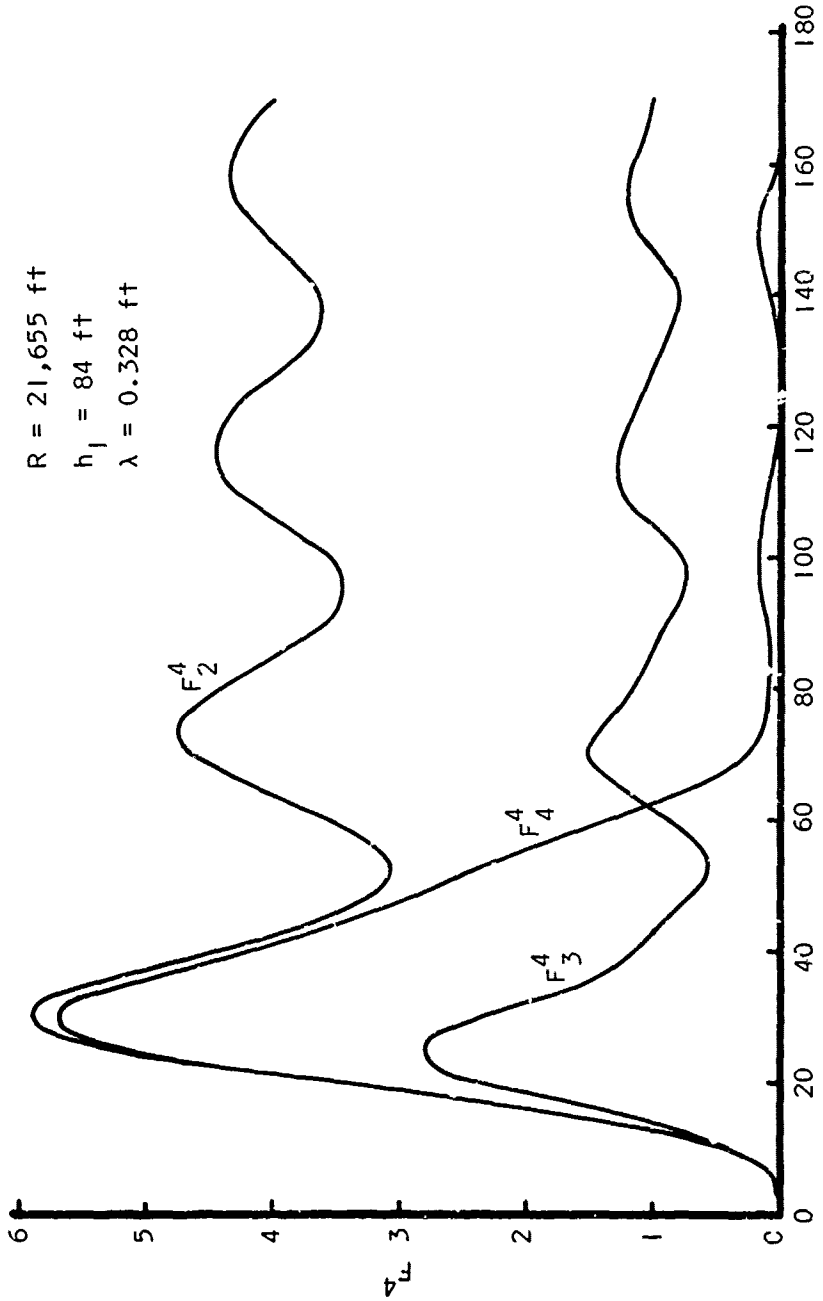

Figure A-5. Variation of F^4 vs. Target Height for Three Coherent Models of Extended Vertical Target.

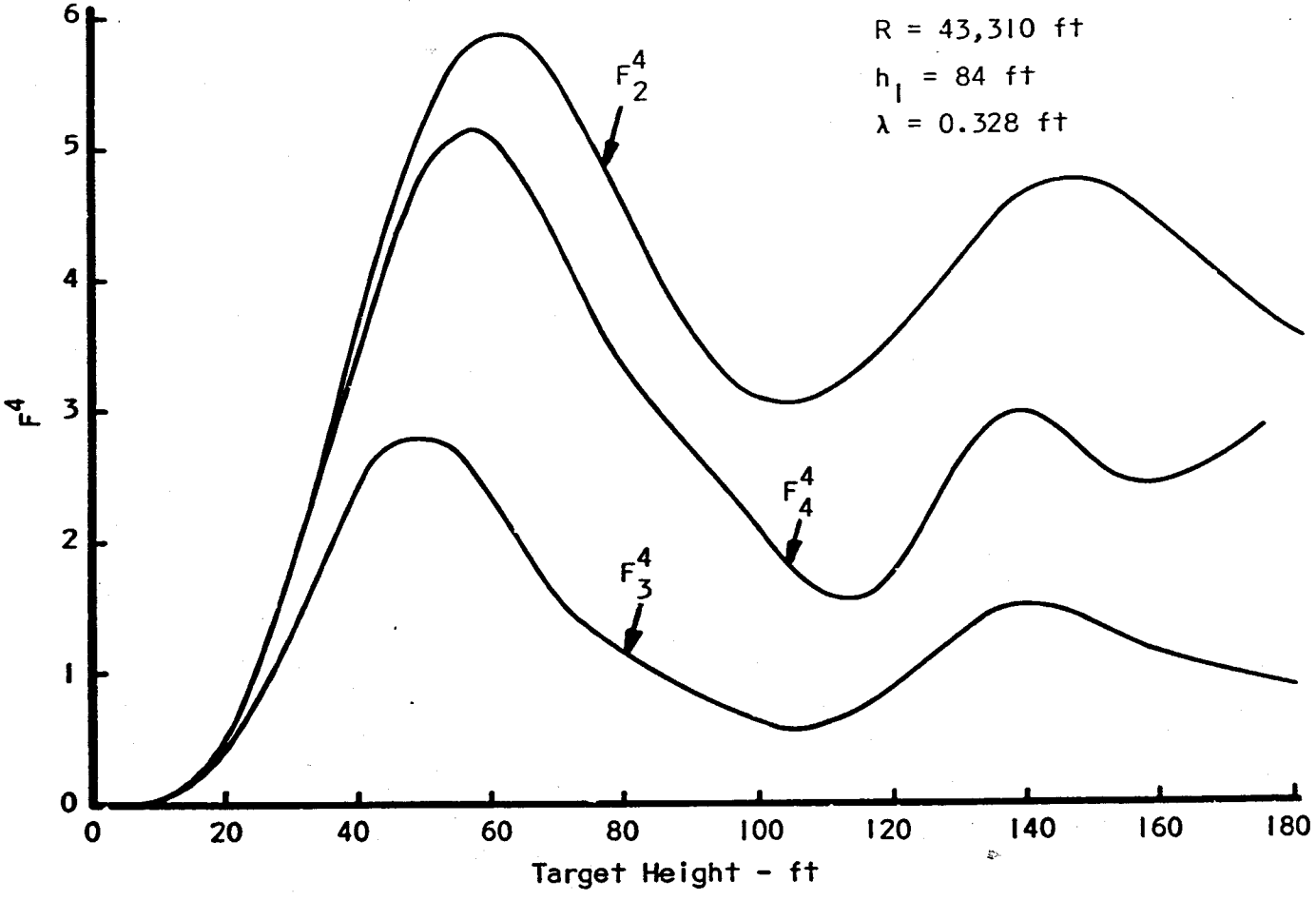

Figure A-6. Variation of F^4 vs. Target Height for Three Coherent Models of Extended Vertical Target.

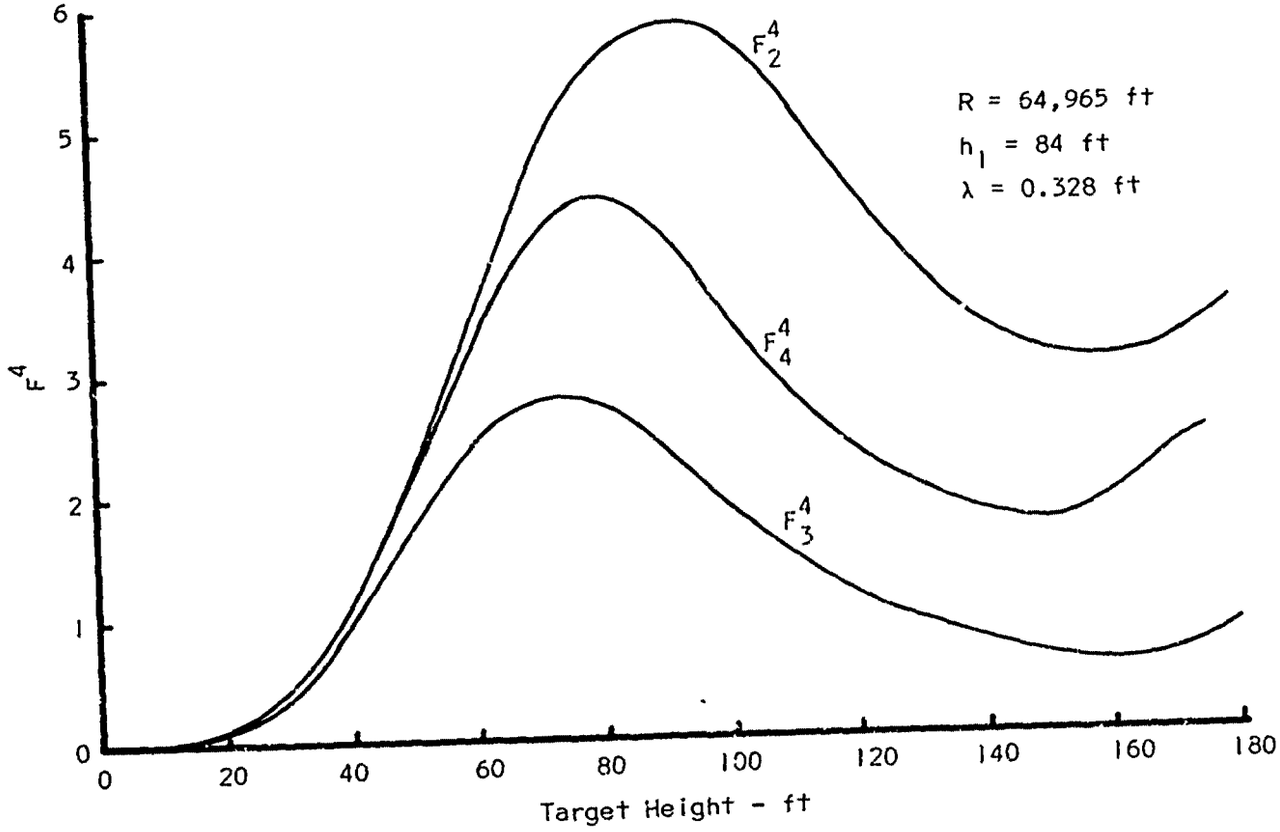

Figure A-7. Variation of F^4 vs. Target Height for Three Coherent Models of Extended Vertical Target.

(no phase considered). In computing F_4^4, the free-space, normal-incidence return at the actual distance involved was computed in each case (all phase information retained) and used as the normalizing factor. This method of normalizing can make a decided difference at the shorter ranges.

Note that over the first lobe, F_4^4 agrees very closely with F_2^4 for the shortest range (21,665 ft). As the range is increased to two and three times this value the amplitude of F_4^4 over the first lobe decreases and begins to approach the values of F_3^4 more closely. The graphs of F_4^4 resemble those of F_2^4 and F_3^4 in that each tends to rise sharply as h initially increases from zero.

As h increases to larger values, F_4^4 tends eventually to approach an asymptotic value. However the value of the asymptote is highly dependent on the phase factor $e^{-j(2\pi h_1^2/\lambda R)}$ in Eq. (A-21), and may have any value between 0 and 4. If range instead of plate height is chosen as the independent variable, the asymptotic behavior is quite different and is determined by the relation between plate height and antenna height. Since such behavior is not substantiated in general by measured data, the implication is that a uniform plate extending vertically from the surface is really not a satisfactory model for a complex target such as a ship.

A-5. Vertical Plate Elevated Above Surface

The radar return from a complex target such as a ship may be dominated at some aspects by the return from a relatively few areas on the target. Regular surfaces, both flat and curved, dihedrals, etc., can return very strong signals at times. Also the vertical dimension of any given "hot-spot" (major scattering center) may be small compared to the overall size of the target. Thus, even if several lobes of the interference pattern are distributed over the target, the hot-spot may still be confined to a fraction of one lobe.

In such a case, relative motion between an elevated hot-spot and an interference-pattern lobe can cause significant variations in the radar return from that spot.

A theoretical estimate of the return from an elevated target can be obtained by averaging F between the heights h_a and h_b which bound the target. An evaluation was made retaining both limits in Eq. (A-15) and the result can be simply related to Eq. (A-21). If this equation is regarded as being of the form

$$F^4 = \frac{|f(h)|^2}{|g(h)|^2} \quad , \tag{A-22}$$

then F_5^4 for a plate extending between heights h_a and h_b can be written as

$$F_5^4 = \frac{|f(h_b) - f(h_a)|^2}{|g(h_b - h_a)|^2} \quad . \tag{A-23}$$

Eq. (A-23) provides a means of estimating the average value of F^4 for a coherent plate extending between two arbitrary heights. Of special interest, however, is the variation in the return from a plate of fixed size as it takes on different positions in an interference lobe. Such relative motion between a hot-spot on a ship target and the interference pattern might be caused by roll, pitch, or heave of the ship, or by bending of the interference pattern due to atmospheric effects. If a plate whose vertical dimension is less than one lobe width is moved up or down in the interference pattern, return from the plate should be maximum when the plate is centered on a lobe maximum. Similarly, the return should be minimum where the plate is centered on a lobe minimum (null).

A computer program was constructed to evaluate Eq. (A-23) and calculations were made for plates of varying vertical size which were centered on maxima and minima. These runs were made for R = 12,993 ft , h_1 = 81 ft , and λ = 10 cm ; the parameters give a lobe width of approximately 24 ft. Graphs of F_5^4 as a function of the plate's vertical dimension are shown in Fig. A-8 for plates centered on several different nulls and peaks. For zero plate width (i.e., a point target), F_5^4 would be 16 (12 dB) for a peak and zero for a null. For any given plate size, comparison of F_5^4 for the plate centered on a peak with that for the plate centered on an adjacent null gives a measure of the fluctuation in radar echo to be expected if the plate moved between these two points, a distance of about 12 ft for this example. Obviously very large variations in return power could occur for some plate sizes.

Another situation that was investigated briefly was the range variation of F_5^4 for an elevated flat plate at a fixed height. As might be expected intuitively, the results were intermediate between those for a point target and for one extending upward from the surface to a certain height. In particular, the oscillations were damped out, as contrasted to the situation for the point target, but the damping was not rapid. The relative peaks were smooth topped, as for the target extending up from the surface, while the relative nulls were much more cusped, more like the sharp nulls of the point target. This was only a preliminary investigation and the area should be a fruitful one for additional work, since there is some evidence that experimental data might fit this pattern (see Chapter V).

A-6. Tilted Linear Targets at Low Grazing Angles

The radar cross-sections of simple coherent targets extending upward from the surface of the sea and tilted slightly away from vertical have been studied by several investigators. We note that the effects of the height-varying field may be treated most generally by considering a linear aperture

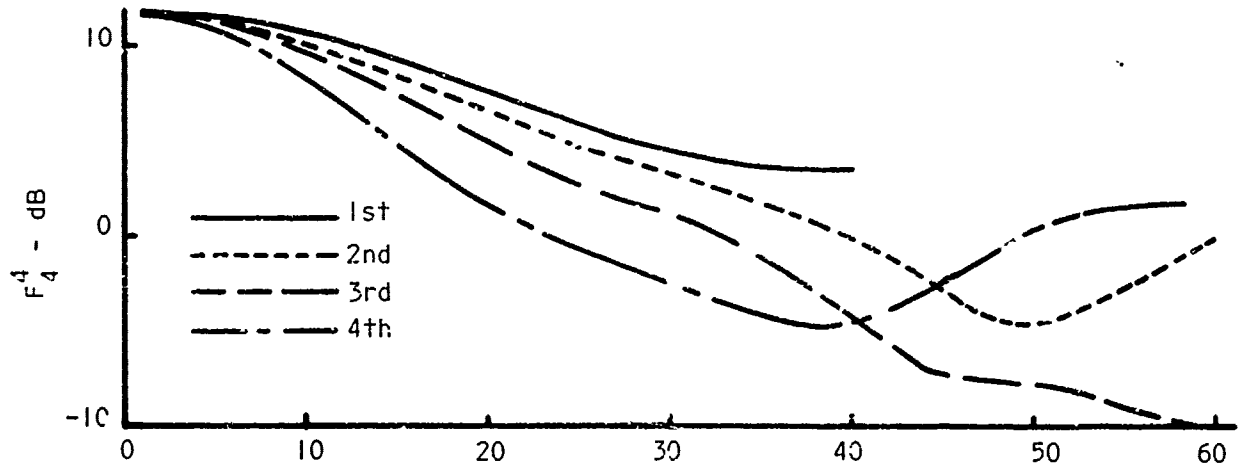

(a) Target Centered on Interference Maximum

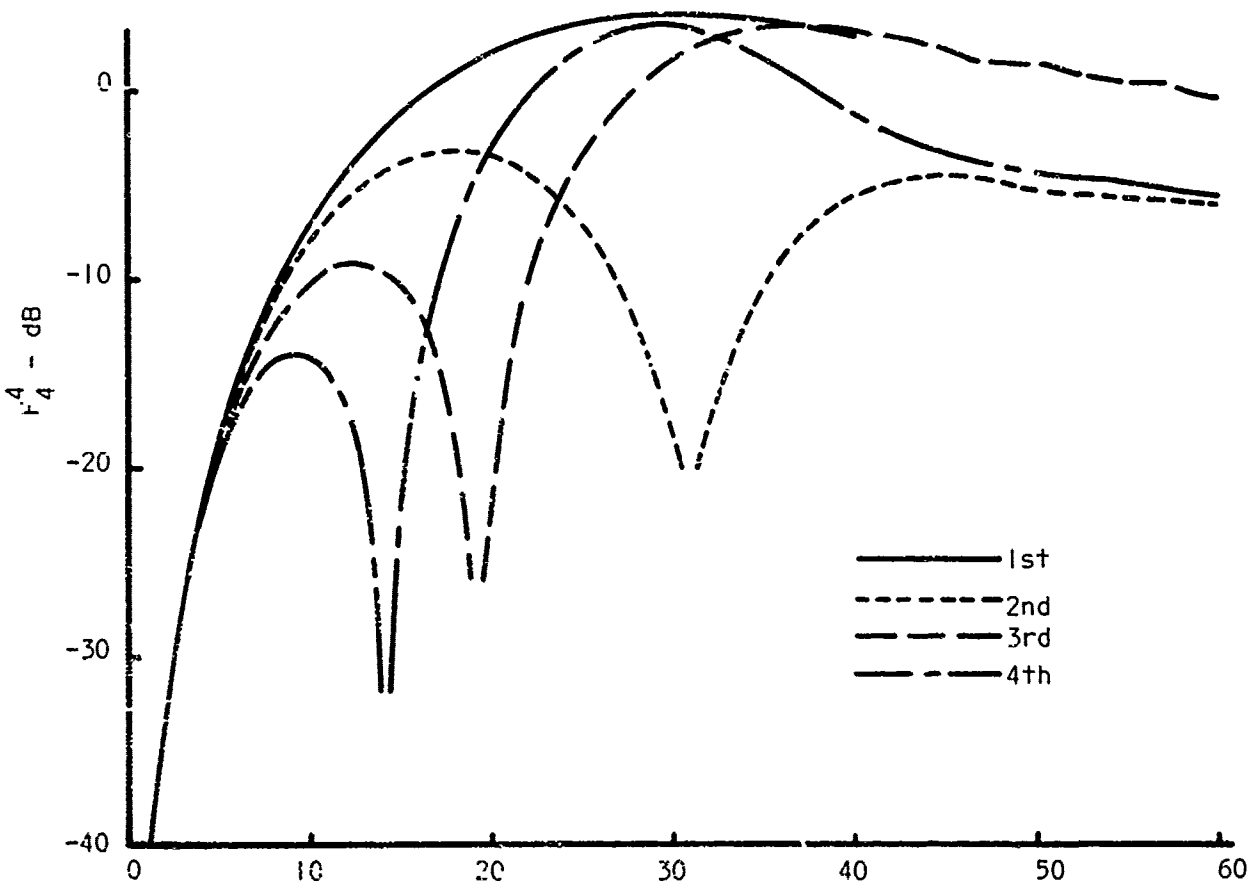

(b) Target Centered on Interference Minimum

Figure A-8. Variation of F^4 vs. Target Size for Coherent Elevated Target Centered on First Four Interference Maxima and Minima (R = 12,993 ft, h_1 = 81 ft, λ = 10 cm).

and specializing to a flat plate of uniform width or a cylinder of constant radius by using the appropriate multiplicative constant.

Kinder [69] has derived an expression for the cross-section of a rectangular plate when the plate is inclined a few degrees toward or away from the radar. Kinder's investigation is perhaps the most general of those located since his derivation retains the complex reflection coefficient in the result and also allows for the plate to be suspended above the surface.

An investigation was made by Freehafer [16] in which the target was a cylinder projecting upward from the surface and the assumption of perfect reflection ($\rho = 1$, $\varphi = \pi$) was introduced early in the analysis. It can be shown that when these values are substituted into Kinder's expression the results are identical except for the difference in multiplicative constants, Freehafer's being for a cylinder of radius r, and Kinder's for a rectangular plate of width b and height h. Marcus [70] has obtained results equivalent to Freehafer's.

An investigation by Perlin and Logan [71] also assumed a cylindrical target with results similar to Freehafer's. Perlin and Logan did introduce the additional parameter of transverse tilt in addition to tilt forward and backward, and found the effects to be quite small. The assumption of perfect reflection was made, and when the transverse tilt in their expression is assumed to be zero, the result is the same as the others except for a factor that produces a slightly asymmetric behavior between forward and backward tilts. For all small angles of tilt, however, the effect of this factor is essentially negligible.

Since the above derivations produce similar expressions for the effect of tilt, and that of Kinder is the most general, only his result will be presented. The target is a rectangular plate of "vertical" dimension h (strictly

speaking, h is the vertical dimension under zero tilt conditions) as shown in Fig. A-9, and width b normal to the paper. Although Kinder's derivation

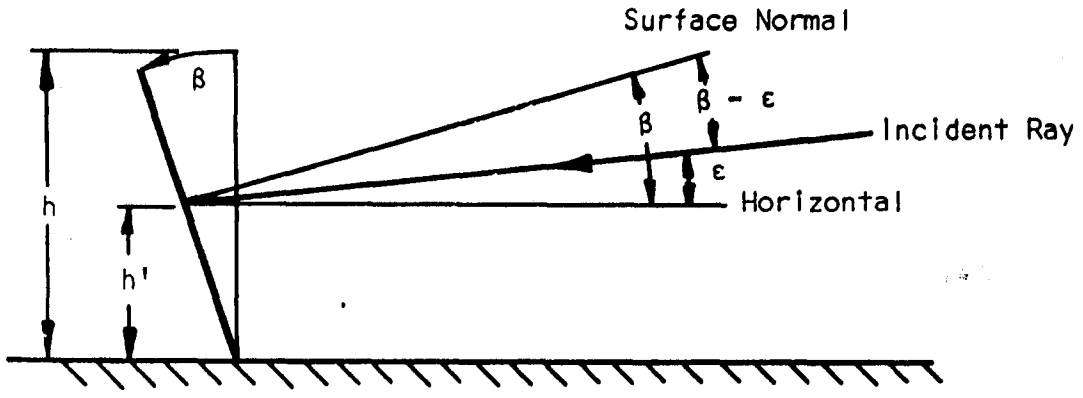

Figure A-9. Geometry for Tilted Target.

includes an angle α to describe rotation of the plate about the vertical axis, this parameter will be omitted here (i.e., $\alpha = 0$). The plate is then assumed to be oriented as shown in Fig. A-9 so that the normal to the plate lies in the vertical plane containing the incident ray. (Rotation through α causes the results given below to be multipled by $[\sin (kb \sin \alpha)/kb \sin \alpha]^2$.) The tilt angle β is defined to be positive when the plate is tilted away from the illuminating radar, and the grazing angle between the incident ray and the horizontal plane is ϵ. The center of the plate is at height h' and the plate is not restricted to be in contact with the surface. The effective cross-section of the plate is then determined to be

$$\sigma = \sigma_o K_1^2 K_2 \qquad \text{(A-24)}$$

In this equation, the first factor σ_o is the far-field normal-incidence cross-section of the plate; the second factor K_1^2 is also concerned with free-space effects and is the usual $(\sin x)/x$ approximation to account for phase

variations in the direct illumination due to off-normal incidence; the third factor K_2 accounts for the interaction of the direct and reflected waves as a function of the various parameters, including β. These factors can be expressed as

$$\sigma_o = 4\pi(hh/\lambda)^2 \quad , \tag{A-25}$$

$$K_1 = \frac{\sin[kh \sin(\beta - \epsilon)]}{kh \sin(\beta - \epsilon)} \quad , \text{ and} \tag{A-26}$$

$$K_2 = 1 + (V/U)^2 + (W/U)^2 + 2(V/U)(1 + V/U)\cos\xi + 2(W/U)\cos 2\xi \quad , \tag{A-27}$$

where $U = K_1$,

$$V = 2\rho \frac{\sin[kh \sin\beta \cos\epsilon]}{kh \sin\beta \cos\epsilon} \quad ,$$

$$W = \rho^2 \frac{\sin[kh \sin(\beta + \epsilon)]}{kh \sin(\beta + \epsilon)} \quad , \text{ and}$$

$$\xi = -\varphi - 2kh'\cos\beta \sin\epsilon \quad .$$

Of the three factors shown in Eq. (A-24), the product of the last two, $K_1^2K_2$, accounts for all the effects of tilt and the presence of the sea and is common to the results obtained by Freehafer, Perlin and Logan, and Kinder. To obtain the cross-section of a tilted cylinder from Eq. (A-24), it is only necessary to replace the initial factor with the far-field normal-incidence cross-section of a cylinder, $2\pi rh^2/\lambda$.

Although Kinder has obtained a fairly general expression for the return from a surface target by introducing the tilt geometry and retaining the

reflection parameters, his derivation utilizes the same assumptions on phase as those made in obtaining F_2^4 for the coherent case, Eq. (A-19). This is shown by the fact that if the tilt angle is set equal to zero and perfect reflection assumed, Eq. (A-24) reduces to Eq. (A-18). It follows that his result is valid only under the same conditions for which the coherent F_2^4 is valid, namely that no more than one or two lobes of the interference pattern are on the target.

To illustrate the predicted effect of target tilt, examples of the cross-section of tilted cylinders were computed using Eq. (A-24) with perfect surface reflection and σ_o for a cylinder. Fig. A-10 shows the cross-section normalized to square wavelength as a function of tilt angle for cylinders of radius $r = 0.5\lambda$ and four different heights when viewed at a grazing angle $\epsilon = 0.3^o$. This figure is similar to those presented by Perlin and Logan and is appropriate to targets veiwed from a low, relatively fixed position such as a ship. (Note that the σ_o used for a cylinder is linear in r and assumes no resonance effects.)

A different presentation of the effects of target tilt was made by Freehafer and is illustrated by Fig. A-11. This figure shows the computed cross-section of a cylinder with $h = 40\lambda$ and three different tilt angles as a function of a normalized range $R/h_1 = \csc \epsilon$. These curves would be appropriate for targets viewed from a moving platform such as an aircraft. The curve for zero tilt may be seen to be identical in form to that for F_2^4 in Fig. A-4 except for the reciprocal relations between the abscissae. Note that the cross-section of a tilted cylinder undergoes violent oscillations as the grazing angle increases (R/h_1 decreases) and that computations show a maximum occurs when the direct ray from the radar is normal to the cylinder. The region for R/h_1 greater than about 160 corresponds to the R^{-8} region for this target height.

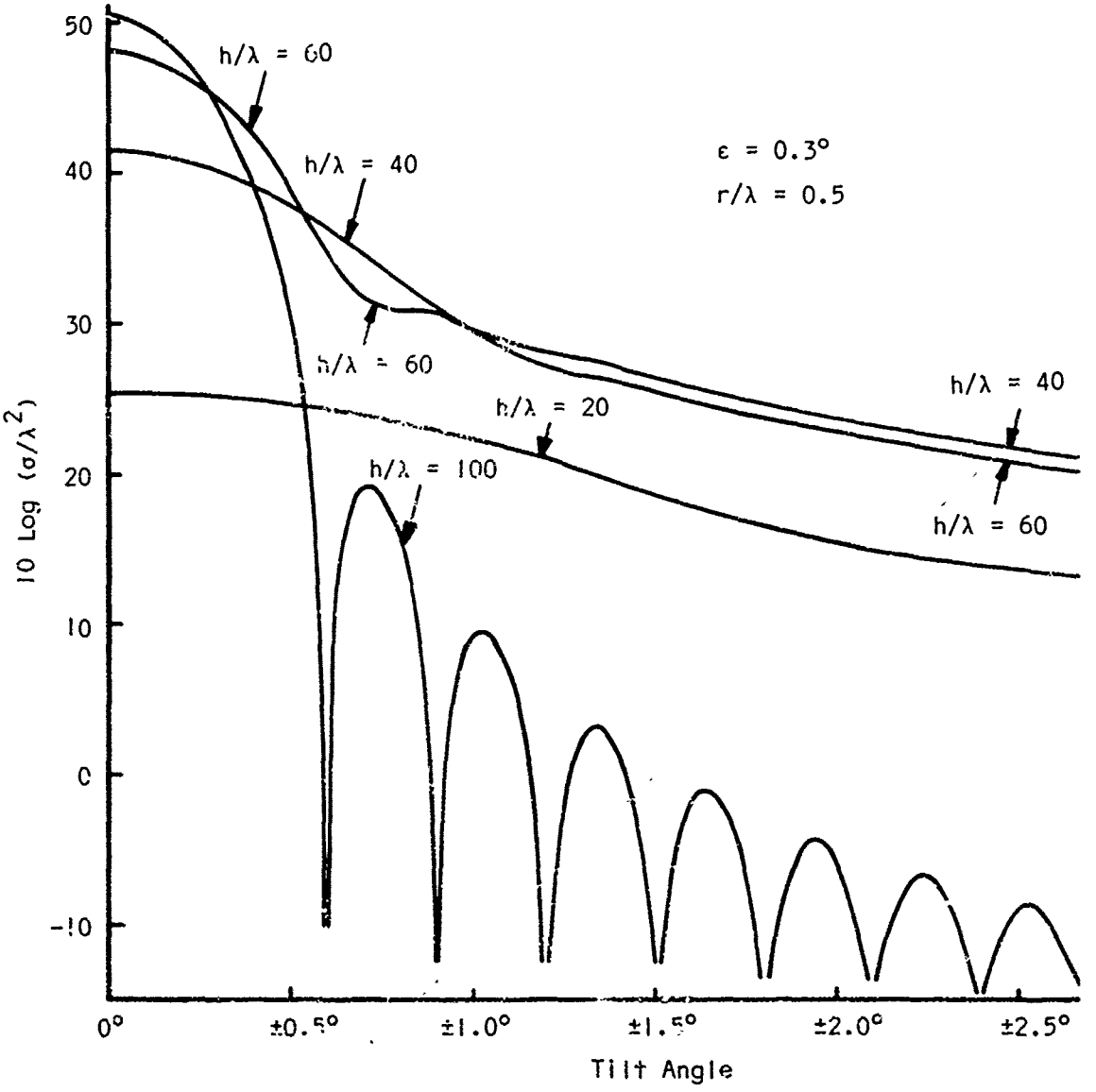

Figure A-10. Normalized Radar Cross-Section vs. Tilt Angle for Extended Cylinders of Several Heights.

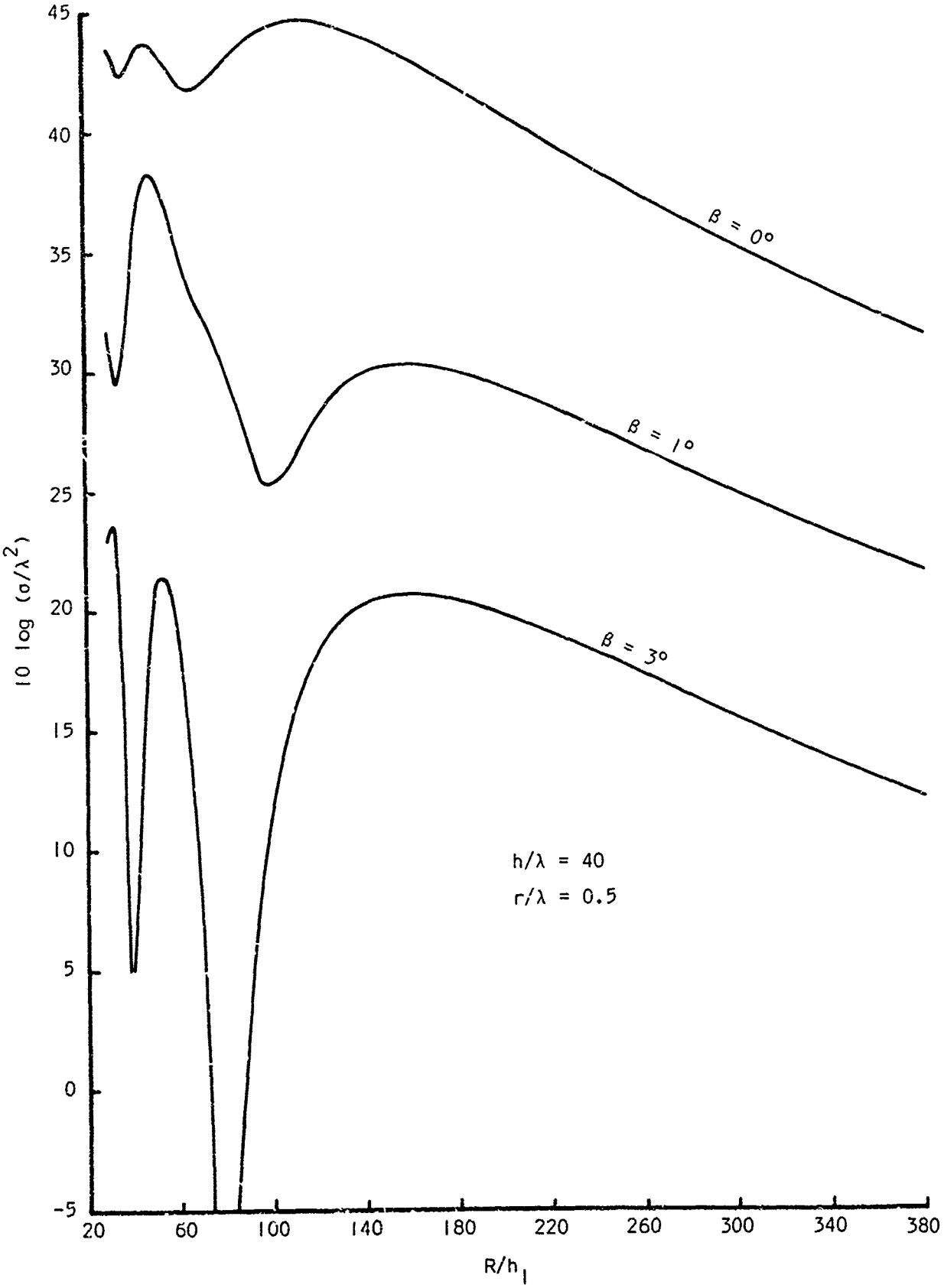

Figure A-11. Normalized Radar Cross-Section vs. Normalized Range for Extended Cylinder with Several Tilt Angles.

The curves in Figs. A-10 and A-11 must be thought of as specific examples and no simple generalizations are evident for the tilted case.

A-7. Russian Treatment of F^4

Recent Russian articles by Peresada have been concerned with vertical and tilted targets extending upward from the sea [72, 73, 74]. The concept of an attenuation function V is introduced and is essentially the same as the pattern propagation function F if any effects of antenna gain function are negligible. For a coherent scatterer extending vertically from the surface, V^4 was found to differ markedly from the F^4 of other studies. In particular, V^4 reaches much larger values than does F_2^4 of our Eq. (A-19) which is for the same physical model. Although V is determined for the spherical earth, we have made some computations using flat-earth approximations and believe that we have reconciled the major difference between the Russian results and those obtained elsewhere.

In our treatment of F^4 for an extended target we have determined the factor by which the far-field, free-space, normal-incidence cross-section, σ_o, must be multiplied to obtain the effective cross-section in the presence of the reflecting earth. Our value of F^4 therefore is equivalent to the product $K_1^2K_2$ which multiplies σ_o in Eq. (A-24). As noted there, K_2 is actually the factor which results from the presence of the earth, while K_1^2 is based on the usual $(\sin x)/x$ approximation to the diffraction pattern which accounts for off-normal viewing of the target. Although Peresada has worked exclusively with Fresnel integrals, he has, in effect, chosen to normalize to $K_1^2\sigma_o$ instead of σ_o alone and his denominator should reduce to this in the far-field. He thus accounts for the off-normal incidence of the free-space target which would result if the geometry were preserved and the earth simply removed. Even in the near field, the equivalent K_1^2 appears in the denominator of V, and when the function in his denominator takes on a very small value the magnitude of V is greatly increased. To summarize, in the far-field we would have

$$F^4 = \sigma_{eff}/\sigma_o \quad , \qquad \text{and} \qquad V^4 = \sigma_{eff}/K_1^2\sigma_o \quad . \tag{A-27}$$

The fact that the Russian treatment is normalized to a function instead of a constant appears to account for the major difference between V and F; either relation would be satisfactory as long as consistency was maintained. We believe that normalization to "maximum" free-space cross-section is more satisfactory in practice because of the ease of visualizing changes in F^4 as system parameters are varied. In a sense, however, the Russian treatment may be considered to be the purer one because it simply introduces the reflecting earth into a situation which is otherwise geometrically the same as the one for free space. It may be noted that Peresada makes the same assumptions on uniform phase as those which led to Eqs. (A-19) and (A-24) and we believe the same limitations on target size apply to his work.

A-8. Non-Uniform Distribution of Cross-Section with Height

Each of the simplified models for extended targets considered in preceding sections of this Appendix has been based on an inherent cross-section per unit surface area that did not vary with height. Assumptions on phase were made to allow integrals to be evaluated easily for the three models. Nevertheless, there can be no doubt that complex targets such as ships are not well represented by these gross simplifications, and the matter of more realistic representations will be considered here very briefly.

Implicit in the incoherent model is the assumption that the random scatterers will take on a full range of relative phase relationships within a short time, so that the ensemble average of the model will approximate the time-average behavior of the target. The result for F_1^4 given in Eq. (A-14) is based on uniform distribution of scatterers from the surface up to height h. While this may be a fairly good model for a target such as a splash, it probably

does not closely approximate a ship whose projected area, and hence, probably its cross-section also, varies greatly as a function of height.

Insofar as the incoherent model itself represents ships and other sea targets, a height-varying cross-section function may be multiplied by F_o^4 and the product averaged over the overall height. Such a procedure is discussed in Section 6-5 of Kerr, and examples given for summing the contributions from separate horizontal strips used to represent the vertical distribution of cross-section. Kuhn and Sutro [67] give analytical results for parabolic and sine-square distributions of cross-section, and Durlach [4] has results for exponential and Gaussian distributions.

It may be noted that the height distribution of cross-section affects the theoretical transition range. As shown in Table A-I, the value of $\lambda R_t/h_1 h$ is 5.37 for the case of uniformly distributed cross-section; Kuhn and Sutro give 4.95 as the value for the parabolic distribution and 4.65 for the sine-squared distribution, both of which have their maximum value at h/2. These results further indicate the uncertainty in R_t even on a theoretical basis.

When the phase effects of the incident field can be assumed to be random, the problem can be treated as above on the basis of averaging power. For a coherent target, such as a flat plate, this cannot be done and approximations based on uniformity of phase have been discussed above in Section A-2. A more exact treatment would require that the illuminating field and target reflectivity be treated as phasors and the problem approached on the basis of scattered fields from which cross-section can be determined.

Fig. A-12 depicts amplitude variations of both target reflectivity and illuminating fields that might represent some possible situations. Although only amplitudes are shown, the illuminating fields are labeled as $|FE_o|$ to imply that both F and E_o are phasors. The target characteristics are labeled in terms

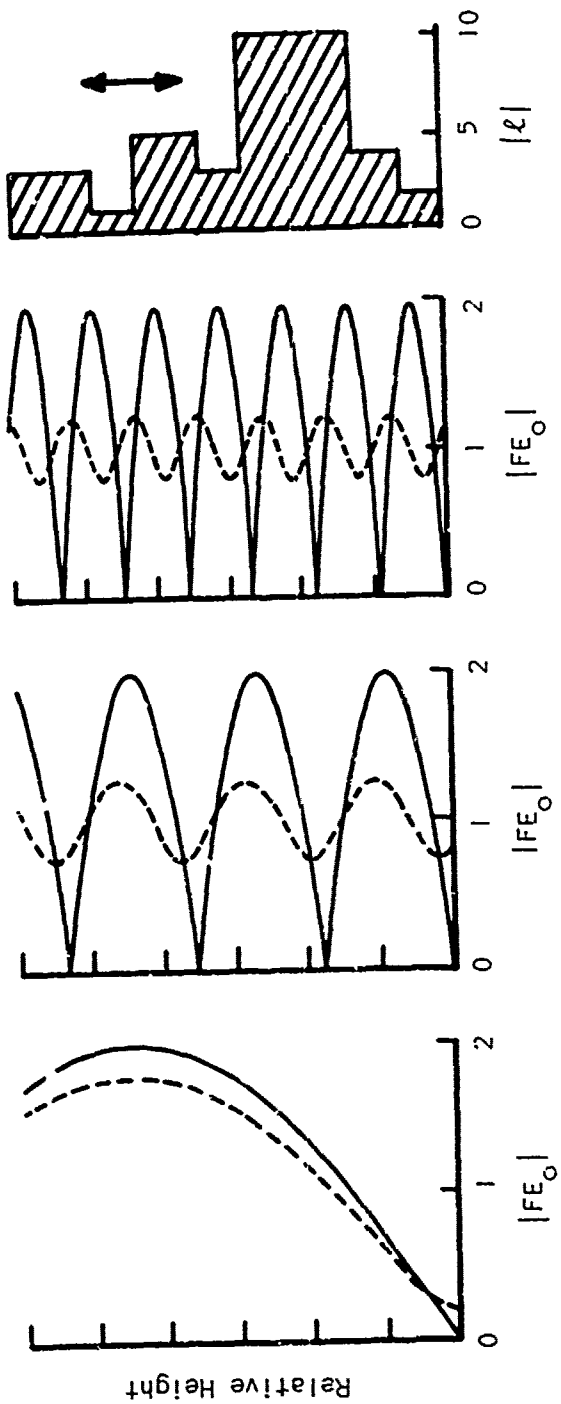

Figure A-12. Schematic Representation of Variation of Magnitudes of Illuminating Field and Target Scattering Length with Height Above the Sea. (Solid Lines Depict Horizontal Polarization and Dashed Lines Vertical Polarization.)

of scattering length ℓ which is also a phasor, and whose magnitude equals $\sqrt{\sigma/4\pi}$ [4, 5]. This approach is closely analogous to that taken in predicting the cross-section of aircraft [75] except that the illuminating field is not now uniform but varies in both amplitude and phase across the target or target elements.

Fig. A-12 illustrates how the form of a non-uniform field incident on a non-uniform target might vary in different circumstances. The entire target might be illuminated by a portion of a single interference lobe, or several interference lobes might illuminate just one part of the target. That relative motion might occur between field and target and cause variations in effective cross-section is suggested by the vertical arrows. While not intended to depict precisely a particular circumstance, the difference in illumination between horizontal polarization (solid lines) and vertical polarization (dashed lines) is also shown.

A-9. Targets Viewed at High Angles

In considering possible models for a target viewed at non-grazing angles, the concept of interference lobes in the illuminating field does not appear to be particularly useful. In fact, the usual roughness of the sea will probably destroy the ability of the indirect rays to interfere with the direct rays and produce an interference structure. Under these circumstances, the average value of the pattern propagation function would be unity, and while sea reflection might contribute some fluctuation to the return, the previously developed models of an average F^4 do not seem appropriate. Other possibilities will be treated briefly.

The overall characteristics of a ship suggest that many portions might be approximated by simple shapes. A multitude of surfaces are presented by masts, yardarms, shrouds, antennas, weapons, deck machinery, etc., and energy reflected from any of these surfaces can contribute to the radar return.

The relative importance of any given reflecting surface can vary considerably with slight changes in viewing angle. However, the presence of substantial near-vertical and near-horizontal relatively smooth surfaces suggests that dihedral and trihedral forms might be particularly important, particularly in view of their high efficiency as radar reflectors.

Considering now the 90° dihedral, it may be noted that this is a retro-directional scatterer which may be represented by an equivalent flat plate oriented perpendicular to the incident ray. In order for the incident ray to be returned, it must strike both of the plane surfaces in a double-bounce mechanism. The dimensions of the equivalent flat plate will vary with the angle of view, as shown in Fig. A-13 for a dihedral with legs of equal length. The size of the equivalent flat plate will be limited by the length of the shorter side if the legs are unequal.

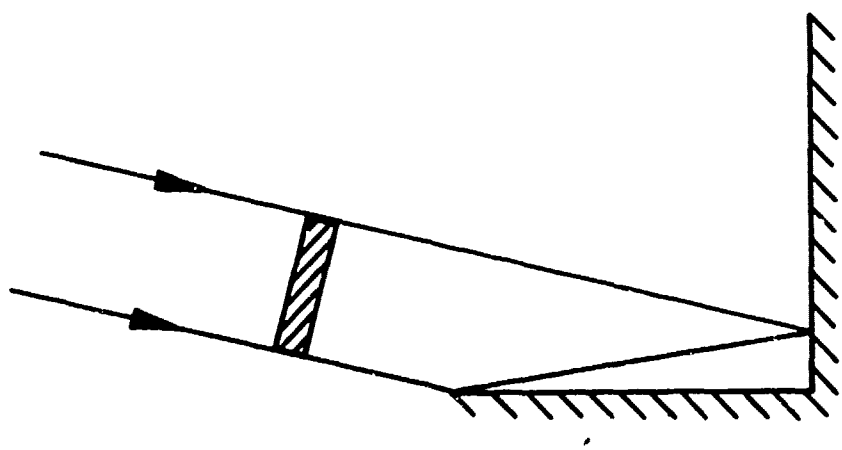

Figure A-13. Flat-Plate Equivalent to a Dihedral Reflector.

Although we argue above that there will usually not be a reflected ray off the sea at high incidence angles, this may not always be the case. It is possible that dihedrals will sometimes be formed with the sea as one surface for some combinations of polarization, wavelength, and incidence angle. The general problem of dihedrals with surfaces which are not perfectly reflecting, as well as a number of other aspects of the representation of complex targets,

has been investigated by the University of Michigan [76]. It may also be noted that the dihedral angle does not have to be exactly 90° for the reflector to have appreciable cross-section [77] although the return is degraded by departures from the right-angle condition.

A preliminary attempt has been made by DuWaldt [19 to calculate the cross-section of a Navy attack transport (APA) by identifying its major scattering surfaces. Flat-plate equivalents were used for dihedral and trihedral reflectors, including those formed with the sea. Davies' theory of scattering from rough surfaces [78] was used to calculate cross-section for several azimuth angles and elevation angles from 0° to 90°. The cross-section was modified by allowance for a Lambert scatter component to represent the numerous minor items not included otherwise. A value of 60 was used for the Davies roughness parameter, and the Lambert component was taken to be 1% of the deck area and independent of viewing angle.

Results of the calculations were compared with data taken on a YAGR (see Section 3-1) which is a ship of somewhat the same general type. On the quarter, the calculated values were some 20 dB lower than the (adjusted) measured values, and DuWaldt attributes this to the fact that the trihedrals in the ship structure were ignored and the dominant contribution at this aspect was therefore from the Lambert component. Beam aspect showed reasonable agreement, and bow and stern aspects had calculated values which were high. It may be noted here that the experimental data were taken with vertical polarization while DuWaldt assumed perfect reflectivity of the sea in setting up dihedrals using the sea and vertical ship surfaces, thereby neglecting the influence on reflection coefficient of both roughness and polarization. With some refinement, the general approach seems to be worthwhile for making estimates of overall cross-section of ships.

REFERENCES

1. "Abstracts on Radar Reflectivity of Sea Targets, Volume I," H. A. Corriher, Jr. and B. O. Pyron, Georgia Institute of Technology, Engineering Experiment Station, Technical Report 1, Vol. I, on Project A-914, Contract Nonr-991(12), December 1966, AD 813 995L. (Each transmittal of this document outside the Department of Defense must have prior approval of Air Programs, Code 461, Office of Naval Research.)

2. "Abstracts on Radar Reflectivity of Sea Targets, Volume II (U)," H. A. Corriher, Jr. and B. O. Pyron, Georgia Institute of Technology, Engineering Experiment Station, Technical Report 1, Vol. II, on Project A-914, Contract Nonr-991(12), December 1966, Secret-1, AD 381 645L. (Each transmittal of this document outside the Department of Defense must have prior approval of Air Programs, Code 461, Office of Naval Research.)

3. PROPAGATION OF SHORT RADIO WAVES, D. E. Kerr, Editor, MIT Radiation Laboratory Series, Volume 13, McGraw-Hill Book Company, Inc. (1951).

4. "Influence of the Earth's Surface on Radar," N. I. Durlach, Massachusetts Institute of Technology, Lincoln Laboratory, Technical Report 373 (ESD-TDR-65-32), Contract AF 19(628)-500, January 1965, AD 627 635.

5. "Reflection and Transmission of Radio Waves," M. Katzin, Chapter 4 of AIRBORNE RADAR, D. J. Povejsil, R. S. Raven, and P. Waterman, D. Van Nostrand Company, Inc. (1961).

6. "Radar Cross Section of Ship Targets," M. Katzin, Naval Research Laboratory, Report RA-3A 213A, January 1944, ATI 37 552.

7. "Radar Cross Section of Ship Targets, II," W. S. Ament, M. Katzin, and F. C. Macdonald, Naval Research Laboratory, Report R-2232, February 1944, ATI 28 604.

8. "Radar Cross Section of Ship Targets, III," W. S. Ament, M. Katzin, and F. C. Macdonald, Naval Research Laboratory, Report R-2295, June 1944, ATI 51 543.

9. "Radar Cross Section of Ship Targets, IV," W. S. Ament, M. Katzin, and F. C. Macdonald, Naval Research Laboratory, Report R-2332, July 1944, ATI 37 551.

10. "Radar Cross Section of Ship Targets, V," F. C. Macdonald, Naval Research Laboratory, Report R-2466, March 1945, ATI 47 476.

11. "Radar Cross Section of Ship Targets, VI," W. J. Barr, Naval Research Laboratory, Report R-2467, April 1945, ATI 76 027.

12. "Radar Cross Section of Ship Targets, VII," W. S. Ament, W. J. Barr, and F. C. Macdonald, Naval Research Laboratory, Report R-2524, May 1945, ATI 15 264 or ATI 76 011.

13. "Radar Cross Section of Ship Targets, VIII," W. J. Barr, Naval Research Laboratory, Report R-2793, March 1946, ATI 72 901.

REFERENCES (Cont.)

14. "A Radar Directory (U)," E. B. Soltwedel, Rand Corporation, Research Memorandum RM-2000, August 1957, Confidential-4, AD 150 674.

15. "Overwater Observations at X and S Frequencies on Surface Targets," O. J. Baltzer, V. A. Counter, W. M. Fairbank, et al., Massachusetts Institute of Technology, Radiation Laboratory, Report RL 401, July 1943, ATI 13 714.

16. "Radar Echoes from Periscopes," J. E. Freehafer, Massachusetts Institute of Technology, Radiation Laboratory, Report RL 172, March 1943, ATI 25 449.

17. "Radar Echoes from Ships," J. T. Ransone, Jr., W. T. Davis, and J. C. Daley, Naval Research Laboratory, Memorandum Report 1368, October 1962, AD 474 135L. (U.S. Government only; others to Director, Naval Research Laboratory, Washington, D. C. 20390.)

18. "Ship Cross Sections," J. A. Lieske, Johns Hopkins University, Applied Physics Laboratory, Report BPD64U-10, 27 April 1964.

19. Private communication with Dr. B. J. DuWaldt of Aerospace Corporation re IOC 65-4030.3-208 of 24 August 1965 and IOC 65-4020.3-230 of 18 October 1965.

20. "Radar Cross-Section Measurement of a Ship at Four Frequencies," J. C. Daley, L. E. Hearton, and J. T. Ransone, Jr., Naval Research Laboratory, Letter Report 5270-3A:JCD:bjg, April 1966.

21. "Airborne Backscatter Study at Four Frequencies," J. C. Daley, Naval Research Laboratory, Letter Report 5270-20A:JCD:bjg, August 1966.

22. "Radar Backscatter from Complex Targets," J. C. Daley, Naval Research Laboratory, Letter Report 5270-23A:JCD:bjg, October 1966.

23. "A High-Resolution K-Band Ship Search Set," W. M. Fairbank, W. T. Harrold, and G. I. Sheckels, Massachusetts Institute of Technology, Radiation Laboratory, Report RL 576, 7 December 1944, ATI 25 472 or ATI 35 696.

24. "Preliminary Report on the Observation of Snorkels and Sea Clutter Using Coherent Airborne Radar," J. J. Kovaly, G. S. Newell, W. C. Prothe, and C. W. Sherwin, University of Illinois, Control Systems Laboratory, Report R-27, Contract DA 11-022 ORD-721, November 1952, AD 2 883.

25. "A Classification of Radar Reflectors in Use at Present," Trinity House (Great Britain), Research and Development Section, paper presented at Sixth International Technical Conference on Lighthouses and Other Aids to Navigation, 26 September 1960, AD 242 001.

26. "A Note on the Theoretical Maximum Range to Be Expected from a Radar Reflector," Trinity House (Great Britain), Research and Development Section, paper presented at Sixth International Technical Conference on Lighthouses and Other Aids to Navigation, 26 September 1960, AD 242 128.

REFERENCES (Cont.)

27. "Radar Reflectors Now Used in the Aids to Navigation System of the United States," C. R. Adams, U.S. Coast Guard, Civil Engineering Division, paper presented at Sixth International Technical Conference on Lighthouses and Other Aids to Navigation, 26 September 1960, AD 242 142.

28. "Measurements Using a Polarization Instrumentation Radar on Navigational Buoys," I. D. Olin and F. D. Queen, Naval Research Laboratory, Report 5701, November 1961, AD 268 727.

29. "Comparisons of Horizontal, Vertical, and Circular Polarization on Marine Targets at Eastney," O. Nourse and I. J. Arkieson, Admiralty Surface Weapons Establishment (Great Britain), Technical Note TX-59-4, October 1959.

30. "Radar and Ice," L. S. Le Page and A. L. P. Milwright, Journal of the Institute of Navigation 6, 113-27 (April 1953).

31. "The Detection of Ice by Radar," L. S. Le Page and A. L. P. Milwright, Marine Observer 24, 150-62 (1954).

32. "A Record of Radar Performance in Ice Condition," R. E. Perry, Journal of the Institute of Navigation 6, 74-85 (January 1953).

33. "Properties of Radar Echoes from Shell Splashes," H. Goldstein, Physical Review 70, 232-33 (1946).

34. "Radar Echoes from Air-Laid Mine Splashes," R. Beringer, J. G. Carver, and C. W. Hoover, Jr., Yale University, Edwards Street Laboratory, Technical Report 5, Contract Nonr-609(02), 15 March 1952, ATI 204 613 or TIP C-8394.

35. "Interim Survey of MILORD Design and Development Program," F. Dixon, Georgia Institute of Technology, Engineering Experiment Station, Technical Report 1 on Project A-129, Contract NObsr-64055, 31 December 1953, AD 323 979.

36. "1952 Observations of Mine and Shell Splashes with the Firing Error Analysis Radar (FEAR)," H. A. Corriher, Jr., Georgia Institute of Technology, Engineering Experiment Station, Technical Report 2 on Project A-129, Contract NObsr-64055, 15 November 1954.

37. "Technical Evaluation of the MILORD Mine-Watch Radar," H. A. Corriher, Jr., Georgia Institute of Technology, Engineering Experiment Station, Final Report on Project A-129, Contract NObsr-64055, 30 September 1956, AD 306 247.

38. "Growth Characteristics of Splashes from Inert-Loaded Projectiles," I. E. Perlin, N. A. Logan, and F. Dixon, Georgia Institute of Technology, Engineering Experiment Station, Technical Report 5 on Project 124-27, Contract NOrd-10020, 30 September 1948, ATI 204 749.

REFERENCES (Cont.)

39. "Theory of the Performance of Radar on Ship Targets," M. V. Wilkes, J. A. Ramsay, and P. B. Blow, Air Defence Research and Development Establishment (Great Britain), Joint Report ADRDE RO4/2/CR252 and CAEE 69/C/149, July 1944, AD 396 529 (DDC reference only).

40. "A Theory of the Performance of Radar on Ship Targets," M. V. Wilkes and J. A. Ramsay, Proceedings of the Cambridge Philosophical Society 43, 220-31 (1947).

41. "Entfernungsabhängigkeit der Radarrückstrahlung in Erdbodennähe (Range Dependence of Radar Return in the Vicinity of the Earth)," G. Beck, Technischen Hochschule München (Germany), summary of a doctoral dissertation, 1965.

42. "Range Requirements in Radar Cross-Section Measurements," R. G. Kouyoumjian and L. Peters, Jr., Proceedings of the IEEE 53, No. 8, 920-28 (August 1965).

43. "Identification of Naval Spoofs," L. R. Koller, Harvard University, Radio Research Laboratory, Report 411-129, November 1944, ATI 15 385.

44. Unclassified section from "Measurements Using a Polarization Instrumentation Radar on Selected Targets (U)," I. D. Olin and F. D. Queen, Naval Research Laboratory, Report 5755, April 1962, Secret-3, AD 329 363.

45. "Statistics of Ship Radar Cross-Section Data," R. E. Harrison, Aerospace Corporation, Report TR-669(9990)-5, (in preparation, April 1966).

46. "Snorkel Detection Using Airborne Coherent Radar II," J. J. Kovaly, G. S. Newell, W. C. Prothe, and C. W. Sherwin, University of Illinois, Control Systems Laboratory, Report R-36, Contract DA 11-022 ORD-721, April 1953, AD 8 006.

47. "Design Characteristics of Coherent Radar for Snorkel Detection," C. W. Sherwin, University of Illinois, Control Systems Laboratory, Report R-39, Contract DA 11-022 ORD-721, November 1953, AD 21 780.

48. "Radar Areas of Small Landing Craft," W. S. Ament, F. C. Macdonald, and D. L. Ringwalt, Naval Research Laboratory, Memorandum Report 117, January 1953, AD 9 209.

49. "Radar Areas of Small Landing Craft, II," W. S. Ament and F. C. Macdonald, Naval Research Laboratory, Memorandum Report 317, June 1954.

50. "A Preliminary Report on Frequency Characteristics of Moving Targets in Sea Clutter," J. J. Kovaly and W. C. Prothe, University of Illinois, Control Systems Laboratory, Report R-24, Contract DA 11-022 ORD-721, July 1952, ATI 164 130.

51. "Development in Radar Homing Missiles for the Period March 1, 1944 to May 1, 1945," P. R. Stout, R. F. Carlson, L. Myrtle, and D. L. Huth, Massachusetts Institute of Technology, Contract OEMsr-240, June 1945, ATI 35 569.

REFERENCES (Cont.)

52. "Report of Trials to Determine the Variation of the Apparent Reflective Point of Plain [sic] 10 cm Waves from a Destroyer," J. F. Coales and M. Hopkins, Admiralty Signal Establishment (Great Britain), Report M.627, July 1944, AD 396 535.

53. "Systems Properties of Jumping-Frequency Radars," B. G. Gustafson and B-O Ås, Phillips Telecommunication Review 25, No. 1, 70-76 (July 1964).

54. "Theory of Reduction of Submarine Echoes by Shielding Screens," R. Weinstock, Harvard University, Radio Research Laboratory, Report 411-99, October 1944, ATI 15 351.

55. "Interim Report on Radar Camouflage Studies for Submarine Snorkel and Periscope," F. C. Macdonald, Naval Research Laboratory, Letter Report 3460-82/48(A), December 1948.

56. "Radar Camouflage," M. M. Andrews, O. J. Baltzer, E. L. Hudspeth, and C. E. Mandeville, Massachusetts Institute of Technology, Radiation Laboratory, Report RL 766, July 1945, ATI 24 717.

57. "Radar Reflections from Small Surface Targets," V. R. Widerquist and J. E. Boyd, Georgia Institute of Technology, Engineering Experiment Station, Technical Report 17 on Project 124-27, Contract NOrd-10020, August 1950, ATI 202 182.

58. Private communication with Mr. A. W. Boekelheide of Aerospace Corporation re IOC 66-2353.2-9 of 17 January 1966.

59. "An Airborne, Four-Frequency, Frequency Stabilized, Coherent Radar System," N. G. Hamm, E. G. McCall, F. C. Macdonald, and J. T. Ransone, Jr., Proceedings, 7th National Convention on Military Electronics, 57-59, (September 1963).

60. "Dynamic Measurement of Radar Cross Sections," I. D. Olin and F. D. Queen, Proceedings of the IEEE 53, 954-61 (August 1965).

61. "Final Report on Phase 1, Covering the Period 23 December 1964-30 November 1965 (U)," F. L. Beckner, University of Texas, Defense Research Laboratory, Report DRL-535, Contract N123-(62738)52022A(X), 18 January 1966, Confidential-4, AD 371 123.

62. "Radar Target/Clutter Measurements Program (U)," F. L. Beckner, University of Texas, Defense Research Laboratory, Report DRL-545, Contract N123-(62738)55231A(X), 14 September 1966, Confidential-4, AD 382 765.

63. "ARIS Orientation Manual," RCA Service Company, Missile Test Project, 1 December 1965, AD 476 363.

64. "Some Measured Electromagnetic Characteristics of a PTF (U)," C. M. Kuch and E. H. Hackney, North American Aviation, Inc., Space and Information Systems Division, Report SID 66T-75, 27 August 1966, Secret-3.

REFERENCES (Cont.)

65. "Clutter Reduction Radar (U)," E. R. Flynt, F. B. Dyer, R. C. Johnson, et al., Georgia Institute of Technology, Engineering Experiment Station, Final Report on Project A-725, Contract NObsr-91024, (to be published 31 December 1967), Confidential-4.

66. THE SCATTERING OF ELECTROMAGNETIC WAVES FROM ROUGH SURFACES, Petr Beckmann and Andre Spizzichino, The Macmillan Company (1963).

67. "Theory of Ship Echoes as Applied to Naval RCM Operations," T. S. Kuhn and P. J. Sutro, Harvard University, Radio Research Laboratory, Report 411-93, July 1944, AD 15 371.

68. "Research and Measurements on Aircraft Equipment Against Sea Targets," O. Stuetzer, paper in "Electromagnetic Wave Propagation and Absorption," Air Materiel Command, Translation F-TS-1973-RE, August 1944, ATI 23 143.

69. "Investigation of the Reflection from Ships at a Wavelength of 54 Cm," H. Kinder, Air Materiel Command, Translation F-TS-1996-RE, January 1944, ATI 43 351.

70. "Theory of Radar Return from the Schnorkel," P. M. Marcus, Massachusetts Institute of Technology, Radiation Laboratory, Report RL 671, January 1945, ATI 51 426.

71. "A Theoretical Study of Radar Reflections by Cylinders," I. E. Perlin and N. A. Logan, Georgia Institute of Technology, Engineering Experiment Station, Technical Report 10 on Project 124-27, Contract NOrd-10020, 15 July 1949, ATI 93 809.

72. "Diffraction in a Non-Uniform Field," V. P. Peresadä, Radiotekhnika i Elektronika 4, No. 3, 384-87 (1959).

73. "Diffraction by a Plate Located at the Earth in the 'Line-of-Sight' Zone," V. P. Peresada, Radiotekhnika 17, No. 6, 24-28 (1962).

74. "Radar Visibility of Marine Objects," V. P. Peresada, Foreign Technology Division, Air Force Systems Command, Report FTD-MT-63-281 (TT-64-71498), 28 May 1964, AD 606 763.

75. "Radar Cross-Section Estimation for Complex Shapes," J. W. Crispin, Jr. and A. L. Maffett, Proceedings of the IEEE 53, No. 8, 972-82 (August 1965).

76. "Studies in Radar Cross-Sections-XVI: Microwave Reflection Characteristics of Buildings," H. Weil, R. R. Bonkowski, T. A. Kaplan, and M. Leichter, University of Michigan, Engineering Research Institute, Report 2255-12-T (RADC TR-55-489), Contract AF 30(602)-1070, 1 May 1955, AD 83 901.

77. "Polarization Dependence of Radar Echoes," J. N. Hines and J. A. McEntee, Ohio State University Research Foundation, Report 612-13, Contract AF 30 (635)-2811, 31 October 1956, AD 114 242.

78. "The Reflection of Electromagnetic Waves from a Rough Surface," H. Davies, Proceedings of the IEE 101 Pt. IV, 209-14 (1954).

DISTRIBUTION LIST FOR FINAL REPORT, VOLUME I, CONTRACT Nonr-991(12)

Office of Naval Research (2)
Department of the Navy
Washington, D. C. 20360

ATTN: Air Programs Branch, Code 46

Office of Naval Research (1)
Resident Representative
Georgia Institute of Technology
103-104 Electronics Research Bldg.
Atlanta, Georgia 30332

Commanding Officer (1)
Office of Naval Research
Branch Office London
Box 39 Navy #100
Fleet Post Office
New York, New York 10453

Naval Research Laboratory (7)
Washington, D. C. 20390

ATTN: Dr. M. I. Skolnik, Code 5300 (1)
Mr. F. C. Macdonald, Code 5270 (1)
Mr. I. W. Fuller, Jr., Code 5310 (1)
Dr. I. D. Olin, Code 5347 (1)
Mr. N. W. Guinard, Code 5278 (1)
Mr. J. C. Daley, Code 5278 (1)
Technical Library, Code 2027 (1)

Naval Air Development Center (7)
Johnsville, Warminster
Pennsylvania 18974

ATTN: Mr. Joseph Turco, AETD (5)
Mr. E. L. Chipman, AETD (1)
Mr. E. E. Koos, AETD (1)

Department of the Navy (1)
Office of the Chief of Naval Operations
Washington, D. C. 20350

ATTN: Mr. M. R. Moore, Op-07TE

Navy Space Systems Activity (4)
Hq SSD, AF Unit Post Office
Los Angeles, California 90045

ATTN: Dr. Egon E. Muehlner (1)
Mr. George Candella (3)

Naval Air Systems Command (6)
Department of the Navy
Washington, D. C. 20360

ATTN: Mr. C. A. Good, AIR-5383A (2)
Mr. E. Kelly, AIR-53523A (1)
Mr. Harold H. Landfried,
AIR-5333D4 (1)
Mr. Vytas A. Tarulis, AIR-53321D (1)
Technical Library, AIR-604A (1)

Naval Ship Systems Command (4)
Department of the Navy
Washington, D. C. 20360

ATTN: Mr. P. E. Taylor, Code 03521 (1)
Mr. F. P. Theriot, Code 6175B (1)
Electronic Warfare Branch,
Code 6176 (1)
Rewson Project, Code 6050 (1)

Navy Electronics Laboratory (1)
San Diego, California 92152

ATTN: Mr. James Whitaker

Naval Missile Center (1)
Point Mugu, California 93041

ATTN: Mr. T. M. Barrett, Code 5311

Naval Ordnance Laboratory (1)
Corona, California 91720

ATTN: Mr. Fred Alpers

Naval Ordnance Test Station (1)
China Lake, California 93557

ATTN: Mr. Ed Parks

Naval Avionics Facility (1)
21st and Arlington Avenue
Indianapolis, Indiana 46218

ATTN: Mr. Paul L. Brink

Naval Radiological Defense Laboratory (1)
San Francisco Naval Shipyard
San Francisco, California 94135

Naval Scientific and Technical (1)
Intelligence Center
U.S. Naval Observatory, Bldg. 52
Massachusetts Avenue at 34th Street, N. W.
Washington, D. C. 20390

U.S. Coast Guard (1)
1300 E Street, N. W.
Washington, D. C. 20591

Project AGILE (1)
Advanced Research Projects Agency
The Pentagon
Washington, D. C. 20301

U.S. Army Limited War Laboratory (1)
Aberdeen Proving Ground
Maryland 21005

Rome Air Development Center (1)
Air Force Systems Command
Griffiss AFB, New York 13440

ATTN: Mr. Arthur Frohlich

Foreign Technology Division (1)
Air Force Systems Command
Wright-Patterson AFB, Ohio 45433

Air Force Avionics Laboratory (1)
Wright-Patterson AFB, Ohio 45433

ATTN: Mr. W. W. Welbourne, AVNT

Headquarters TARC (DRT) (1)
Shaw Air Force Base, S. C. 29152

Central Intelligence Agency (1)
Washington, D. C. 20505

Scientific and Technical Information Facility (2)
National Aeronautics and Space Administration
P. O. Box 5700
Bethesda, Maryland 20014

Aerospace Corporation (2)
P. O. Box 95085
El Segundo, California 90045

ATTN: Mr. D. D. Pidhayny

Remote Area Conflict Information Center (1)
Battelle Memorial Institute
505 King Avenue
Columbus, Ohio 43201

Center for Naval Analyses (1)
1401 Wilson Boulevard
Arlington, Virginia 22209

Institute for Defense Analyses (1)
400 Army-Navy Drive
Arlington, Virginia 22202

ATTN: Dr. Stanley Marder, RESD

The Rand Corporation (1)
1700 Main Street
Santa Monica, California 90406

Airtronics, Inc. (1)
Dulles International Airport
P. O. Box 17186
Washington, D. C. 20041

Autonetics (1)
3370 Miraloma Avenue
Anaheim, California 92803

ATTN: Main Technical Library

General Dynamics/Pomona (1)
P. O. Box 1011
Pomona, California 91769

General Electric Company (1)
Valley Forge Space Technology Center
P. O. Box 8555
Philadelphia, Pennsylvania 19101

ATTN: Mr. J. Liston

Grumman Aircraft Engineering Corporation (1)
S. Oyster Bay Road
Bethpage, L. I., New York 11714

Hughes Aircraft Company (1)
P. O. Box 3310
Fullerton, California 92634

Hughes Research Laboratories (1)
3011 South Malibu Canyon Road
Malibu, California 90265

Hughes Aircraft Company (1)
Centinela at Teale Street
Culver City, California 90232

ATTN: Dr. B. J. DuWaldt

Hughes Aircraft Company (1)
Missile Systems Division
Canoga Park, California 91300

ATTN: Mr. A. W. Boekelheide

Micronetics, Incorporated (1)
7155 Mission Gorge Road
P. O. Box 20396
San Diego, California 92120

North American Aviation, Inc. (1)
Space and Information Systems Division
2000 North Memorial Drive
Tulsa, Oklahoma 74115

ATTN: Mr. C. M. Kuch

Raytheon Company (1)
Missile Systems Division
Bedford, Massachusetts 01730

ATTN: Mr. George H. Grant

Raytheon Company/Autometric (1)
4217 Wheeler Avenue
Alexandria, Virginia 22304

ATTN: Mr. A. Biache, Jr.

Sanders Associates, Inc. (1)
95 Canal Street
Nashua, New Hampshire 03301

Sylvania Electronic Systems--West (1)
P. O. Box 188
Mountain View, California 94040

ATTN: Mr. S. N. Watkins

TRW Systems (1)
Washington Operations
1735 I Street, N. W.
Washington, D. C. 20006

ATTN: Mr. E. M. Yanis

TRW Systems (1)
7001 North Atlantic Avenue
Cape Canaveral, Florida 32920

Westinghouse Electric Corporation (1)
Surface Division
Westinghouse Defense and Space Center
P. O. Box 1897
Baltimore, Maryland 21203

Westinghouse Electric Corporation (1)
Aerospace Division
Westinghouse Defense and Space Center
P. O. Box 746
Baltimore, Maryland 21203

Engineering Experiment Station (3)
Georgia Institute of Technology
Atlanta, Georgia 30332

ATTN: Electronics Division

The Johns Hopkins University (2)
Applied Physics Laboratory
8621 Georgia Avenue
Silver Spring, Maryland 20910

ATTN: Dr. I. Katz (1)
Mr. F. E. Nathanson (1)

Massachusetts Institute of Technology (1)
Lincoln Laboratory
P. O. Box 73
Lexington, Massachusetts 02173

Stanford Research Institute (1)
333 Ravenswood Avenue
Menlo Park, California 94025

University of Michigan (2)
Institute of Science and Technology
P. O. Box 618
Ann Arbor, Michigan 48107

ATTN: Radio Science Laboratory (1)
Project MICHIGAN (1)

Defense Research Laboratory (1)
The University of Texas
P. O. Box 8029
Austin, Texas 78712

ATTN: Mr. Don Lauderdale

Defense Documentation Center (20)
Cameron Station
Alexandria, Virginia 22314

British Defence Staff (10)
British Embassy
3100 Massachusetts Avenue, N. W.
Washington, D. C.

ATTN: Staff Information Officer

Australian Joint Services Staff (2)
Australian Embassy
1735 Eye Street, N. W.
Washington, D. C. 20006

ATTN: Defence Science Attache

Canadian Joint Staff (2)
Canadian Embassy
2450 Massachusetts Avenue, N. W.
Washington, D. C.

ATTN: Defence Research Member

UNCLASSIFIED
Security Classification

DOCUMENT CONTROL DATA - R & D

Security classification of title, body of abstract and indexing annotation must be entered when the overall report is classified)

1 ORIGINATING ACTIVITY (Corporate author) Engineering Experiment Station Georgia Institute of Technology Atlanta, Georgia 30332	2a. REPORT SECURITY CLASSIFICATION UNCLASSIFIED 2b. GROUP None

3 REPORT TITLE

Radar Reflectivity of Sea Targets, Volume I

4 DESCRIPTIVE NOTES (Type of report and inclusive dates)

Final Report

5 AUTHOR(S) (First name, middle initial, last name)

Corriher, H. A., Jr., Pyron, Berry O., Wetherington, R. D., and Abeling, A. B.

6 REPORT DATE	7a. TOTAL NO. OF PAGES	7b. NO. OF REFS
30 September 1967	114 + viii	78

8a. CONTRACT OR GRANT NO	9a. ORIGINATOR'S REPORT NUMBER(S)
Nonr-991(12) b. PROJECT NO NR 233-029 c. d.	Final Report, Vol. I, Project A-914 9b. OTHER REPORT NO(S) (Any other numbers that may be assigned this report)

10 DISTRIBUTION STATEMENT

U. S. military agencies may obtain copies of this report directly from DDC. Other qualified users shall request through Air Programs, Office of Naval Research, Washington, D. C.

11 SUPPLEMENTARY NOTES	12 SPONSORING MILITARY ACTIVITY
	Office of Naval Research Air Programs Branch, Code 461 Department of the Navy Washington, D. C. 20360

13 ABSTRACT

Volume I of this two-volume survey presents a broad overview of the state of knowledge of radar reflectivity of sea targets. All forms of targets are considered, including ships and boats, submarines, periscopes and snorkels, wakes, buoys, icebergs, and splashes. Also discussed are the statistical properties of returns, glint, and camouflage. Several approximate theories which have been advanced to explain the radar return of sea targets are reviewed and compared, and additional theoretical work is reported which indicates that there are serious limitations inherent in the commonly used coherent model. The effective cross-section of a target on a reflective surface is emphasized as being the product of the inherent ("free-space") cross-section times F^4, the fourth power of the pattern propagation factor. Suggestions are made for interpreting World War II cross-section values for present-day systems studies. It is recommended that extensive experimental measurement data be obtained on a few targets rather than fragmentary data on many targets. This should lead to better understanding of the general problem and, eventually, to possible techniques for predicting the radar cross-sections of sea targets.

14 KEY WORDS	LINK A		LINK B		LINK C	
	ROLE	WT	ROLE	WT	ROLE	WT
Radar Reflectivity						
Radar Reflectors						
Radar Sea Targets - Theory						
Radar Sea Targets - Experiments						
Radar Targets						
Radar Camouflage						
Glint						
Statistical Properties of Radar Returns						
Ships and Boats						
Submarines						
Snorkels						
Periscopes						
Buoys						
Icebergs						
Splashes						
Wakes (Sea)						
Electromagnetic Scattering						
Radar Cross-Sections						